COMPLETE CHARACTERISTIC CIRCLE DIAGRAMS FOR TURBOMACHINERY

Thesis by

W. M. Swanson

In Partial Fulfillment of the Requirements

For the Degree of

Mechanical Engineer

California Institute of Technology

Pasadena, California

1951

ACKNOWLEDGEMENTS

I am deeply grateful to Professor Aladar Hollander for his inspiration, help, and many suggestions. This association with him has been most enjoyable and valuable.

I should also like to acknowledge my gratitude to the Peerless Pump Division of the Food Machinery Corporation for supplying the pumps on which these experiments were conducted.

To Mrs. Ruth Toy goes a lot of thanks and credit for making this thesis a reality.

SUMMARY

Complete circle characteristics of per cent head and per cent torque plotted parametrically with per cent capacity as ordinate and per cent speed as abscissa are generally derived for an ideal case.

The experimental circle characteristics are presented as determined for an axial flow and mixed flow pump of representative commercial practice and a comparison of the three basic types of turbomachine; axial flow, mixed flow and radial flow (or centrifugal) is made. A new method of plotting power ratio radially on the same axes is also presented and compared for the same three units.

TABLE OF CONTENTS

NOTATION

A	Area
b	Width of section
C_H	Experimental head-speed coefficient
C_h	Cascade correction factor to head
C_L	Lift coefficient
C_Q	Experimental capacity coefficient
C_T	Experimental torque-speed coefficient
c	Absolute velocity (used only with subscripts); also chord length (without subscripts)
D_h	Hub diameter
D_o	Outside diameter
D_R	Representative
F	Force
g	Acceleration due to gravity
H	Head
K_H	Experimental head-capacity coefficient
K_n	Experimental speed coefficient (reciprocal of C_Q)
K_T	Experimental torque-capacity coefficient
n	Rotational speed in revolutions per minute
n_s	Specific speed
P	Power
Q	Capacity
r	Section radius
s	Slant height of truncated cone
T	Torque

t	Airfoil cascade spacing
u	Rotational velocity in feet per second
w	Relative velocity
w_∞	Vector mean of w_1 and w_2
z	Number of blades on impeller
α	Angle of attack of w_∞ with respect to chord line of airfoil
β	Angle between w and u in velocity triangle; also angle between chord line and perpendicular to c_m
γ	Specific weight of fluid
δ	Reciprocal of
η	Power ratio
λ	ψ / ϕ
ρ	Ratio of D_n/D_o; also fluid density
τ	Torque coefficient
ϕ	Euler flow coefficient
ψ	Euler head coefficient
ω	Rotational speed in radians per second

Additional Subscripts

1	Refers to inlet
2	Refers to outlet or exit
m	Refers to meridional component
P	Refers to pump
T	Refers to turbine
u	Refers to rotational component

PART I

INTRODUCTION

The idea of determining operating characteristics at conditions other than those for which a machine (pump) was primarily designed was first presented by Kittredge and Thoma (1, 2) in 1931. The characteristics were given on a percentage basis and merely extended beyond the normal limits. For example, the capacity was carried beyond the value of that for zero torque to where the pump was being run as a turbine, or in the opposite direction to normal (with the normal speed direction maintained) to give a forced power dissipating device. This could be done both for the normal and reverse direction of operation. The results were presented on two basic plots; one at constant speed with head and torque plotted against capacity and the other at constant capacity with head and torque plotted against speed. These can be seen in Figs. 4a and b of Ref. 4. In 1932 tests were begun here at the California Institute of Technology to obtain the complete characteristics for a four inch double suction, centrifugal pump. These were published in 1937 in a paper by Professor R. T. Knapp (3). In this paper the dimensionless characteristics are combined into a single parametric percentage plot of capacity vs. speed with constant percentages of head and torque as parameters. Since this plot gives the complete operating characteristics through every possible phase of operation, through 360 degrees, it was called a circle diagram, or as it is also referred to, the Karman-Knapp circle diagram. The idea of this type of representation was suggested by Theodore von Karman and first worked out and presented by R. T. Knapp.

This paper presents a method of determining what might be called the ideal complete characteristics of a unit knowing only its geometry. A comparison of the ideal and the actual experimental results is given for the radial flow pump (3) and for an axial flow pump of representative commercial practice. The complete circle characteristics are presented for an axial flow unit for the first time, and also those of a mixed flow unit. In addition to the usual circle characteristic plot, a circle power ratio diagram is introduced which represents the ratio of hydraulic to mechanical power, or its inverse plotted radially on the same per cent capacity (ordinate) vs. per cent speed (abscissa) coordinates. This power ratio circle plot gives the complete history of the pump and turbine efficiencies and power ratios under conditions of no useful output for all possible operating conditions.

The various applications of such methods of characteristic representation in determining design features of installation are quite well covered in many references (1, 2, 3, 4, and 5) and will not be repeated here.

The operation of machines under conditions for which they were not designed poses some very interesting questions when noting the results that are obtained. It is seen that most simple pump units operate about as efficiently, or sometimes even better, when operated as turbines. This would suggest the use of a single unit in some installations where both types of operation are dictated. In designing such a unit, care would have to be taken to match both turbine and pump

requirements. This would not be difficult to do if the heads, torques and capacities were fairly close in both cases. To put out the same torque as the pump requires a higher capacity to speed ratio for turbine operation. Thus the conditions could not be merely reversed in going from one type of operation to another. For example, to run one of the pumps tested as a turbine at 100 per cent speed and 100 per cent torque would require about 135 per cent capacity and 140 per cent head.* It also presents the question as to how might the reverse be, or how good a pump would a Kaplan or Francis turbine make. It should make an interesting experiment.

The axial flow unit subject to these tests was designed on what may be termed an extended one-dimensional theory. In Appendix A, a brief comparison is made between the experimental results and two methods of two-dimensional cascade theory as applied to this axial flow geometry.

---

* This, however, is not at the maximum turbine efficiency. At maximum efficiency for 100 per cent torque, the speed is 74 per cent.

PART II

DEVELOPMENT OF A THEORETICAL CIRCLE DIAGRAM

For almost any type of turbomachine it is possible to represent the machine as a two-dimensional airfoil lattice or cascade. The flow pattern and the characteristics of a machine can be developed after first making the following assumptions: (a) there is no prerotation of the flow; (b) the flow is irrotational, two-dimensional and steady; (c) the fluid is ideal and incompressible and (d) there are an infinite number of blades with zero thickness. All of these are not necessary, but simplify the following development.

First, consider the case of a purely axial flow machine where the two-dimensional representation is obtained by unwrapping a coaxial cylinder passed through the impeller as shown in Fig. 1.

Assume the machine is operating as a pump, then the head developed can be calculated from the vane geometry and mass, momentum, and energy conservation conditions. Referring to the cascade as shown in Fig. 1b with the airfoils moving to the right with the velocity u and the fluid approaching with the velocity c, consider what happens as the fluid moves through the vanes. For further simplification consider the flow relative to the blades, then the direction and magnitude of the velocities will be as shown in the velocity diagrams of Fig. 1b and 1c. Because of assumption (d) the relative flow will leave the vanes at the exit vane angle, β_2. There will be no change in the axial component of momentum of the fluid since the axial component of the absolute velocity must remain constant assuming the flow is continuous,

incompressible, and two-dimensional. In the tangential or rotational direction, however, the absolute velocity gains a component. The force needed to move the cascade is equal to the change in the momentum in this direction, or in the case of the cylinder, the torque equals the change in moment of momentum, or

$$T = (\rho Q)(c_{u_2} - c_{u_1})r \text{ and } c_{u_1} = 0 \text{ by assumption (a).}$$

Assuming no losses, the power input from this moment must equal the hydraulic power output, or

$$\omega \cdot T = \rho g Q H = (\rho Q)(c_{u_2})r\omega \text{ , or}$$

$$H = \frac{u_2 c_{u_2}}{g} \text{ foot pounds per pound of fluid flowing.}$$

This is the ideal head developed for the machine running at a given speed (ω) with a given through velocity,

$$Q/A = c_1 = c_{m_1} = c_{m_2} = c_m$$

where c_m is the through flow or meridional component of the absolute velocity. The head for zero capacity or zero through flow velocity can be seen from Fig. 1 to be u_2^2/g where $c_{u_2} = u_2$. A dimensional head coefficient can be arbitrarily defined as the ratio of the head at any capacity to this shut-off head and will be

$$\frac{u_2 c_{u_2}}{g} \frac{u^2}{g} = \frac{c_{u_2}}{u_2} = \psi$$

A capacity coefficient can similarly be defined for the through flow velocity, $\phi = c_{m_2} / u_2$. Now the ideal characteristic for a pump

can be plotted in terms of these coefficients between the limits of zero flow and zero head. For zero flow, $\phi = 0$ and $\psi = 1$; for zero head, $c_{u_2} = 0$, $c_u = 0$ and from Fig. 1, c and d, $\phi = \tan\beta_2$ and $\psi = 0$. The characteristic curve is seen to be a straight line between the two points. Fig. 2 shows this ideal characteristic with an intermediate point showing the linear correspondence with the velocity triangle. It is possible to allow for the more realistic conception of a finite number of vanes but retaining the assumption of a potential flow. Since the actual flow cannot be controlled completely so that all the fluid leaves tangent to the exit vane angle, it will not be turned as much as indicated by the vane geometry; therefore, there will be a smaller increase of the rotational component of momentum, resulting in a smaller head generated than that indicated by the Euler velocity triangles. The actual effective c_u will depend on both the vane angle and the gap-chord ratio, t/c (Fig. 1). This correction will vary linearly as the head increases so that the head may be expressed as $H = C_h \frac{u_2 c_{u_2}}{g}$, or the shut-off head as $C_h \frac{u_2^2}{g}$. This C_h factor was determined by Weinig (6) and is presented by Wislicenus (7, 8). The modified theoretical characteristic will now appear as in Fig. 3.

So far the method of obtaining this ideal characteristic has been derived for but one radius on a specific type of machine. The same method of analysis is valid for any type of machine yielding the same results. Since u_1 will not equal u_2, etc., for a radial flow runner, the subscripts 2 have been retained in the above analysis.

The total characteristic for all meridional radii is found by integrating over the entire flow passage. Characteristics for three radii at a chosen design condition are shown with their corresponding velocity triangles in Fig. 4. This is for a "free-vortex" type runner where the head developed ($u_2 c_{u_2}$ or $r c_{u_2}$) is constant over the passage so that a pressure equilibrium exists across the passage to maintain assumption (b). The runners or blades are designed for <u>one</u> particular operating condition that will produce the desired head at a lift coefficient for the cascade at a relatively small lift-drag ratio. (For a calculation of the characteristics for an actual pump from airfoil cascade data, see Appendix A.) Such a condition might be the head at the point indicated on the ψ vs. ϕ plot of Fig. 4. It can be noted here that for an ideal (no loss) characteristic, that at higher values of head (ψ), something strange appears to happen and above the value of C_h at the hub, the desired head line no longer appears to intersect a characteristic. What happens will become more apparent and will be discussed in a later section.

Now consider what happens outside the one quadrant for which this characteristic has been determined and again consider the characteristic of the next quadrant. If there the capacity is higher than that for zero head, hydraulic power instead of shaft power is being supplied and shaft power is the product or output. There will be a head drop across the pump instead of an increase, the shaft torque will be of the opposite direction and the pump becomes a turbine.

Before continuing, this is a good place to establish direction or sign conventions. All the quantities Q, n, H, and T will arbitrarily be designated positive for operation as a normal pump. The hydraulic power (HQ) as an output and shaft power (Tn) as an input will be positive by definition. These quantities will be negative when opposite from the direction of operation of the normal pump. A positive head is an increase of head across the pump in the normal pump direction and conversely. The signs of the parameters for all types of operation necessary are shown in Fig. 19.

Again consider the region of operation of over capacity maintaining a normal rotational direction. The head and torque are negative, the capacity and speed positive; therefore, the hydraulic power (-H x +Q) is negative, or hydraulic power is being supplied (opposite from pump hydraulic power). The shaft power (-T x +n) is also negative, or an output is resulting. This zone of operation is,by definition, a turbine zone. Note that the ratio of shaft to hydraulic power is positive.

Now consider the extension in the other direction, through shut-off into a region of negative capacity, or reverse flow direction still maintaining the same direction of rotation. The quantities here are -Q, +n. +H, and +T or negative (input) hydraulic power and positive (input) shaft power, or the machine is acting as a forced power-dissipating device. The characteristic now covers all possible modes of operation in the positive rotational direction.

The same type of analysis can be applied if the runner is rotated in the reverse direction (-n). The exit angle, β_2 (formerly β_1) is seen in Fig. 5 to be smaller, thus the value of C_h and tan β_2 will be smaller. In this zone of operation the quantities are -Q, -n, -H and -T, or again the shaft and hydraulic power are positive, or shaft input and hydraulic output. Combining the resulting characteristics, a complete characteristic as shown in Fig.6 is obtained. This is essentially a plot of the head vs. capacity at constant speed.

Now consider a power curve of HQ vs. Q, or dimensionless hydraulic power, $\phi\psi$ vs. ϕ . This curve is a parabola, $P = \phi\psi = C_h \phi (1 - \phi \cot \beta_2)$ with its maximum at $\phi = \frac{1}{2} \tan\beta_2$, $\psi = \frac{C_h}{4} \tan\beta_2$. Since $T\omega = \rho QgH$ the dimensionless shaft power curve will be coincident and the ideal pump efficiency will be everywhere 100%.

It was previously stated that every possible mode of operation was derived and shown on Fig. 6. This is true; however, to get every operating condition the characteristics shown would have to extend to infinity for the zero speed conditions. To overcome this difficulty the characteristics can be given on the basis of $1/\phi$ so that the points that go to infinity in the ϕ direction will be transformed into zeros. The inverse of ϕ is u_2/c_{m_2} and a similar transformation must be made for the head coefficient, $\psi = {}^{c_{u2}} / u_2$ or $\frac{u_2 c_{u2}}{g} / \frac{u_2^2}{g}$. If this is divided by ϕ^2 , $\psi/\phi^2 = \frac{u_2 c_{u2}}{g} / \frac{c_{m_2}^2}{g}$ or a head coefficient based on the through-flow velocity or capacity (Q) is obtained. If $1/\phi$

is denoted by δ and ψ/ϕ^2 by λ then a plot of these quantities as derived from Fig. 6 will appear as in Fig. 7 for the positive flow direction. The equation for the +n characteristic of Fig. 6 was $\psi = C_h(1 - \phi \cot\beta_2)$. Since $\lambda = \psi/\phi^2$, $\lambda = C_h \delta (\delta - \cot\beta_2)$ is the equation of the constant capacity head characteristic of Fig. 7. The curve for the negative flow direction is also sketched in as it would be derived from Fig. 6. The characteristics in the zones of power dissipation are shown dotted since they are not too well defined for some types of turbomachines as will be shown later. Fig. 6 and 7 now contain all the possible modes and conditions of operation. In both these curves it is somewhat deceiving to show both curves on the same coordinate axes, for although the coefficients ϕ and ψ are both positive on the right hand abscissa, for the +n curve, $\phi = \frac{+c_{m_2}}{+u_2}$ and for -n, $\phi = \frac{-c_{m_2}}{-u_2}$. (The same is true for δ.)

To make the picture somewhat more complete a development of the torque characteristics will be briefly considered. On the constant speed reference the torque curve will necessarily be a parabola since the head was derived from the equation

$$\omega \cdot T = \rho QgH \propto Tn \propto P.$$

A power, or $\phi\psi$ curve will be a parabola when plotted against ϕ. With a constant speed reference the torque vs. ϕ must also be parabolic. A schematic representation is shown in Fig. 8. A torque coefficient, τ, is also difficult to define on an ideal and dimensionless basis so that here it will not be shown. From the development of

Figs. 6, 7, and 8 it is not difficult to induce that the torque when plotted dimensionlessly on a constant capacity basis would be a straight line as shown in Fig. 9.

Consider next a mean Euler curve with the exit flow triangle so calculated as to give equal magnitude of absolute and relative velocities (c_2 and w_2) at the design operating condition as a normal pump. (Fig. 10). If this design point is arbitrarily designated as 100% ϕ and 100% ψ and the characteristic is then reduced to a percentage basis, it will appear as in Fig. 11. Fig. 12 would be representative of the negative rotational direction. The principal reasons for different characteristics in the -n direction are different inlet conditions and a different exit vane angle. All of the characteristics can now be expressed as percentages of design point.

Now consider a method to combine them into a single circle plot of per cent Q vs per cent n. Since $\psi = \dfrac{u_2\, c_{u_2}}{g} \Big/ \dfrac{u_2^2}{g} = H \Big/ \dfrac{u_2^2}{g}$ the characteristic of Fig. 11 is essentially per cent H/n^2 vs Q/n for any one particular machine geometry. Choosing any arbitrary point on this characteristic, for example point a, this point can be transformed to any desired parametric head as follows: at point a suppose $Q/n=0.25$ and $H/n^2 = 1.50$, in the Q vs n plot (Fig. 13). Next a value of Q or n for the head desired must be located to locate the point on this line. Suppose it is desired to find the Q and n for 100% H at this Q/n ratio of 0.25. Fig. 11 gives 150% H/n^2 at 25% Q/n, this means that the head is 150% relative to 100% n, or for 100% H, $n = \dfrac{1.00}{\sqrt{1.50}} \times 100 = 82\%$ n.

Thus the head is +100% at 25% Q/n and 82% n as shown. For the entire +100% H curve on this plot the procedure is as follows: from Fig. 11,

$$H/n^2 = (2 - Q/n), \text{ or for 100\% H } (H = +1),$$

$$n^2 = \frac{1}{2 - Q/n}$$

$$2n^2 - Qn = 1 \quad \text{or in general} \quad n(2n - Q) = H$$

In the +n half plane this is half of a hyperbola with the H = 0 at $\frac{Q}{n} = 2$ and n = 0 assymptotes as shown. For H = -1, the equation can be seen to be $2n^2 - Qn = -1$. It is also a hyperbola, half of which is shown with the same assymptotes. If any other per cent head line is desired it is only necessary to substitute the fractional head in the equation

$$2n^2 - Qn = H$$

Fig. 13 has been completed for the case of a very simple machine with straight vanes and no guidance at the inlet for either direction of flow.

Since the machine is still considered as operating under ideal conditions, the percentage torque characteristic will be easily constructed even if the dimensionless coefficients are not easily or clearly defined. Knowing that the curve is (a) a straight line, (b) must pass through the $T/Q^2 = n/Q = 100\%$ and (c) must have a slope of 2, completely defines this curve (Fig. 14). Its equation is

$$T/Q^2 = 2n/Q-1$$

or

$$Q(2n-Q) = T \quad ,$$

again a hyperbola with assymptotes Q = 0 and Q/n = 2. Making the same assumptions as above and using the same procedure, the 100% T lines

can be plotted on the circle diagram as shown dot-dashed in Fig. 13.

This circle diagram is for one very special case. For any particular machine, however, the procedure would be similar. First, the characteristic would be laid out in the zone of normal operation. If the machine were designed as a turbine it may be desirable to call the design turbine condition the 100% condition and begin with the characteristics referred to constant capacity (the straight line torque characteristics). With this type of representation the limits are essentially those of zero shaft power, i.e., zero speed and zero torque. The reverse operation curve (-n in the case of a pump) can be determined from the vane geometry of the guide vanes (determining the inlet flow) and the impeller exit vane angle (formerly the inlet angle for normal operation). These characteristics may be determined from cascade theory or various other two- and three-dimensional theories (8, 9, 10 and others), whichever is the best method of design available for the machine. The percentage characteristics are then determined and the circle diagram plotted from these.

PART III

METHOD OF EXPERIMENTAL REPRESENTATION

For a real machine the original assumptions cannot be maintained and the characteristic curves will not be as simple as those shown in some cases and for some conditions will bear little resemblance. The shaft and hydraulic power will not be coincident because the efficiency will vary from zero to maximum and back to zero and not approach the ideal efficiency of 100%.

Dimensionless coefficients of head, torque, capacity and speed can be defined in much the same manner as were the theoretical coefficients. The dimensionless head can be defined as $C_H = H/\frac{u_2^2}{g}$ where H is the measured experimental head and u_2 is, as before, equal to ωr. The dimensionless capacity will be $\frac{Q/A}{u_2}$. The torque coefficient can be derived in the same way as was the head coefficient. From above,

$$T\omega = \rho g Q H ,$$

or

$$T = \frac{\rho g Q H}{\omega} .$$

Now H is proportional to $\frac{u_2^2}{g}$ and Q to $u_2 A$; therefore an experimental torque coefficient may be defined as $C_T = \frac{T}{g\,\frac{(u\,A)(u/g)}{\omega}}$ where

$A = \frac{\pi}{4} D_R$, $u = \omega r$, $\omega = \frac{\pi n}{60}$, $r = \frac{D_R}{2}$ and D_R is some representative diameter, so that

$$C_T = \frac{T}{\rho \frac{\pi}{4} D_R^5 \left(\frac{\pi n}{60}\right)^2} ,$$

$$C_T = \frac{T}{\frac{\gamma}{g}\frac{\pi^2 n^2}{14400} D_R^5} .$$

These are the coefficients based on constant speed. The dimensionless coefficients based on constant capacity are easily defined as follows:

$$K_n = 1/C_Q ,$$

$$K_H = C_H / C_q^2 ,$$

$$K_T = C_T / C_Q^2 .$$

The ideal head and torque characteristics for positive rotation would appear as in Fig. 15. Fig. 16 represents those for negative rotation. Both the resulting power curves would be similar in shape to the torque curve and the power ratio would be everywhere unity, or 100%. The significance of the zone marked ? is somewhat strange to contemplate and impossible to achieve. It is easily visualized if one considers a single airfoil and the flow necessary for this condition. The torque power is a turbining type power and so is the shaft power since both are negative. Therefore, the flow condition to produce such a phenomenon would be as represented in Fig. 17. The deviation of the actual to ideal flow in this case is in the realm of the ridiculous. The actual case is also easily visualized. The machine remains running in the same direction while the direction of flow is reversed. This means that fluid is being forced through the machine and the machine is trying to force it back again. The torque is positive pumping torque and the speed is positive; therefore, the shaft power is positive. The hydraulic power is negative. Therefore, the ratio is

negative denoting no useful power from the device unless it is desired to use it as a fancy water heater.

Another deviation will result from some small losses at zero head and zero torque. It will take a small amount of torque to maintain the actual machine at zero head across the unit due to friction losses in the passages. At zero torque, some head will have to be supplied. The resultant power curves could then be conjured up to look like those in Fig. 18. The dotted line represents a plausible ideal power curve.

Before going further, the notation for the zones of operation and the signs of the components will be established. With reference to Fig. 19, start with all quantities, n, Q, H and T positive for normal pump operation. The zones on the circle diagram will then be as shown. The zone of reverse turbine is in the positive flow and rotational directions but since the machine operates more efficiently in the reverse flow and rotational directions (third quadrant) this is referred to as the normal or high efficiency turbine zone. The zones B and F are friction loss zones as explained above while D and H are differentiated as being intentional dissipation zones. It may be noted that everywhere the ratio of (QH)/(Tn) (or the reciprocal) is positive, there is a useful power output.

Experimental characteristics of dimensionless head and torque on a constant speed basis are presented in Fig. 20 for a commercial 10 inch, low head propeller pump. These were obtained by running the machine in the positive direction and varying the head and capacity from shut-off through zero head and torque into the turbining region,

and in the other direction by starting at shut-off and running with the flow direction reversed. The experimental apparatus with which this was done will be described in another section. This was done for from 3 to 5 various speeds over a speed variation factor of two and bracketing the design speed of the unit where the limits of the machinery and cavitation would allow. In some cases it was necessary to use lower speeds. By reducing the data to dimensionless values, the accuracy was greatly increased and the adherence of the operating conditions to the similarity or affinity laws* could be checked. In every case these laws were found to hold. Stepanoff (10, p.293) states that propeller pumps do not follow these laws in the case of zero rotation (locked rotor). This condition was examined. It was found that the similarity laws were valid in so far as the head and torque were proportional to the square of the through-flow velocity (for all non-cavitating flow rates) providing the rotor position was held fixed at one position. But it was also found that if the head and torque were plotted against the square of the capacity, different straight lines would be obtained depending on the position in which the rotor was locked. Since these propeller pumps have straightening vanes to convert the rotational component to pressure head, at each position the rotor is locked there will be a different correspondence of the rotor and stator vanes. This will cause geometrically different types of flow with different losses resulting. There is no good reason to give supporting the idea that the flow should not obey the proportionality to flow-velocity

---

* $H \propto n^2$, $T \propto n^2$, $Q \propto n$.

squared law (as long as the critical Reynolds number is exceeded). It seems logical that if a mean value of the slope were taken for the dimensionless head and torque vs. capacity curves for all positions of the rotor at zero speed, this mean value should be the same as a value obtained by extrapolating to the zero speed condition the characteristic plots of head and torque vs. speed at constant capacity. Unfortunately, this was not experimentally verified.

The straight line is an ideal characteristic calculated for the mean diameter of the rotor using available cascade data (8, 6) and the blade angles of the machine.

The efficiency curve was next calculated and the point of maximum efficiency determined. The values of C_Q , C_H and C_T were then read off and assigned as the 100% values. By dividing the curves point by point by these values, a per cent plot was obtained as shown in Fig. 21.

This procedure was repeated for the -n direction and Figs. 22 and 23 obtained.

In a similar manner experimental constant capacity curves were obtained. These are shown in Figs. 24, 25, 26, and 27.

Next a point by point calculation of 100% +H and T, and 100% -H and -T circle characteristics were obtained as described in Part II and plotted to obtain the circle diagram as shown in Fig. 28. The data were plotted on a much larger scale than those shown in these figures. Reproductions of the plotted originals of Figs. 20, 24 and 28 are enclosed in the pocket on the back cover.

By making measurements of the actual blade configuration, the

zero lift angle and cascade head correction factor were determined at the geometric mean section radius. From these data the ideal characteristics were determined and are shown as the straight lines on Figs. 20 and 21. The circle characteristics for the positive directions in the circle diagram are shown dotted on Fig. 28. The coincidence is quite good in the normal pump zone. Within the accuracy of the plots, the head and torque are coincident for all values above 60% Q. Due to the strange behavior of the ideal flow as sketched in Fig. 17, the deviation below this point is quite large. The agreement in the reverse turbine zone (C) is not too good.

Only the 0 and 100% H and T curves are shown; however, the remainder can be derived from these, or they can be derived point by point by substituting the desired head value as described above. Since $H \propto Q^2$, $H \propto n^2$ and $Q \propto n$, given any two, the third is easy to find. Some examples follow.

(A) Find the positive head at +50% and +100% n. From Fig. 28, on $Q/n = 0.5$, the 100% H occurs at Q = 36%, n = 72%, or at H = 100, Q = 36 and it is desired to find H at Q = 50. Since $H \propto Q^2$, $H = 100(50/36)^2 = 193\%$; or at H = 100, n = 72 and at H, n = 100. Therefore, $H = 100(100/72)^2 = 193\%$.

(B) The same procedure as (A) would be used if the Q/n ratio and either Q or n were given.

(C) Given H and either Q or n, find the other. For example, find Q at H = -75% and n = -120%. From Fig. 28, at n = -110% H = -100% at Q = -70%. Therefore, H = -75% will be along the line n = -120%, at $Q = -70(\sqrt{-75}/\sqrt{-100}) = -60.6\%$.

It can be seen that Fig. 28 is merely the superposition of two latitudes of a three-dimensional plot, namely the plus and minus 100% levels. If the solid figure is constructed, it will appear as represented in Fig. 30. Any H-n (constant Q) planes through that figure will cut the figure with a parabolic line of intersection as will any H-Q (constant n) planes. The constant H(Q-n) planes will all have geometrically the same shape as Fig. 28, degenerating into a straight line broken at the origin at H = 0.

As yet there has been no consideration of efficiencies, or more generally, power ratios. It was previously mentioned that the ideal efficiency would everywhere be 100%. The real machine will naturally show a different behavior. These efficiencies or power ratios can be followed through in detail by closely adhering to the sign conventions noted in Fig. 19 and by calling any operation where the hydraulic power (HQ) exceeds the shaft power (Tn) a turbine-type operation, and a pump-type operation will be the converse. First regard these quantitatively in the different zones. In Fig. 21 (or 20) in zone A, the normal pump zone, the hydraulic power (+H x +Q) is positive by arbitrary choice of definition and so is the shaft power (+T x +n). In zone C the conditions are -H x +Q or negative hydraulic power denoting a hydraulic input and -T x +n, a negative shaft power denoting a mechanical power output. The ratio is, however, positive. In the negative speed direction in the reverse pump zone, all the quantities are negative; therefore, both powers are positive, as is their ratio, or again hydraulic output and mechanical input. In the normal turbine region the shaft power is

again negative, or an output (+T x -n) and the hydraulic is input or negative (+H x -Q) and again the region is positive. It should be noted that the normal turbine zone is so called because it would be the zone where the machine would operate (with respect to the normal pump definition) if it had been designed as a turbine, and is consequently the region of the higher turbine efficiency. Another apparent fact is that in all these four zones the power ratios are positive, denoting a useful output. In the other zones it will be seen that there is only one quantity of a different sign, thus the power ratio in any of these, B, D, F, or H, will be negative. In zone B, for example, only H is negative; therefore, (-H x +Q) is hydraulic input and (+T x +n) is shaft input; no useful output. Very fortuitously, exactly the same regime exists in these other three regions. It is possible to plot the power ratio on beyond the points of zero power as seen in Fig. 24. If the ratio is hydraulic to shaft power (η_p) the ratio will approach minus infinity as the shaft power approaches zero ($T \rightarrow 0$). Now it was shown that in the turbine region (C, Fig. 43) the ratio is positive. If η_r is the turbine efficiency ratio (shaft to hydraulic power) then it will be positive in zone C, go to zero at T=0, become negative for negative T and approach minus infinity at H = 0. Suppose the absolute value of these powers is plotted across zone B between H = 0 and T = 0. The shaft power, Tn, will have the same shape as the torque line since these are essentially constant speed characteristics. The hydraulic power curve will approach a parabola. Somewhere in this zone the two power curves must cross and where they do, $\eta = -1$. Here the operation will change

from one type to another. From left to right (in Fig. 43) the sequence would be as follows. In zone A the operation is definitely pump type with a useful output; therefore, η is positive. As H = 0 is passed, η becomes negative, or there is no useful output, but the operation is still designated as a pump type since HQ is greater than Tn in absolute value. As the point where $\eta = -1$ is traversed, Tn becomes greater, the inverse ratio is now considered and a turbine-type operation exists. The ratio becomes positive in zone C and useful mechanical output is the product. The same procedure is seen to be applicable to all such zones between pump and turbine operation.

It would again be advantageous to be able to represent all the power ratios on a single diagram. If the same axes are used as for the characteristics circle and this power ratio plotted radially between the limits of plus and minus one on arbitrarily designated radii, a power circle as shown in Fig. 29 is the result. In one glance this gives a comparison of all the zones of operation with respect to relative efficiency. The angle of best normal pump efficiency will be 45° by definition. This method of complete power ratio representation and its derivation was suggested by Professor A. Hollander of this Institute. The cusp points are interesting in that they would be designated as the points of zero and perpendicular angle of attack on the vanes respectively for each zone of loss and power dissipation.

PART IV

COMPARISON OF RESULTS OF TYPES OF MACHINES

As stated previously, the only complete circle plots in existence were for centrifugal (radial flow) machines. When such a machine is operated as a reverse pump, its impeller operation is similar to that of a forward curved vane compressor. The rotational direction is reversed but the flow direction remains the same. Thus, the zone E is in the second quadrant. An entire set of curves for an eight inch double suction pump is presented in Figs. 32 through 41. The axial flow or propeller type pump when run in the reverse direction will pump in the reverse flow direction, obviously. Both conditions are quite logical and can easily be seen by the construction of the simple Euler velocity triangles.

If an ideal circle diagram were to be constructed for a radial flow machine it would appear as in Fig. 31. Where the H and T go to ∞ along the Q and n axes, they have been connected across (solid line for H, dotted for T) showing what happens for a real fluid. The significance of these infinities of torque and head is of interest. It can most easily be described by visualizing an airfoil in these flow conditions. Consider first the $Q = 0$ axis. For no flow the relative and rotational velocities will be coincident, or the vane is in a flow field that is perpendicular to the axis of rotation, or the only force that can be exerted by an ideal fluid is also perpendicular to the shaft; thus there is no force to exert a torque and $T = 0$ for $Q = 0$. At first this would seem to signify that H must also be zero. However,

considering that Tn = QH, Q and T are zero (since T $\rightarrow \infty$ as Q $\rightarrow$ o or for any finite n, T must be zero), while n is finite shows that H must also be finite. A similar analysis can be made for the infinities along the Q axis. In a real machine there will be losses due to mismatching of guide vanes and volutes, and separation losses due to incorrect angles of flow relative to the vanes resulting in a finite mechanical power absorption (in the case of the n axis).

From only a casual observance it would appear that the radial flow machine follows the ideal somewhat more closely. At first it might be ascribed to the fact that radial flow machines have a higher vane solidity than the axial flow and would have more control and entail fewer losses. On the other hand, during normal pump operation (Fig. 32) the radial flow machine is seen to stall off at low relative flow rates more than the axial flow. Yet the torque curve is seen to more nearly comply to the ideal for the radial flow; also the efficiency is relatively better near shut-off for the radial-flow or lower specific speed type. This general trend is shown by Stepanoff (10, Ch.9). However, there are a few finer points to be considered than specific speed alone. Near shut-off the axial flow pump designed on the free vortex method will be pumping at one section radius (tip) and acting as a dissipating device trying to pump the other way at another radius (hub).* This is not a general type of behavior, but is due in this particular case to the decreasing solidity with increasing radius resulting in the curves

---

* At first glance this seems like the reverse should be true, However, considering the development in Appendix A, the above is correct.

shown in Fig. 4 and due to the fact that the blades are nearly constant chord.

It is interesting to visualize the flow around the vanes of a machine in the various zones of operation. Fig. 42 shows a simple representation of a mean section radius for an axial flow machine with the approximate resultant flows. The section line divides the stator from the rotor so that each is shown with the flow moving relative to it. At the off-design points there will also be circulatory flows in the radial plane which further decrease the efficiency.

This basic difference in the reverse pump zones gave rise to some speculation about which direction a mixed flow machine would pump in the reverse rotation direction, in which quadrant would zone E lie. Another complete set of characteristics and the resultant circle diagram were determined and are presented in Figs. 43 through 52. It can be seen that the reverse pump zone is in the third quadrant, or the axial effect predominates. This was expected since the mean passage angle was at an angle of 35° to the axis of rotation (Appendix C).

This unit shows a loop in the normal pump zone of operation (Fig. 43). This instability of operation was obtained experimentally and showed a curious behavior. Approaching from the high capacity side, the operation was smooth up over the peak to the drop off point. At this point there was a sudden decrease of head and the operation became noticeably noisy. Since this noise did not seem to be affected by any changes made in the static head, it was attributed to separation and unstable vortex motion. This noise continued on into the

zone of power dissipation. On approaching from the other side this regime of less efficient flow continued along the lower portion of the loop until a point was reached where the flow again became somewhat unstable with no further variation in the external circuit. This rise was not as unstable as the drop, however, and the operation was stable for periods long enough to get good H and Q readings, while the drop was sudden. The beginning of this loop (with decreasing Q) seems to be initiated by the sudden and violent inception of secondary circulatory flows. The corresponding loop in the efficiency curve would also point to this conclusion. Why these should start and stop at different points depending on the approach direction is another question that still remains to be answered.

Comparisons of the power ratio circles (Figs. 29, 41 and 52) are of interest with respect to a comparison of the efficiencies at the useful zones other than the normal pump. Comparing zones E, the axial flow pump is seen to have a best efficiency of 34%, or 42.5% of the normal pump maximum efficiency. This is quite good, especially considering that the blades are running as upside-down-backwards airfoils, the guide vanes are running in reverse and the three bearing hub support vanes are disturbing the exit flow. The airfoil difficulty is not as effective as it might, however, for even though the blades were patterned after NACA 44xx airfoils, they are quite blunt at the trailing edges also as shown in a comparison of the 4407 airfoil with a measured blade profile (Fig. 53). This rounding of the trailing edge has the effect of decreasing the maximum normal

pump efficiency, but increasing all the others. In reverse pumping, the radial flow pump suffers from poor angles of attack (shock losses), high relative speeds, large separation losses since Q is still positive, and a bad mismatch of volute. The efficiency here is only 9%, or 10.8% of normal pump. For any normal flow direction operation where there is little energy supplied, or energy is taken out, the centrifugal machine is under a great disadvantage due to expanding flow. Since the mixed flow machine is torn between the two, large circulatory motions are set up resulting in poor reverse pump efficiency, 9% maximum as a reverse pump which is 11% of the value of best efficiency as a normal pump.

In the reverse turbine zone (C) the axial flow machine is running with the blades at an excessive angle of attack giving a large drag and the guide or diffusor vane angles are off. The efficiency is surprisingly good however; 50% at the point of best reverse turbine efficiency or 62.5% of the best efficiency as a normal pump. The radial flow shows a poor efficiency here which may be primarily attributed to separation losses with mismatched inlet angles and volute. The maximum efficiency is again only 9% as a reverse turbine. The mixed flow is between the two with 26% maximum as a reverse turbine or 32% of the normal pump maximum.

As a normal turbine, the axial flow gives nearly as good efficiency as when operating as a normal pump. Since the flow is reverse, the rounded edge is at the trailing edge instead of the leading edge. This is of little effect since these blades are thin and nearly symmetrical

with respect to the thickness function and since they are sand cast. The same is nearly true of the impeller vanes as seen in Fig. 53. In the case of the impeller the effect is shown by a narrower and more peaked efficiency curve. The maximum normal turbine efficiency is 78% , or 97.5% of the normal pump efficiency. The radial flow case is not too representative of what is usually found. The maximum normal turbine efficiency is only 70%, or 84% of normal pump. Usually the unit will show a better efficiency as a turbine than as a pump. In turbine operation the flow is convergent into the eye from the volute, a desirable condition with respect to separation. It is true that energy is also being extracted from the fluid; however, the ratio of this energy loss to the static head increase would be the deciding criterion. Usually the vanes are thin and symmetrical so that they operate as well one way as the other. Since the efficiency is for the unit, the reason for the low efficiency shown may be attributed to the split inlet nozzle and the fact that the passages would be designed for flow in the other direction. The mixed flow unit is fairly close with 78% maximum normal turbine efficiency or 95% of maximum normal pump efficiency. The reason that it is not greater may be due to diffusion of the entering flow as well as reversed fore and aft blade ends.

A short discussion was previously given on the cusps shown on the power ratio circles. If the unit were a two-dimensional axial flow with flat plate blades, the cusps would be diametrically opposite to each other, those in zones B and F (Fig. 29) being at the zero attack angles and those in D and H for a 90 degree angle of attack.

For a symmetrically cambered plate, the D and H cusps would be opposed, but the B and F zones would vary from a 180 degree intersection by the included camber angle. A rough comparison was made; the angle given by the cusps measured 8 degrees and the camber angle measured at the geometric mean section radius is 8 1/2 degrees. If the camber were symmetric this angle should be evenly divided with respect to the D and H cusp line. The fact that it is not indicates a non-symmetrical camber. The camber here is at 40% of the chord.

In the case of a radial flow machine, a log spiral vane should give the B and F cusps on a straight line through the center. It may be noted that these zero angle of attack angles are also noted on the characteristic circle diagram as the H = T = 0 lines on the ideal diagram and somewhere between H = 0 and T = 0 on the experimental diagram. In the case of the radial flow in the reverse directions, these zero angles are difficult to define since there is so much interaction of impeller, inlet, and volute effects. The T = 0 lines being in opposite quadrants of the characteristic circle diagram is easily visualized. The H = 0 in the second quadrant is not so easy. This is a case of effective zero lift angle of attack but without having the flow parallel to the leading and trailing edges. This also explains the finite value of T being relatively large at H = 0. The finite H at T = 0 and the sloping right end of the efficiency curve shown in Fig. 36 are similarly explained. The H cusp for +n should be closer to 90 than 180 degrees for the radial flow. As the solidity increases, this angle will vary increasingly from 90 degrees. All of these phenomena are further complicated by three-dimensional effects.

The mixed flow shows a mixture, but predominantly axial tendencies.

There has been made available an axial flow pump of the same specific speed as the mixed flow, the experimental characteristics of which are shown here. Obviously, the two will not have similar characteristics. Completion of the characteristics for this unit would provide an interesting comparison with respect to different designs based on the same specific speed.

To get a better comparison of all three types of unit, a large print with all six circle diagrams is presented and will be found in the pocket of the back cover. This shows at a glance the basic difference between the radial and axial flow units with the mixed flow between the two, but showing more resemblance to the axial flow type of characteristic.

PART V

EXPERIMENTAL EQUIPMENT AND TECHNIQUE

Since this project was purely experimental, the pump modifications were designed and the circuit modifications and installation were made as part of the project.

The circuit used including service pump, dynamometer, throttle valve, venturis and power supplies is a multiple unit in use at the Hydraulic Machinery Laboratory of the California Institute of Technology. This circuit is used for basic research on turbomachinery. The circuit and its components and the method of measurements are described in detail in Ref. 11. Fig. 54 is a sketch showing the installation of the units into this circuit. The circuit is shown for the normal flow direction with the unit operating as a normal pump. Flow enters from the inlet header, then passes through the straightening vanes; the inlet static pressure goes to one side of a mercury manometer that can be read to one thousandth of a foot of mercury with the aid of a vernier, through a high efficiency vaned elbow, through a 10 to 8 inch reducer (14 inches in length), into the bowl unit, into another reducer, through a standard 10 inch pump elbow as supplied with the pump by the manufacturer, passes through another set of straightening vanes. The outlet pressure is led to the other side of the manometer, and to the outlet header. Since it was desired to determine the efficiency of the bowl unit alone, the losses of the various components were measured between the points a through f (shown in the sketch) for both directions of flow and plotted on log paper. They were found to be the same for both directions and proportional to the square

of the flow velocity for all flow rates used. The velocity profiles in two perpendicular directions were determined at points b, c, d, e, and f for positive flow and at a, b, d, and e for negative flow. All of these were not necessary but it was desired to determine the action of the elbows and vane sections. It is interesting to note that the loss in the lower elbow was only about one quarter of that for the top elbow. The lower compared very closely with the losses expected due to pipe friction alone for the equivalent lengths of passage. For negative flows the manometer was connected to piezometer rings a and e so that the pressure was always measured downstream of the vanes where the flow was axial. A velocity profile taken at c showed the velocity distribution to be nearly uniform at the impeller approach.

The head was read to the nearest 0.001 foot of mercury and readings could be repeated to plus or minus 0.002 feet. The speed was set and controlled with a negligible error as described in Ref. 11. The capacity was determined to the nearest 0.01 cfs by reading a mercury manometer and getting Q from a calibration chart. The torque was measured with a combination of dead weights for coarse increments and a hydraulic bellows and precision pressure gage for the fine increments. A make-up system in the hydraulic line made it possible to measure the torque on a null point basis so that the dynamometer was always at the same position in the cradle bearings during measurement. The bellows was mounted to the frame with the free end against the dynamometer torque arm. There was a fair amount of scatter in the torque readings; however, the overall accuracy was considered good since

from 3 to 5 complete sets of data were independently taken for each zone of operation. The accuracy of the data can be illustrated from the points that were plotted for four runs in the reverse pump quadrant for the axial flow pump. An average of 28 points per run was taken; the points of H vs. Q plotted for the four speeds and reduced to dimensionless form plotted such a uniform and even line that it was hardly necessary to draw a line through them. For this particular set, the torque data plotted up equally well.

REFERENCES

1. Thoma, D., "Vorgange beim Ausfallen des Antriebes von Kreiselpumpen", Mitteilungen des Hydraulischen Instituts der Technischen Hochschule Munchen, Heft 4, 1931. S 102-104; Verlag von R. Oldenbourg, Munchen.

2. Kittredge, C. P. and Thoma, D., "Centrifugal Pumps Operated Under Abnormal Conditions", Power, Vol.73, 1931, pages 881-884. (English translation of Ref. (1)).

3. Knapp, R. T., "Complete Characteristics of Centrifugal Pumps and Their Use in the Prediction of Transient Behavior."
   (a) Preprints of ASME University of California and Stanford summer meeting, June 1934. (for 4" pumps)
   (b) Transactions ASME, Vol.59, 1937, pages 683-689 (for 8" pumps)

4. Stepanoff, A. J., "Special Operating Conditions of Centrifugal Pumps", Hydraulic Institute Fourth Annual Contest Engineering Papers, 1944.

5. Knapp, R. T., "Centrifugal Pump Performance as Affected by Design Features", Transactions ASME, April, 1941, pages 251-260.

6. Weinig, F., Die Strömung um die Schaufeln von Turbomaschinen, J. A. Barth, Leipzig, 1935.

7. Wislicenus, G. F., Fluid Mechanics of Turbomachinery, Chapters 7 and 9, McGraw-Hill Book Co., N. Y., 1947.

8. Wislicenus, G. F., "A Study of the Theory of Axial Flow Pumps", Transactions ASME, Vol.67, 1945, page 451.

9. Rouse, H. F., Engineering Hydraulics, Chapter 13, "Hydraulic Machinery", John Wiley and Sons, Inc., N. Y., 1950.

10. Stepanoff, A. J., Centrifugal and Axial Flow Pumps, Wiley, 1948.

11. Knapp, R. T., Hollander, A., Acosta, A. J., and Osborne, W. J., "Laboratory Developments for Study of Flow in Rotating Channels", paper presented at the Annual Meeting of the ASME, 1948.

12. Robinson, R. L., "A Theoretical Analysis of Two-Dimensional Cascade Flow with Application on an Axial Flow Pump", Thesis for the Degree of Mechanical Engineer, California Institute of Technology, 1950.

13. O'Brien, M. P., and Folsom, R. G., "The Design of Propeller Pumps and Fans", University of California Publications in Engineering, Vol.4, No.1, 1939.

PART VI

FIGURES

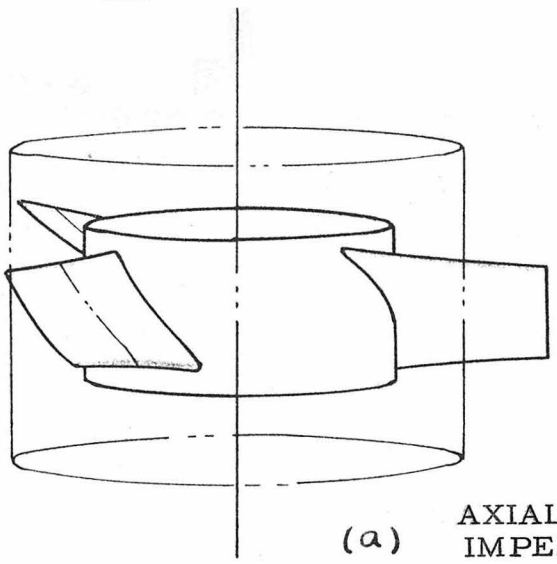

(a) AXIAL FLOW IMPELLER

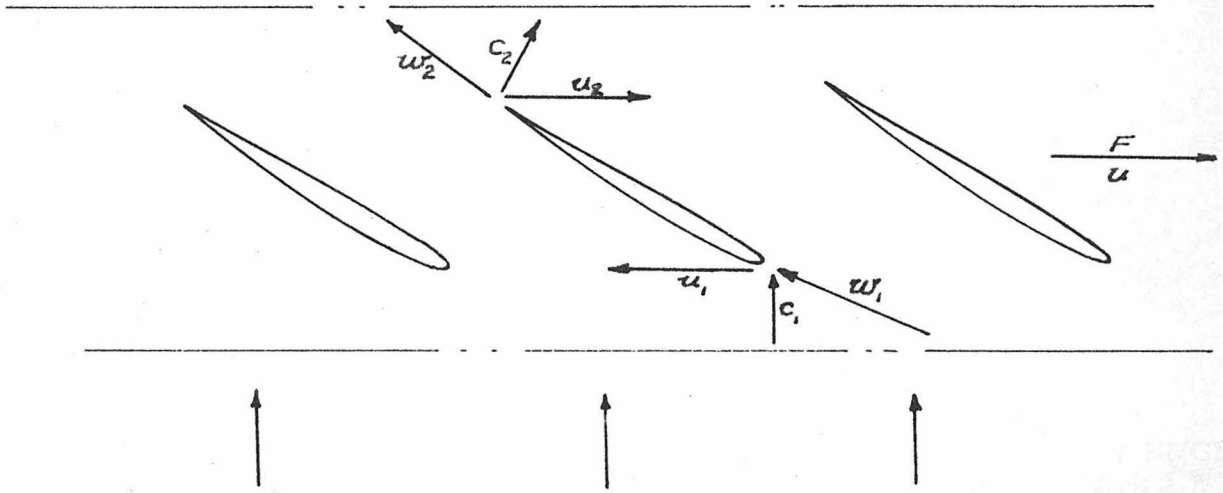

CYLINDRICAL SECTION THROUGH ABOVE

(b)

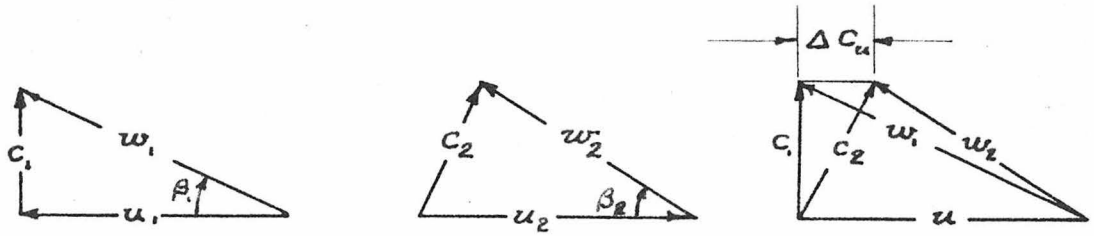

VELOCITY TRIANGLES FOR ABOVE SECTION

(C)

FIG. 1

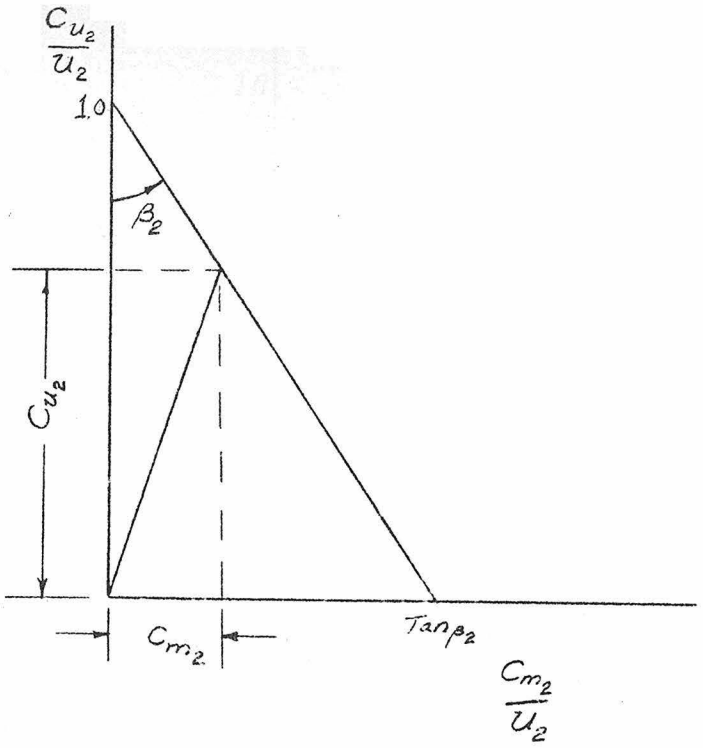

(a) IDEAL EULER CHARACTERISTIC ($\mathcal{U}=1$)

NOTE LINEAR CORRESPONDENCE BETWEEN VELOCITY TRIANGLE AND ABOVE CHARACTERISTIC

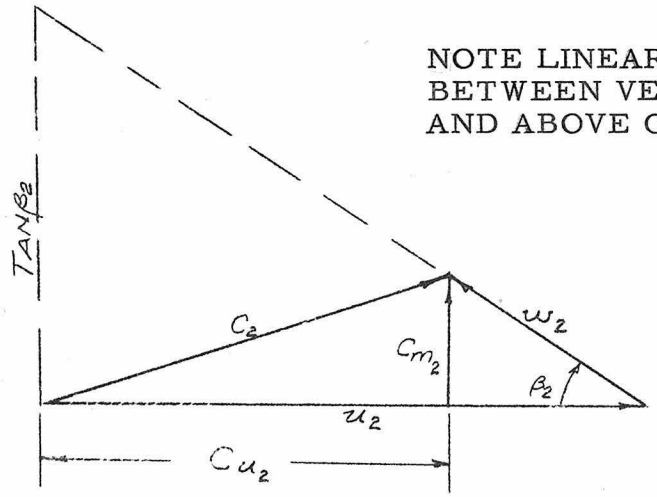

(b) VELOCITY TRIANGLE

FIG. 2

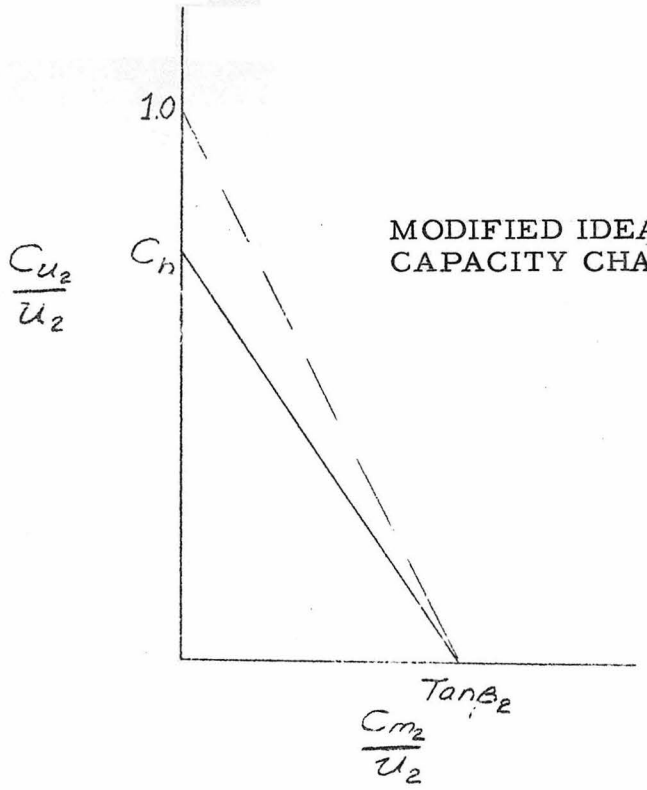

MODIFIED IDEAL HEAD-CAPACITY CHARACTERISTIC

FIG. 3

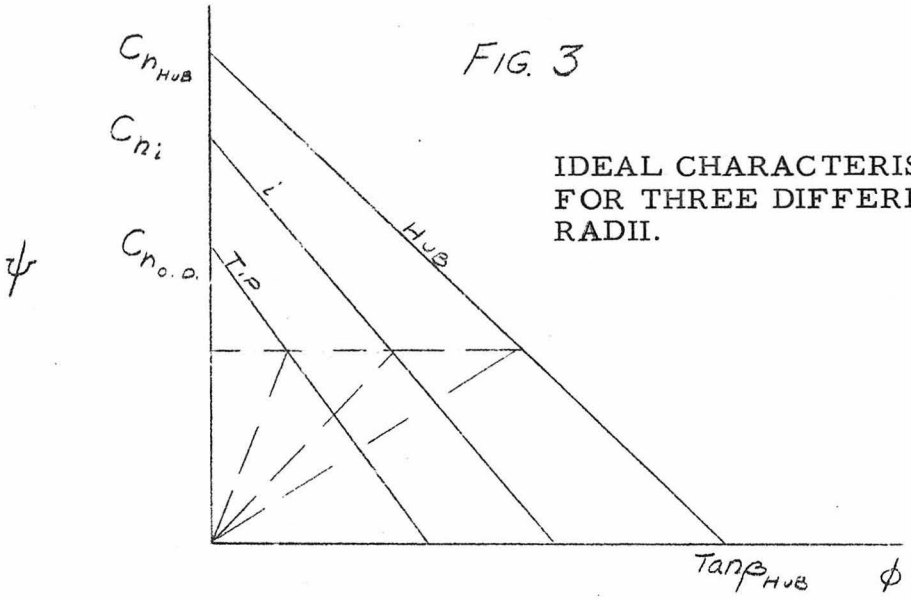

IDEAL CHARACTERISTICS FOR THREE DIFFERENT RADII.

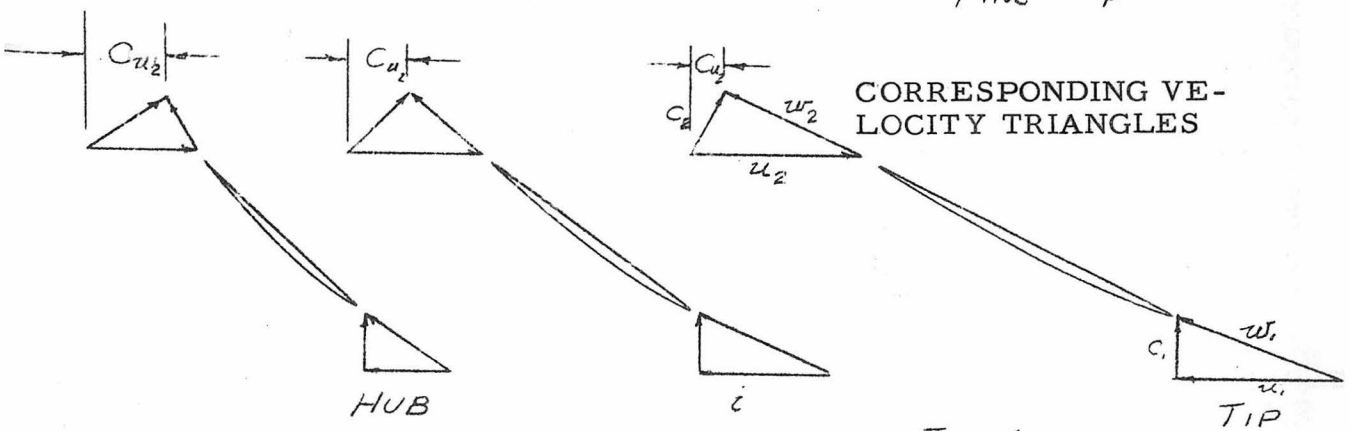

CORRESPONDING VELOCITY TRIANGLES

FIG. 4

FLOW DIRECTIONS FOR REVERSE PUMP CONDITION

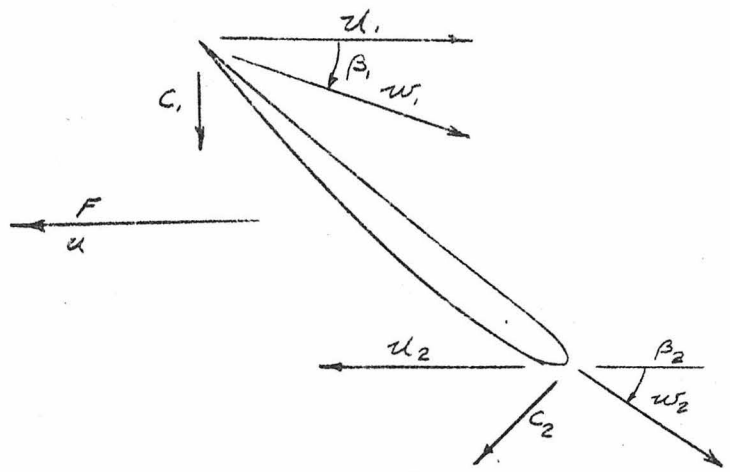

FIG. 5

HEAD - CAPACITY CHARACTERISTICS
FOR POSITIVE AND NEGATIVE ROTATION

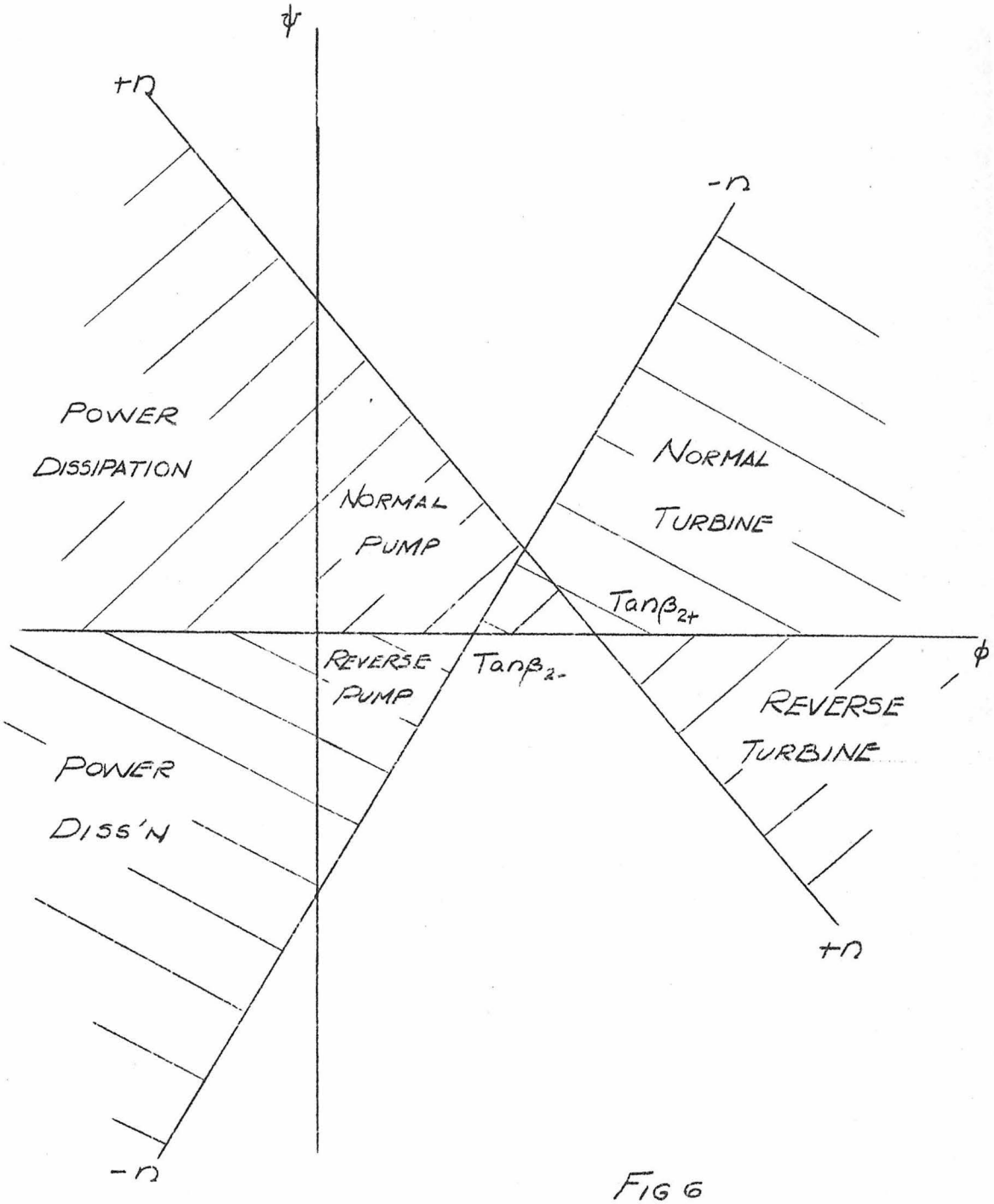

FIG 6

HEAD - SPEED CHARACTERISTICS
FOR POSITIVE AND NEGATIVE FLOW

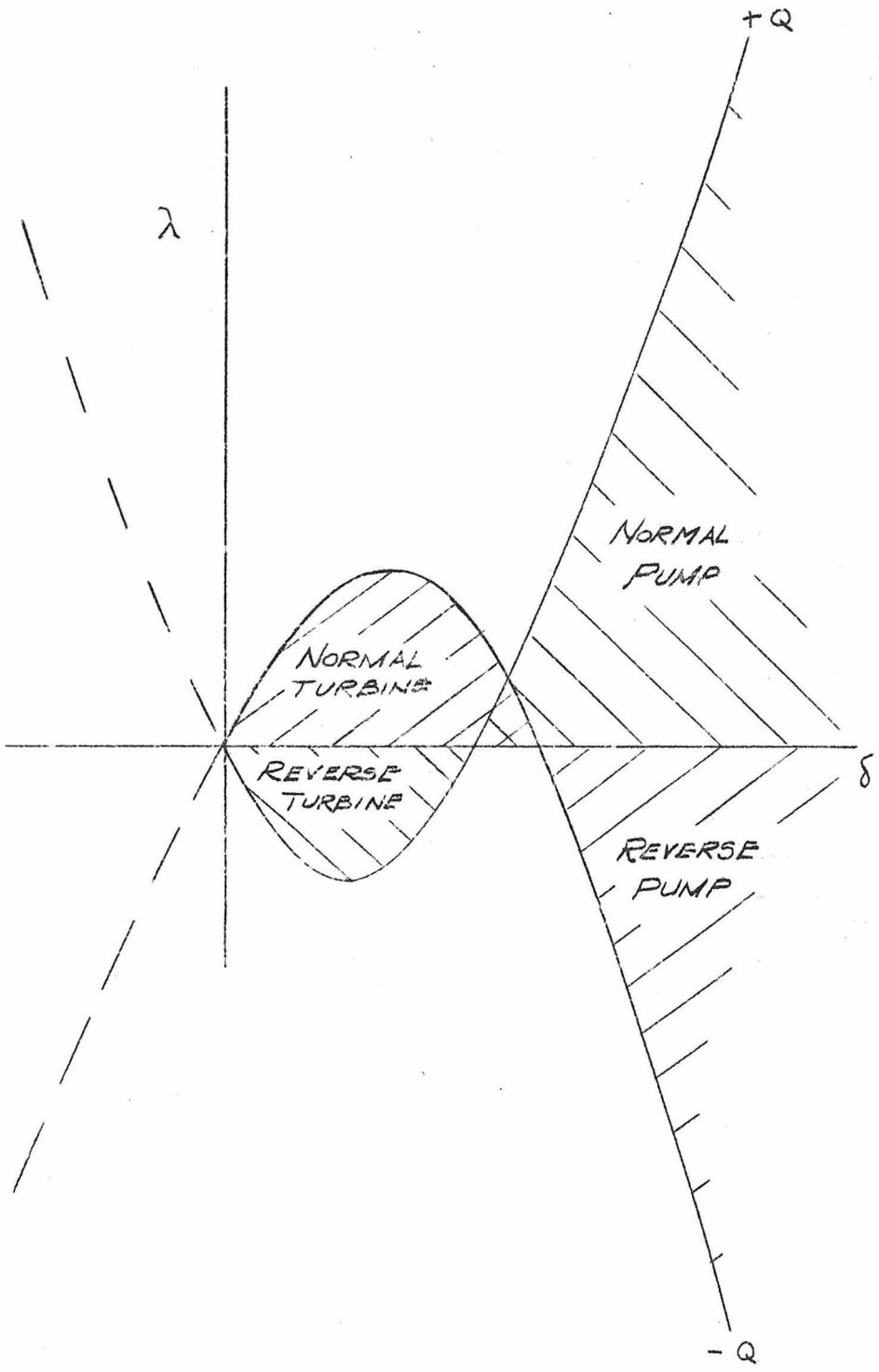

FIG. 7

TORQUE - CAPACITY CHARACTERISTICS
FOR POSITIVE AND NEGATIVE ROTATION

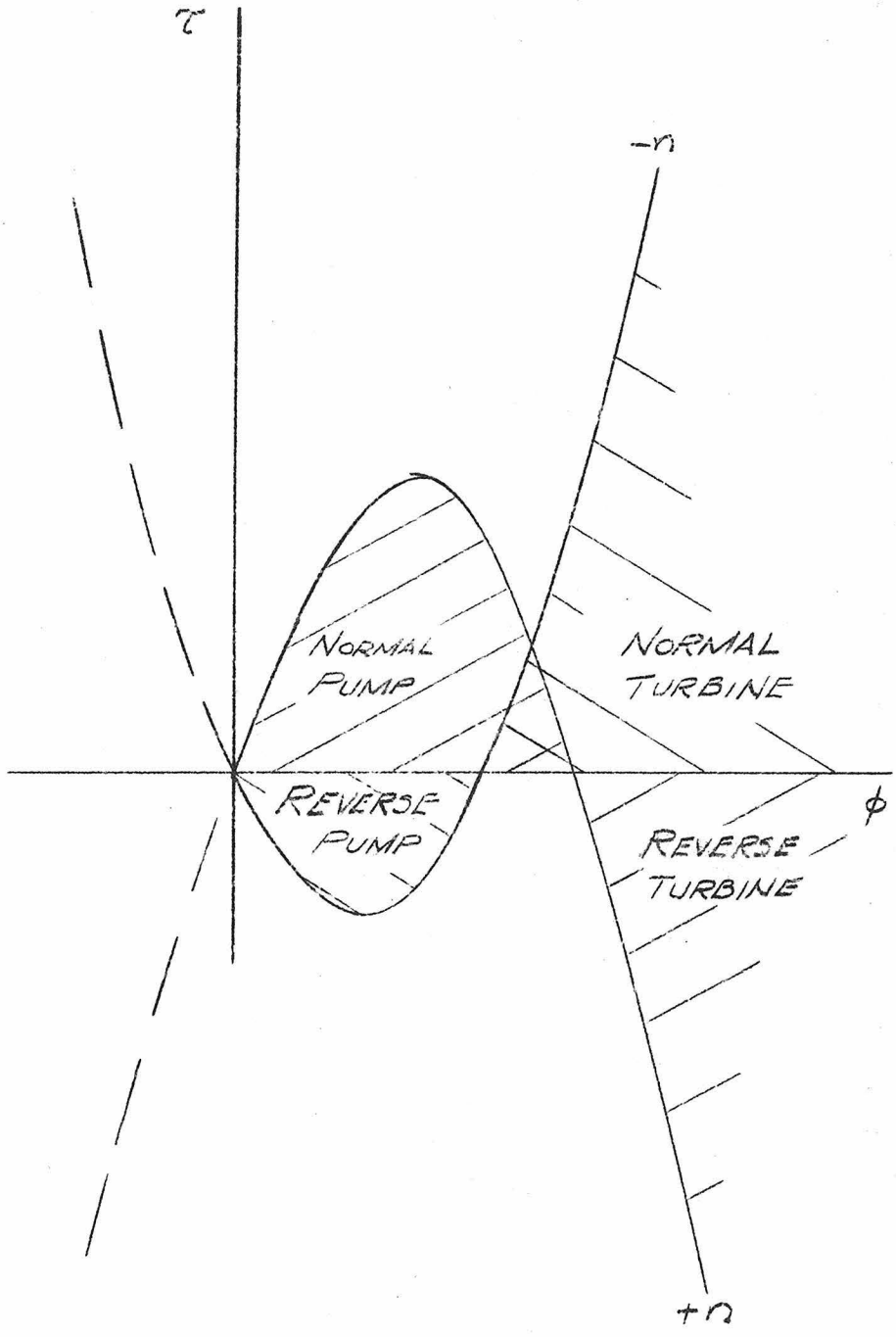

FIG. 8

TORQUE - SPEED CHARACTERISTICS
FOR POSITIVE AND NEGATIVE FLOW

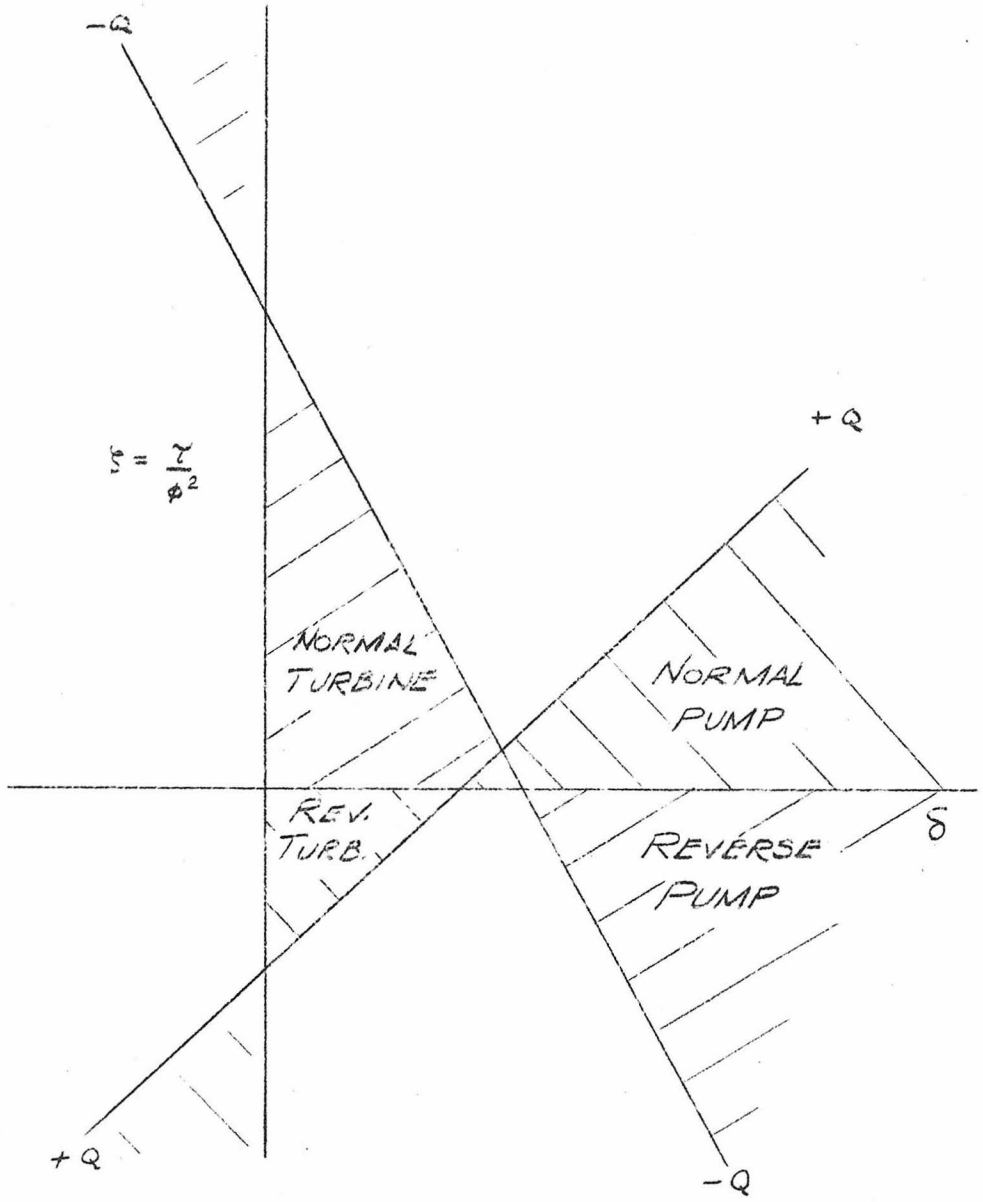

FIG. 9

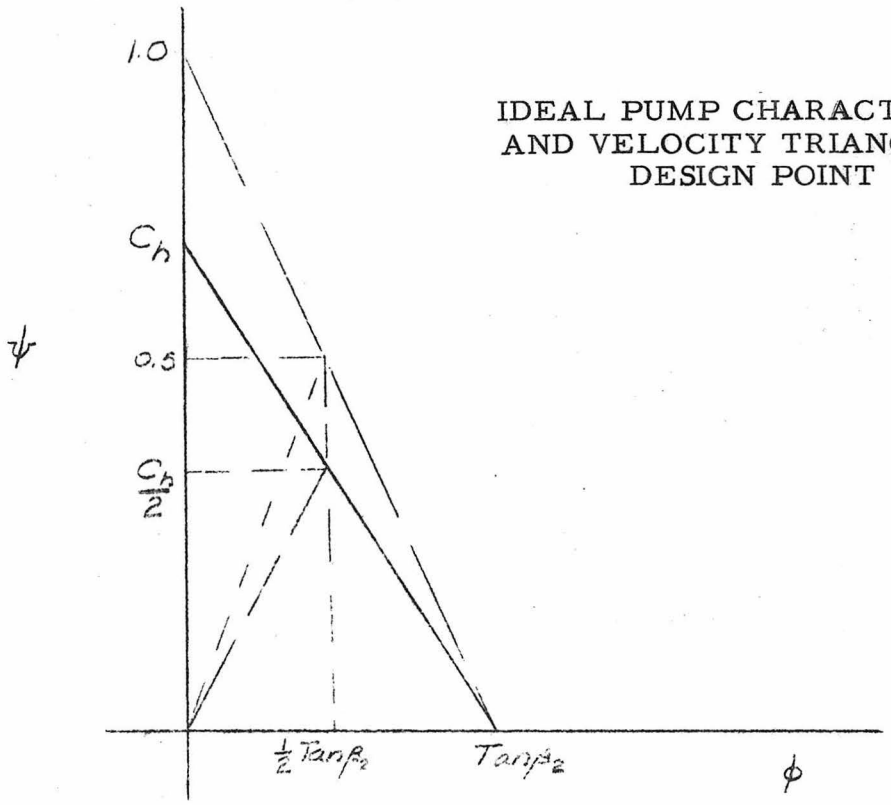

IDEAL PUMP CHARACTERISTIC AND VELOCITY TRIANGLES AT DESIGN POINT

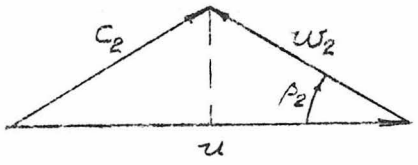

EULER VANE ANGLE DIAGRAM

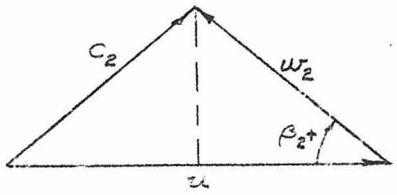

FLOW DIAGRAM

FIG. 10

PERCENTAGE HEAD - CAPACITY CHARACTERISTIC
FOR POSITIVE ROTATION

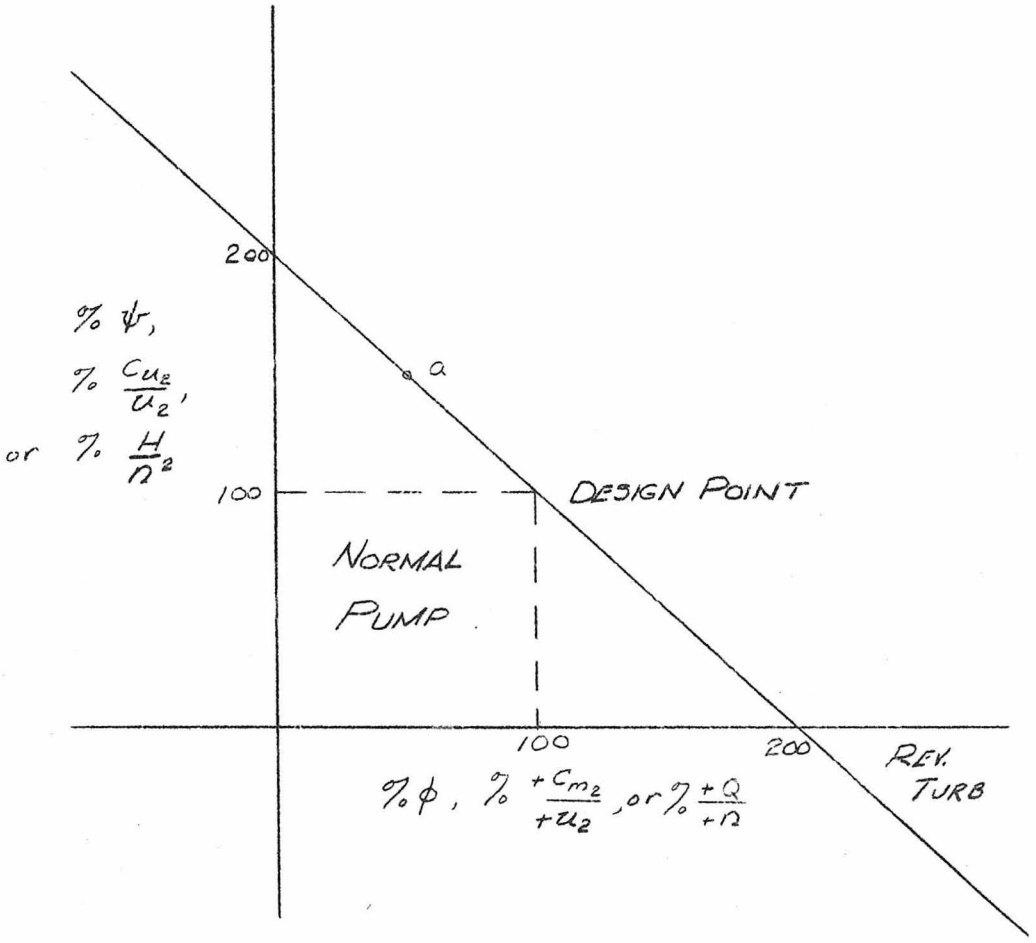

FIG 11

PERCENTAGE HEAD - CAPACITY CHARACTERISTIC FOR NEGATIVE ROTATION

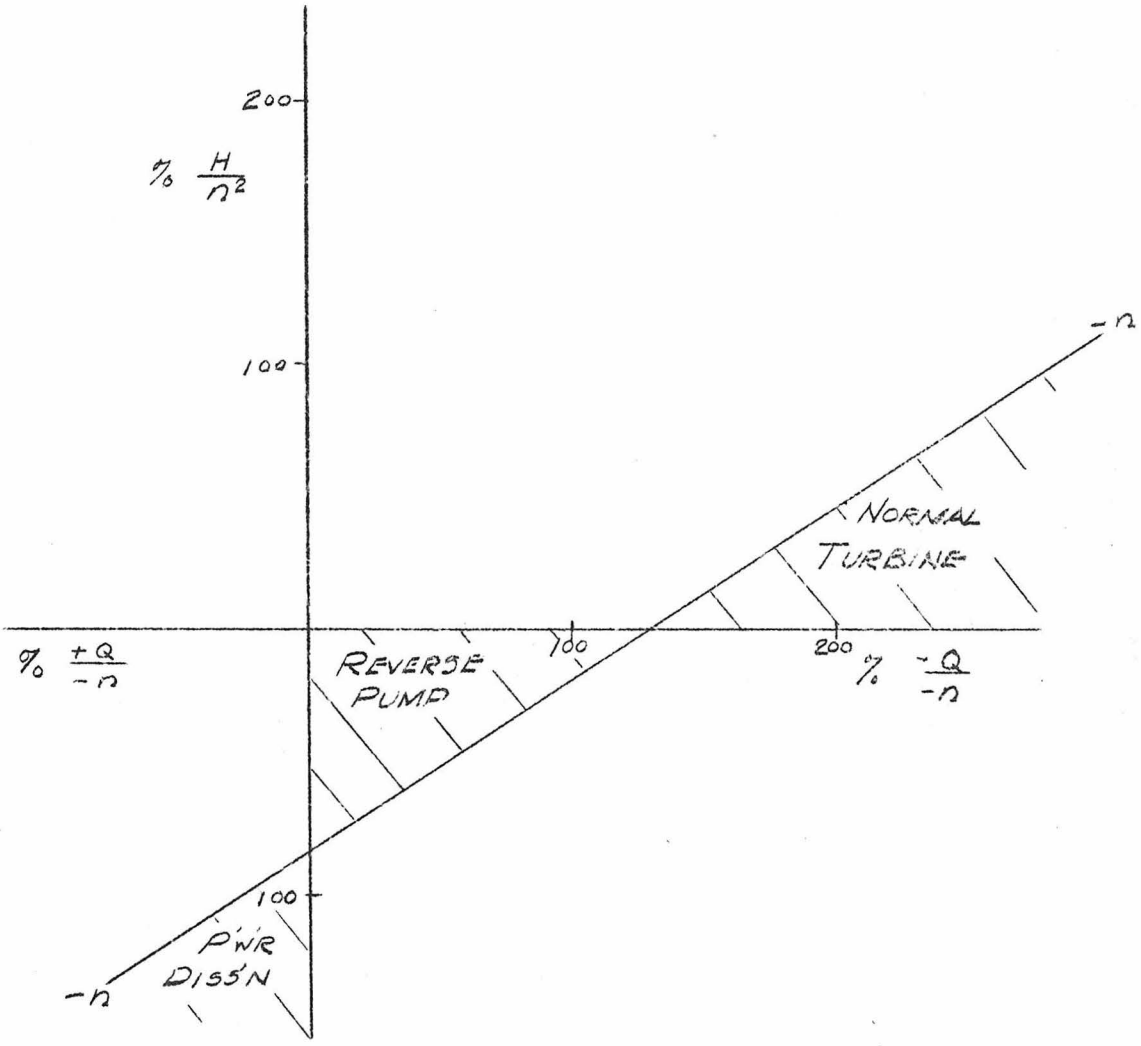

FIG. 12

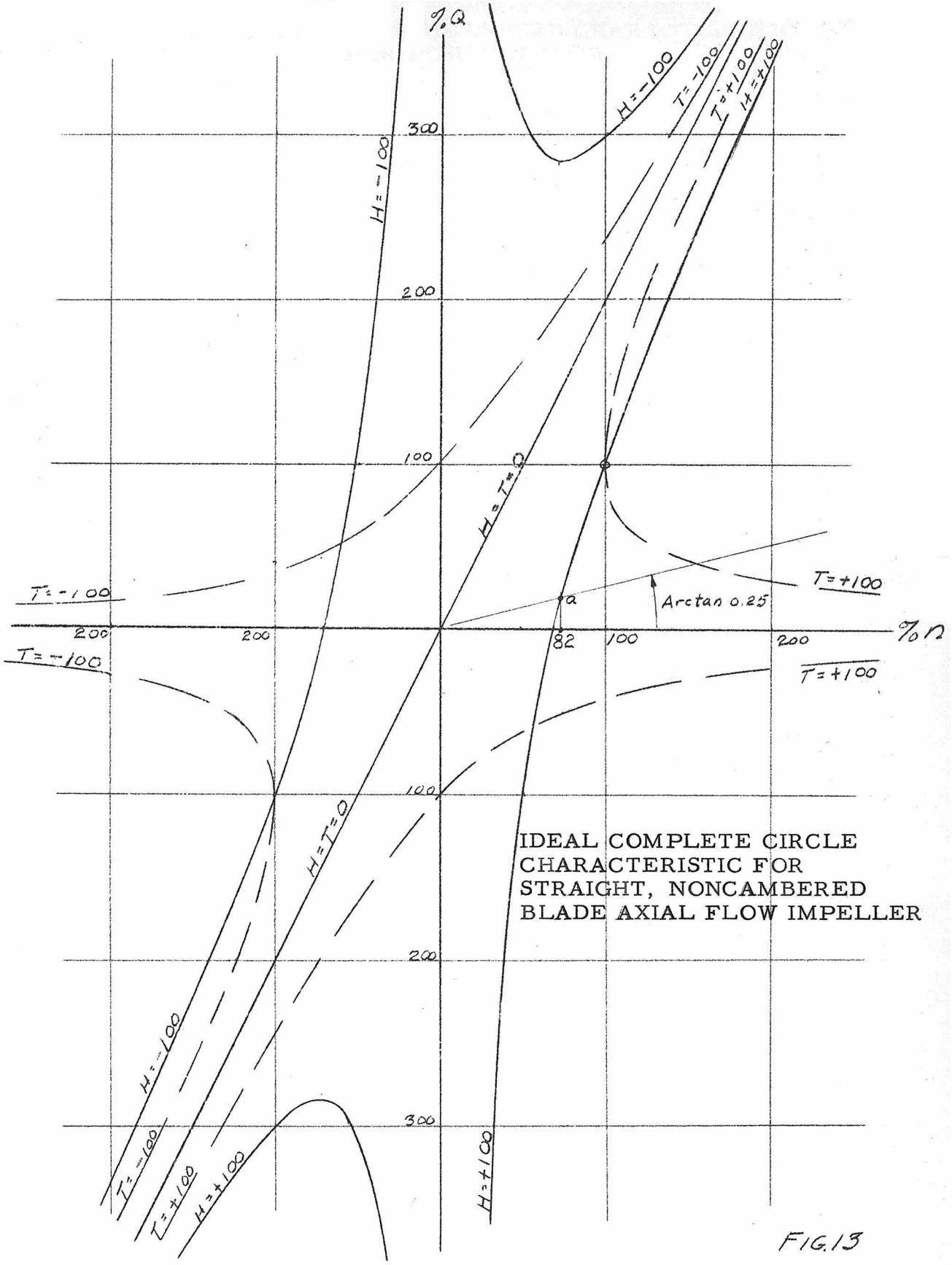

IDEAL COMPLETE CIRCLE CHARACTERISTIC FOR STRAIGHT, NONCAMBERED BLADE AXIAL FLOW IMPELLER

FIG. 13

PERCENTAGE TORQUE - SPEED CHARACTERISTIC
FOR POSITIVE FLOW

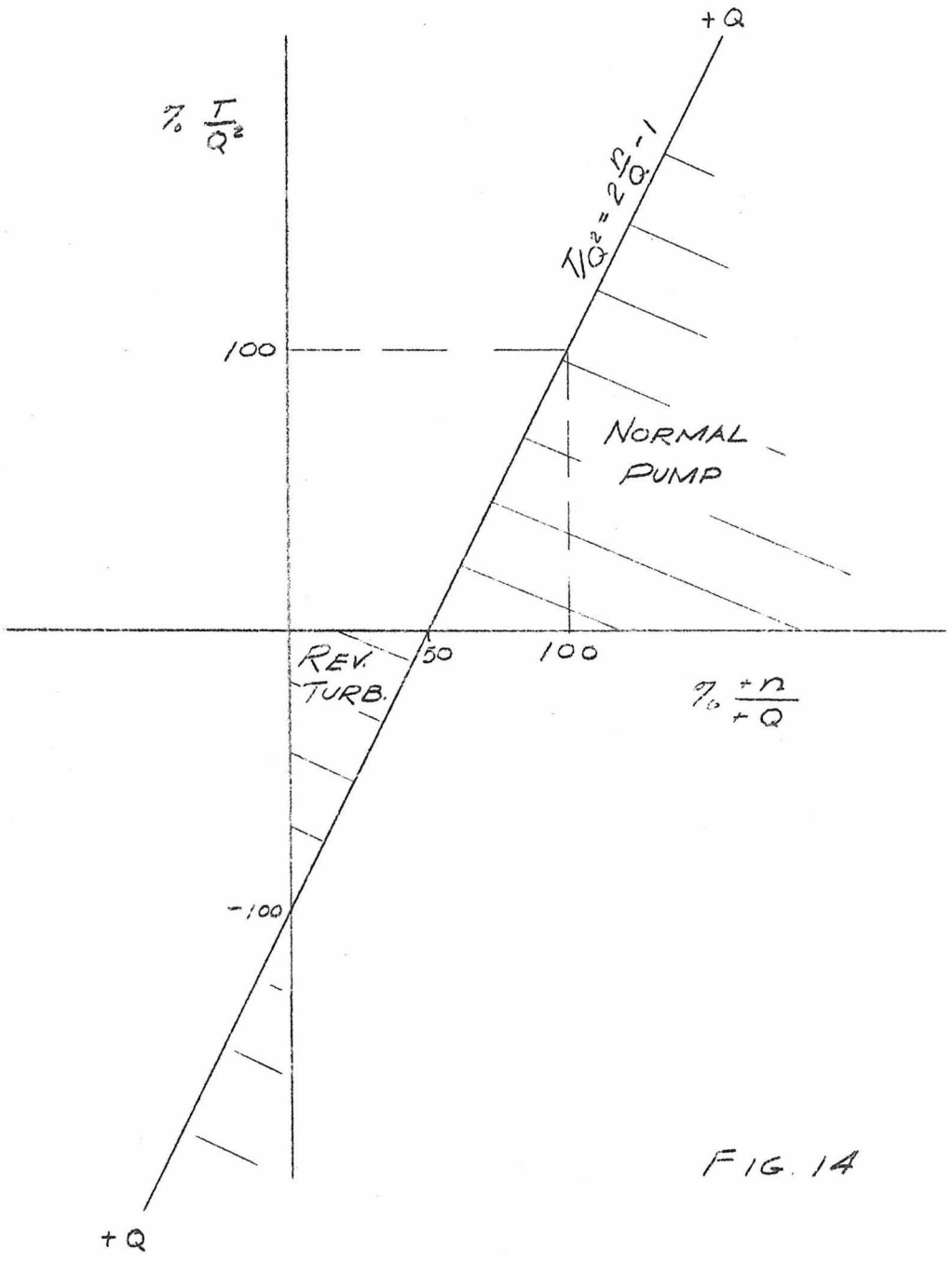

FIG. 14

IDEAL HEAD AND TORQUE - CAPACITY CHARACTERISTICS
FOR POSITIVE FLOW

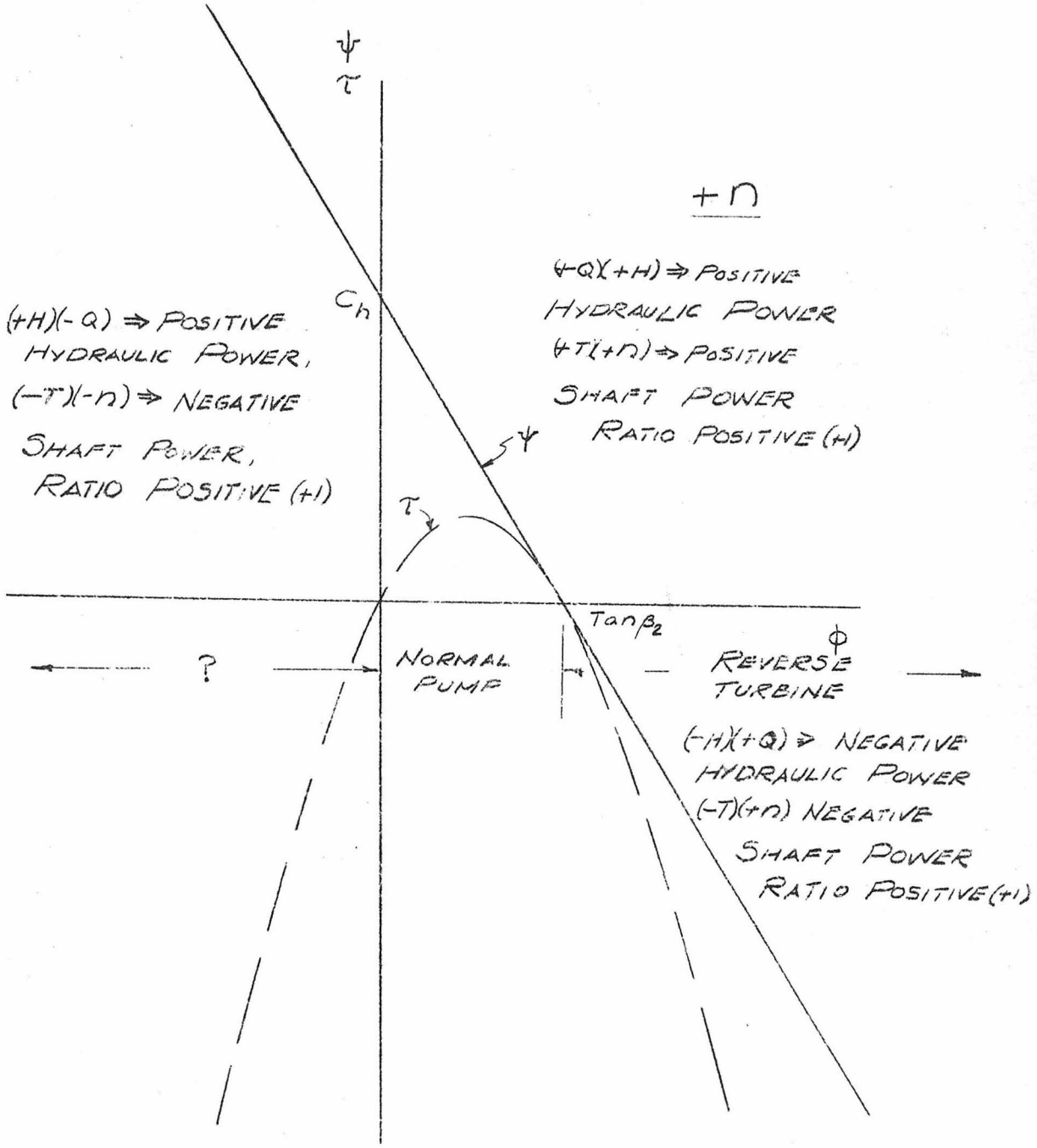

FIG. 15

IDEAL HEAD AND TORQUE - CAPACITY
CHARACTERISTICS FOR NEGATIVE FLOW

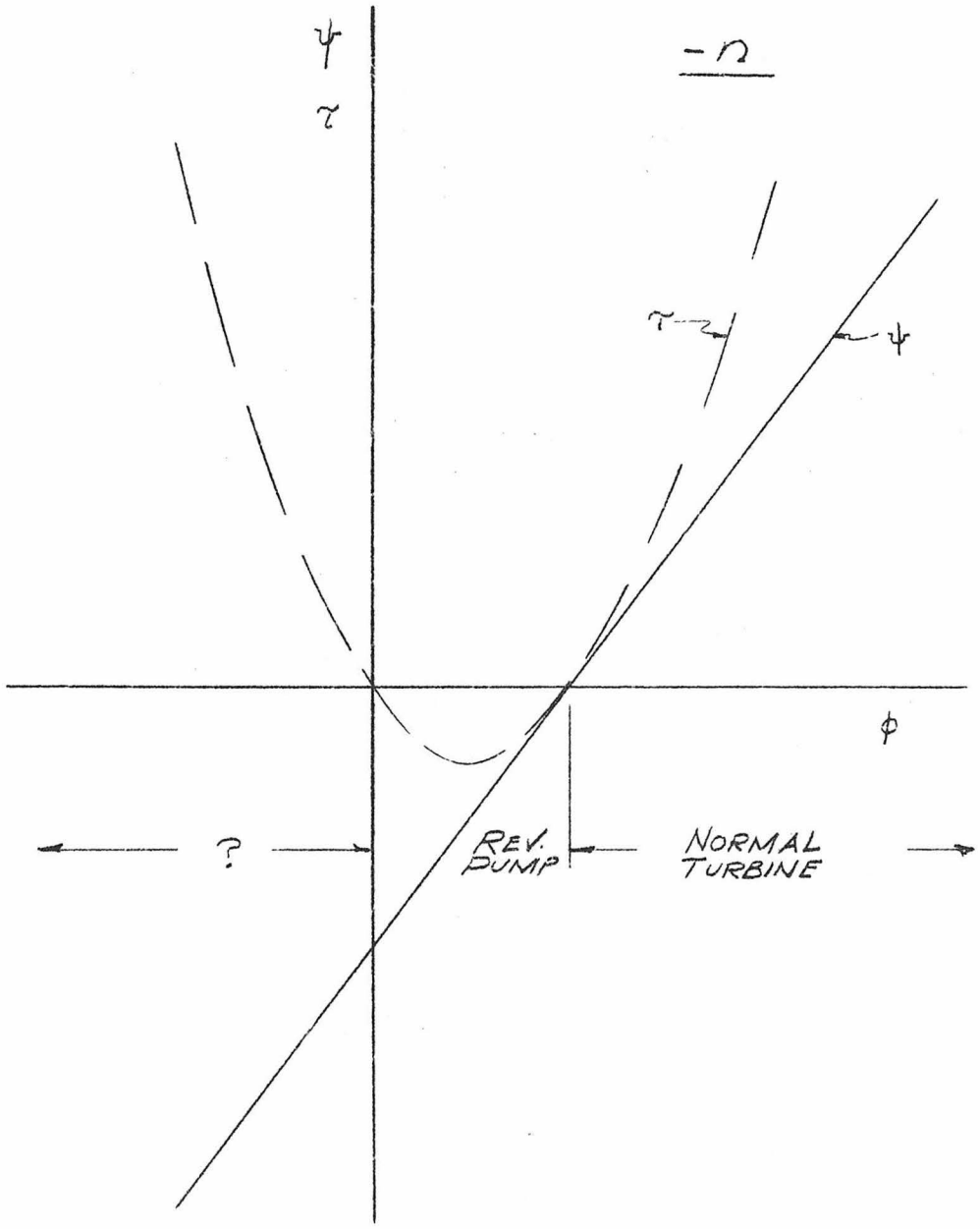

FIG. 16

IDEALIZED FLOW REPRESENTATION FOR
OPPOSED FLOW AND ROTATIONAL DIRECTIONS

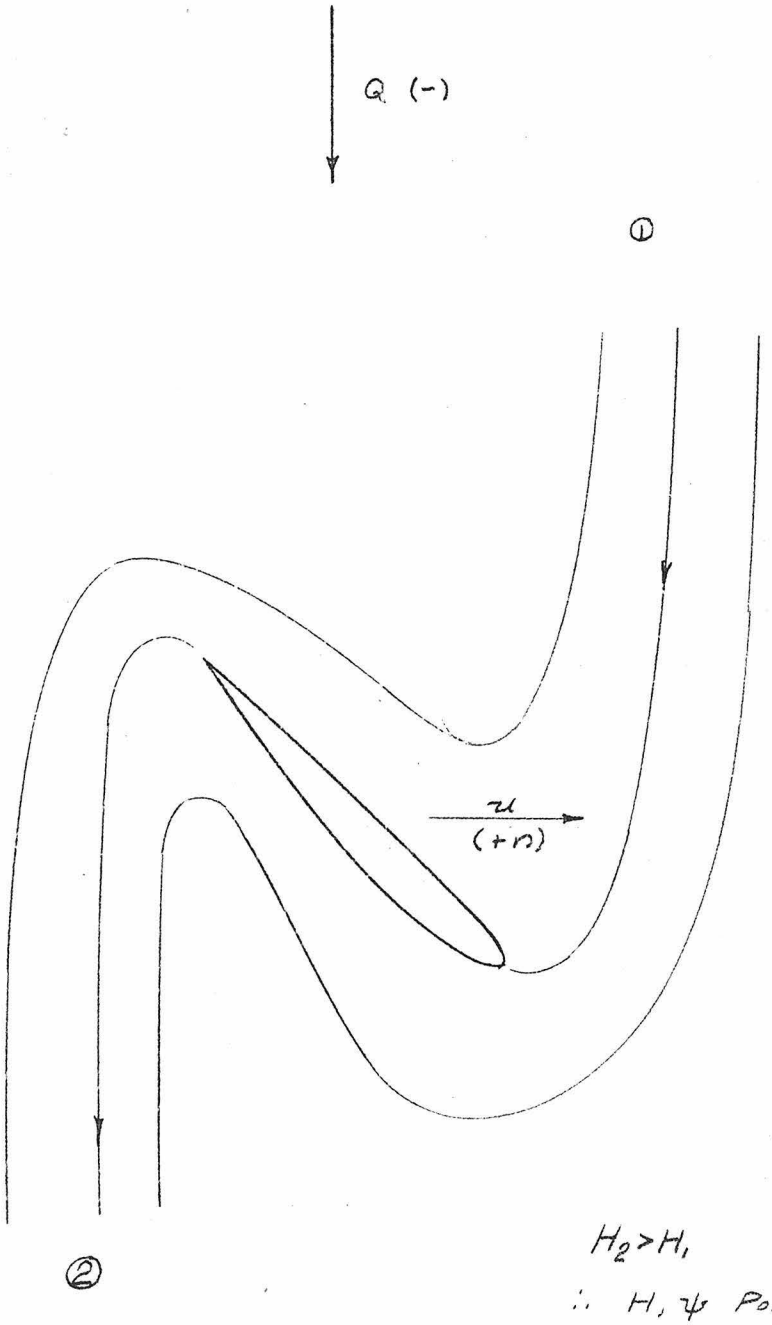

FIG. 17

IDEAL AND ACTUAL
POWER CURVE COMPARISON

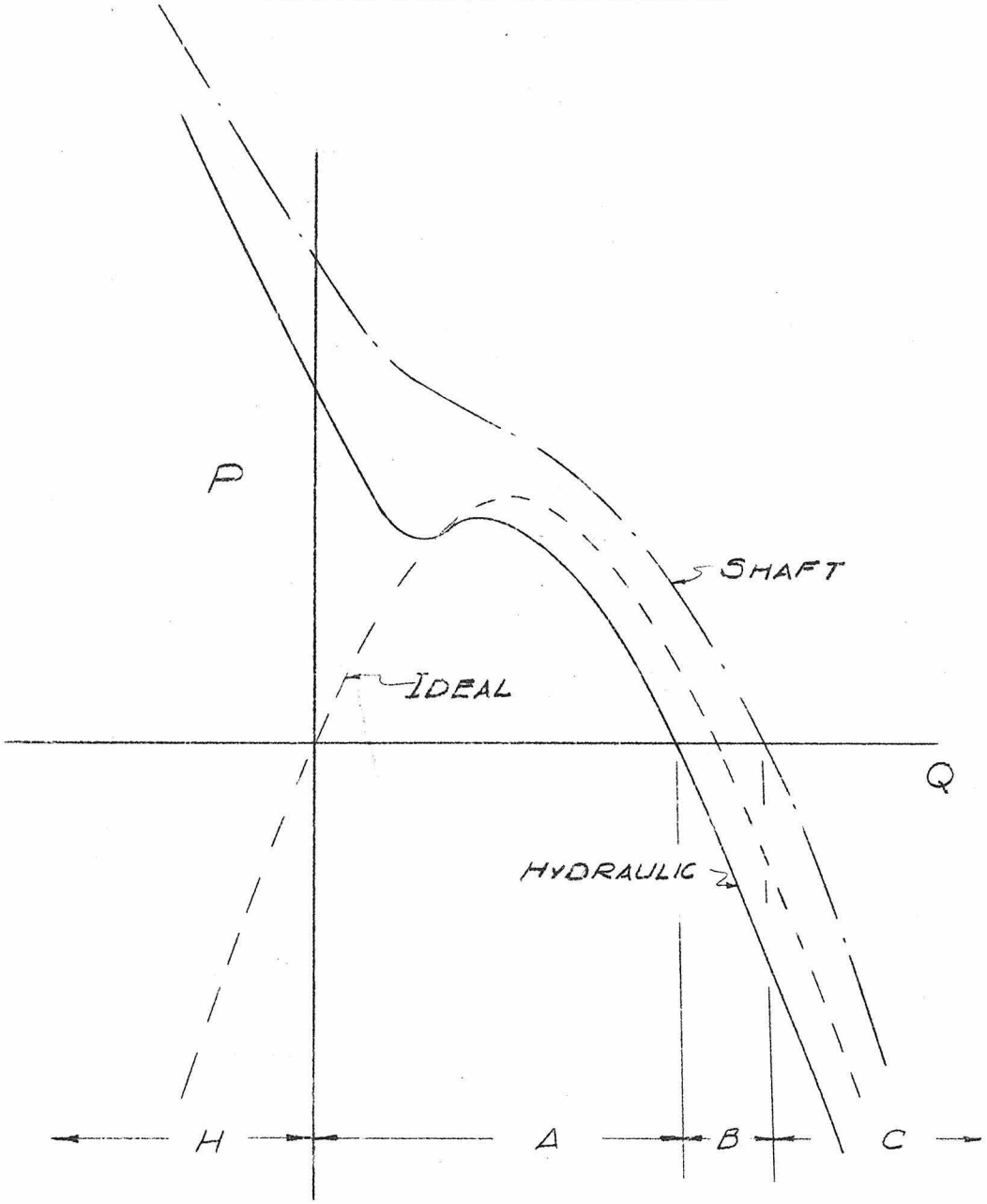

FIG. 18

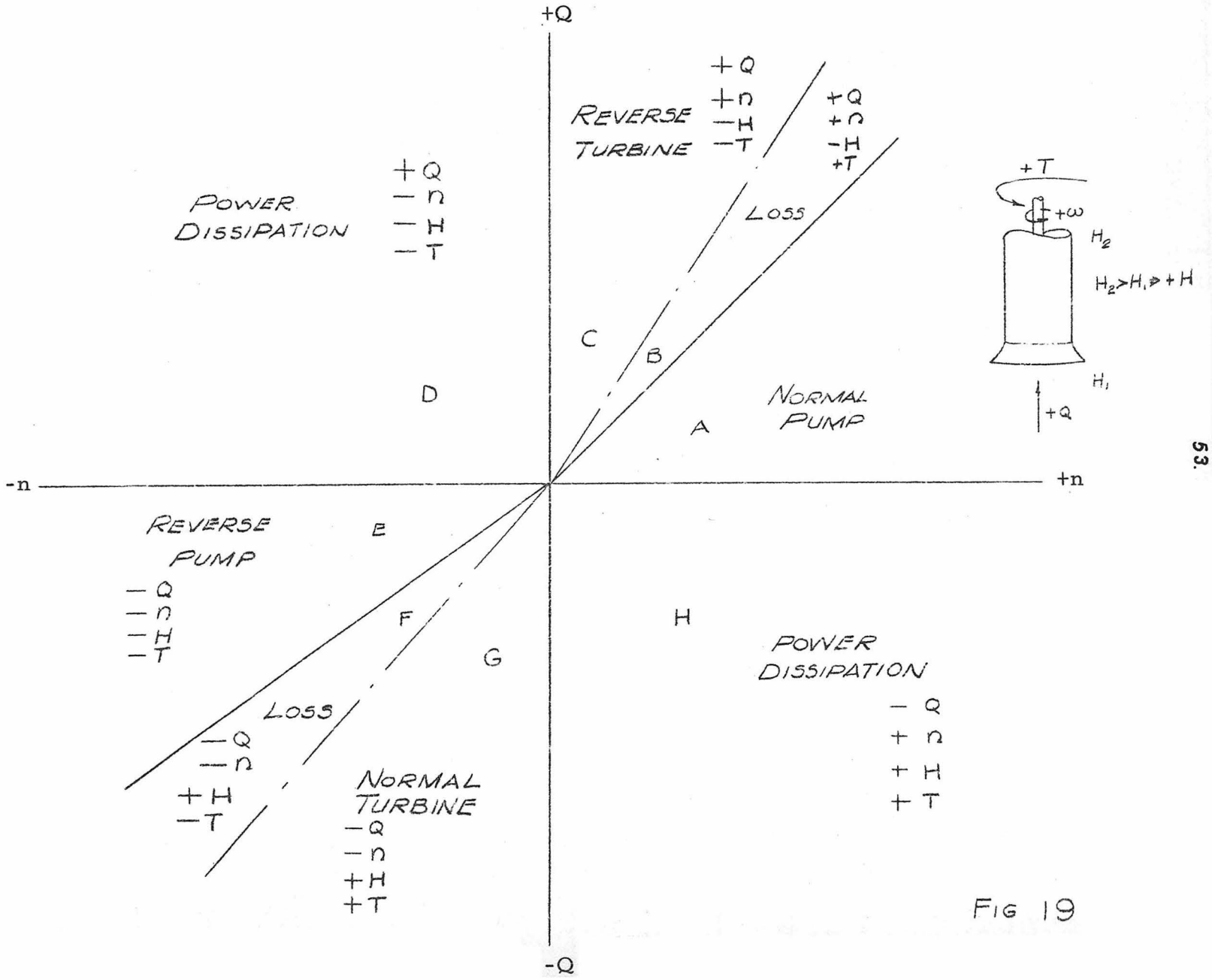
+Q
-Q
+n
-n
+Q
+n
−H
−T
REVERSE TURBINE
+Q
+n
-H
+T
LOSS
+T
+ω
H2
H2>H1⇒+H
H1
+Q
POWER DISSIPATION
+Q
−n
−H
−T
C
B
D
A
NORMAL PUMP
REVERSE PUMP
E
−Q
−n
−H
−T
F
G
H
POWER DISSIPATION
−Q
+n
+H
+T
LOSS
−Q
−n
+H
−T
NORMAL TURBINE
−Q
−n
+H
+T

FIG 19

HEAD-AND TORQUE - CAPACITY CHARACTERISTICS
FOR POSITIVE ROTATION

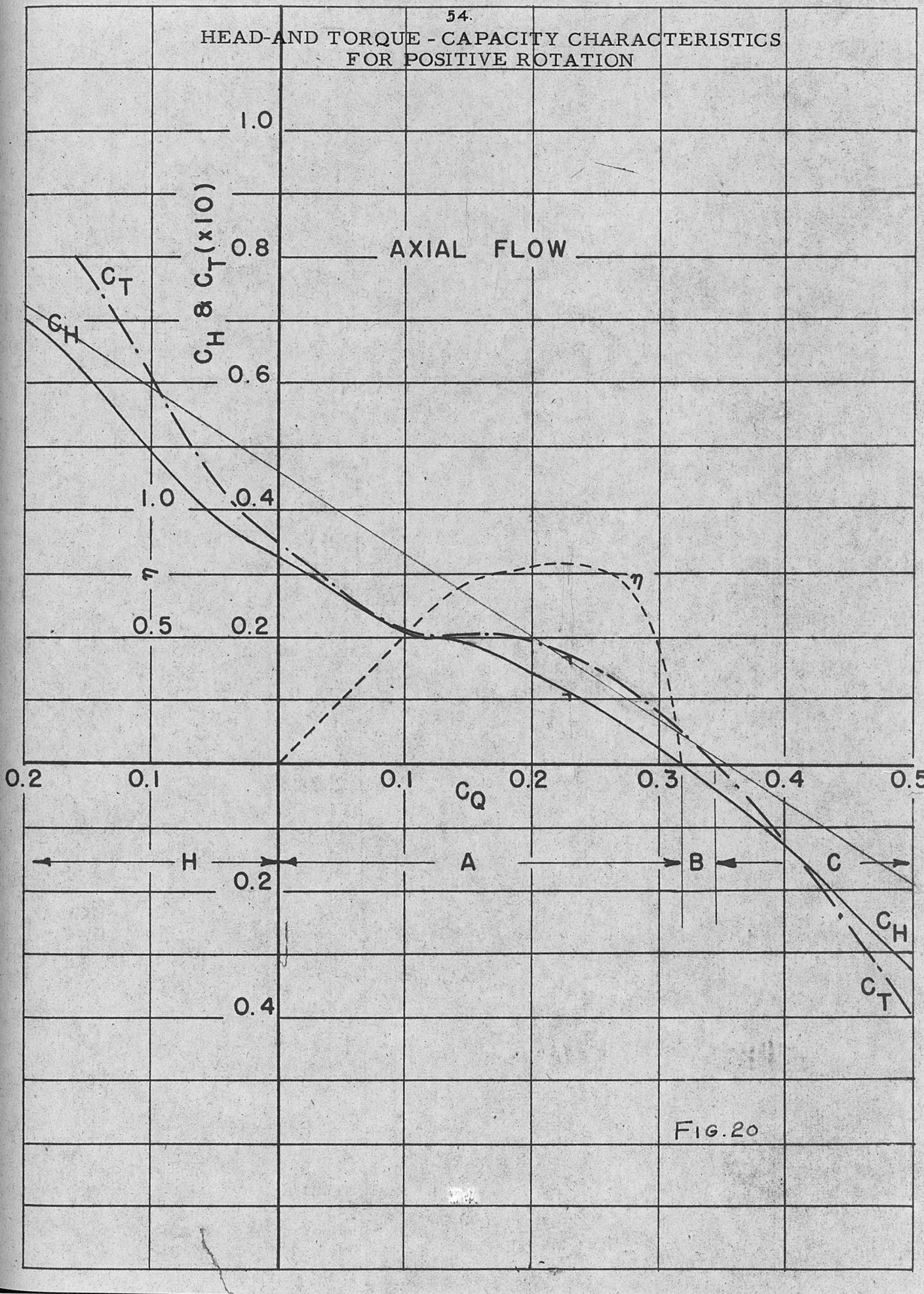

FIG. 20

PERCENTAGE HEAD-AND TORQUE - CAPACITY CHARACTERISTICS FOR POSITIVE ROTATION

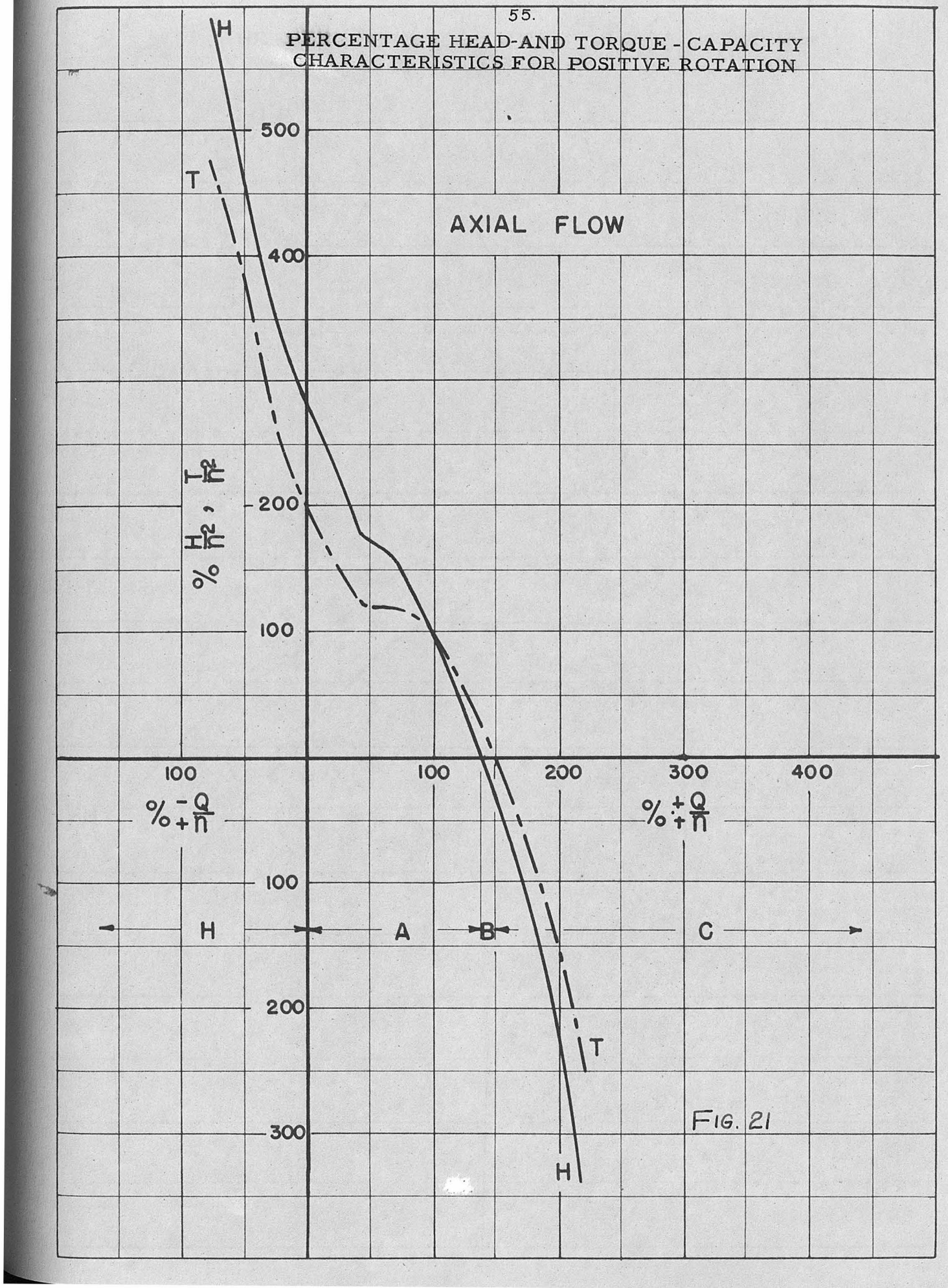

FIG. 21

HEAD AND TORQUE - CAPACITY CHARACTERISTICS
FOR NEGATIVE ROTATION

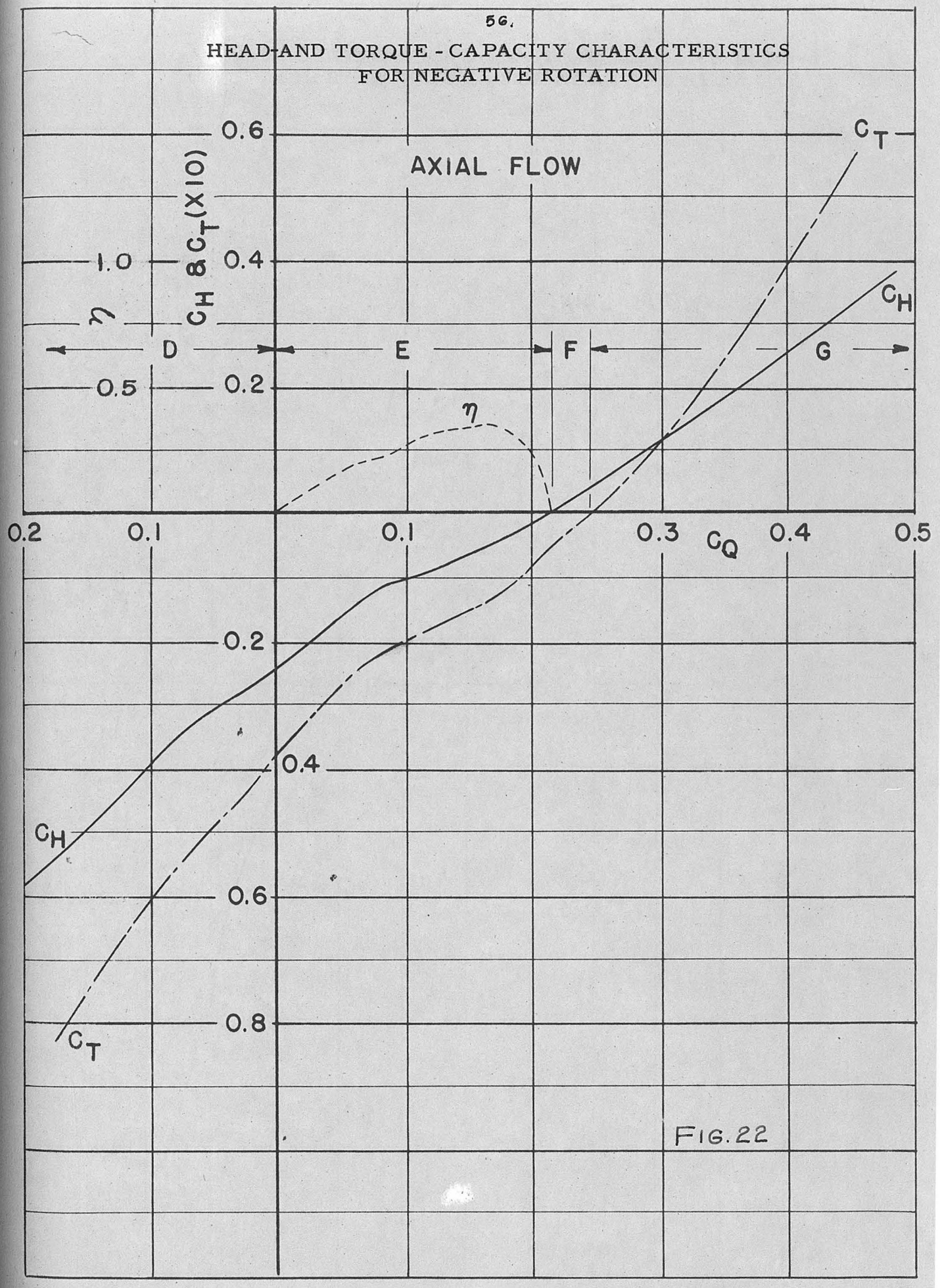

FIG. 22

PERCENTAGE HEAD-AND TORQUE - CAPACITY CHARACTERISTICS FOR NEGATIVE FLOW

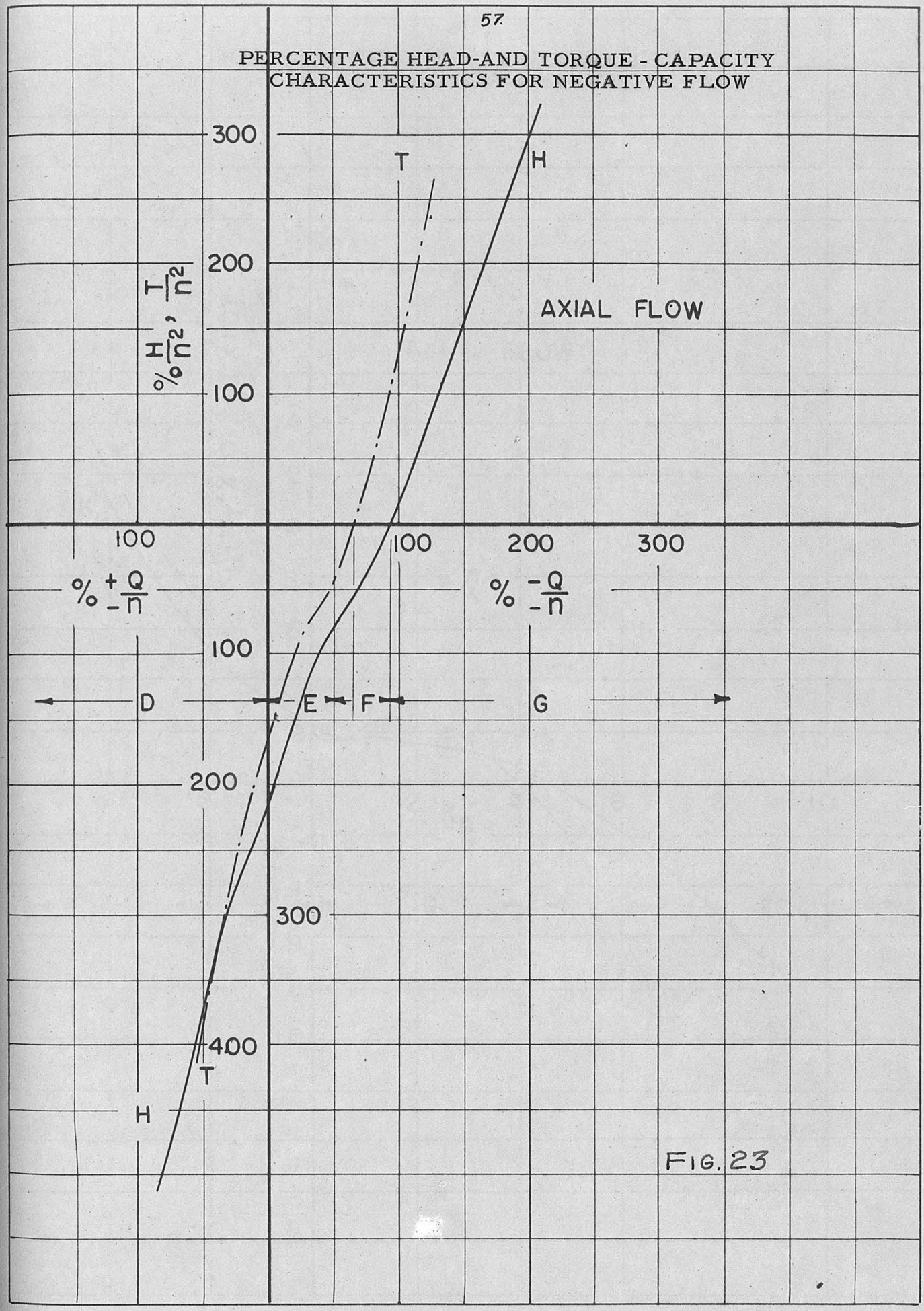

FIG. 23

HEAD-AND TORQUE - SPEED CHARACTERISTICS
FOR NEGATIVE ROTATION

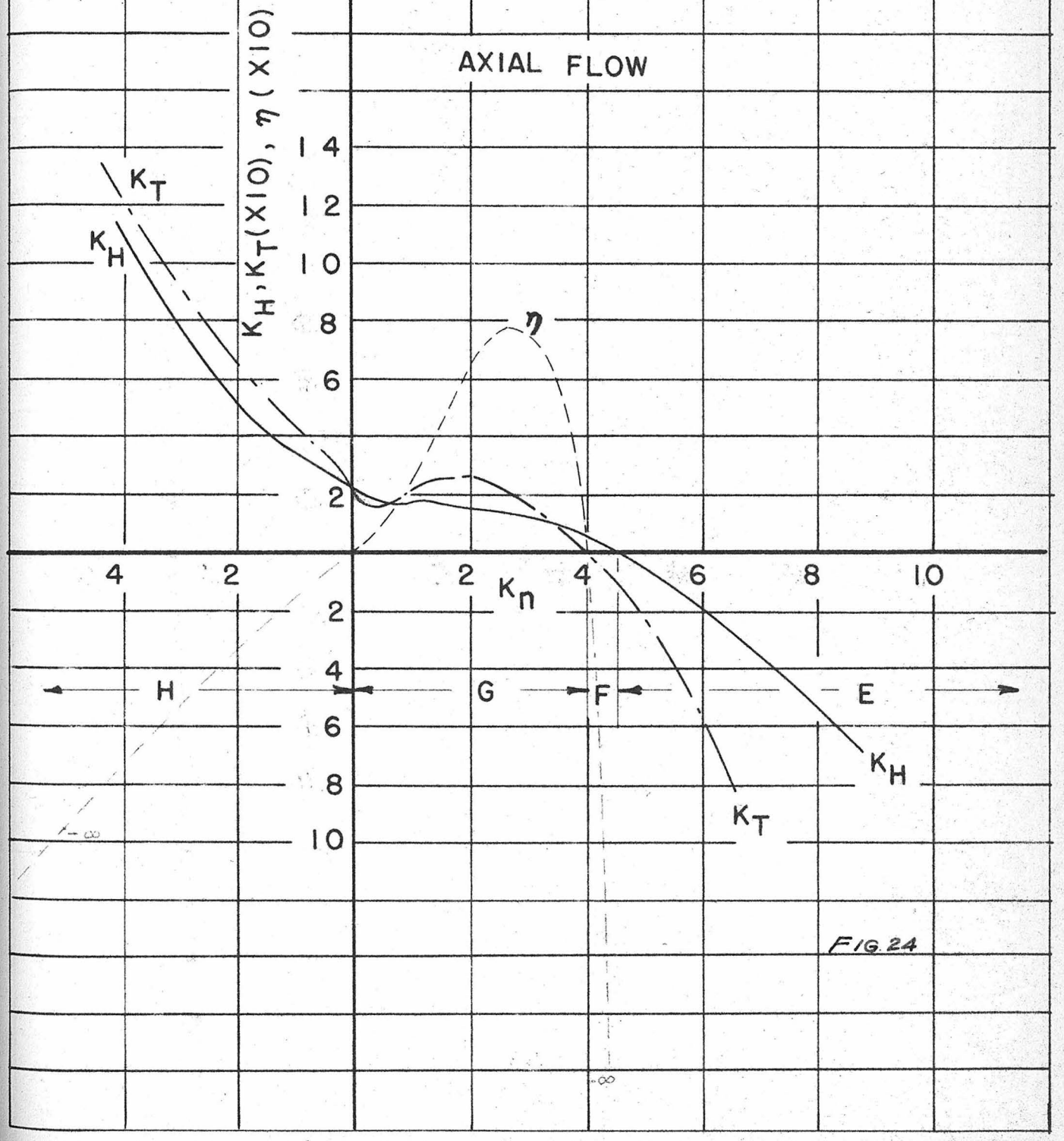

FIG. 24

PERCENTAGE HEAD-AND TORQUE-SPEED CHARACTERISTICS FOR NEGATIVE FLOW

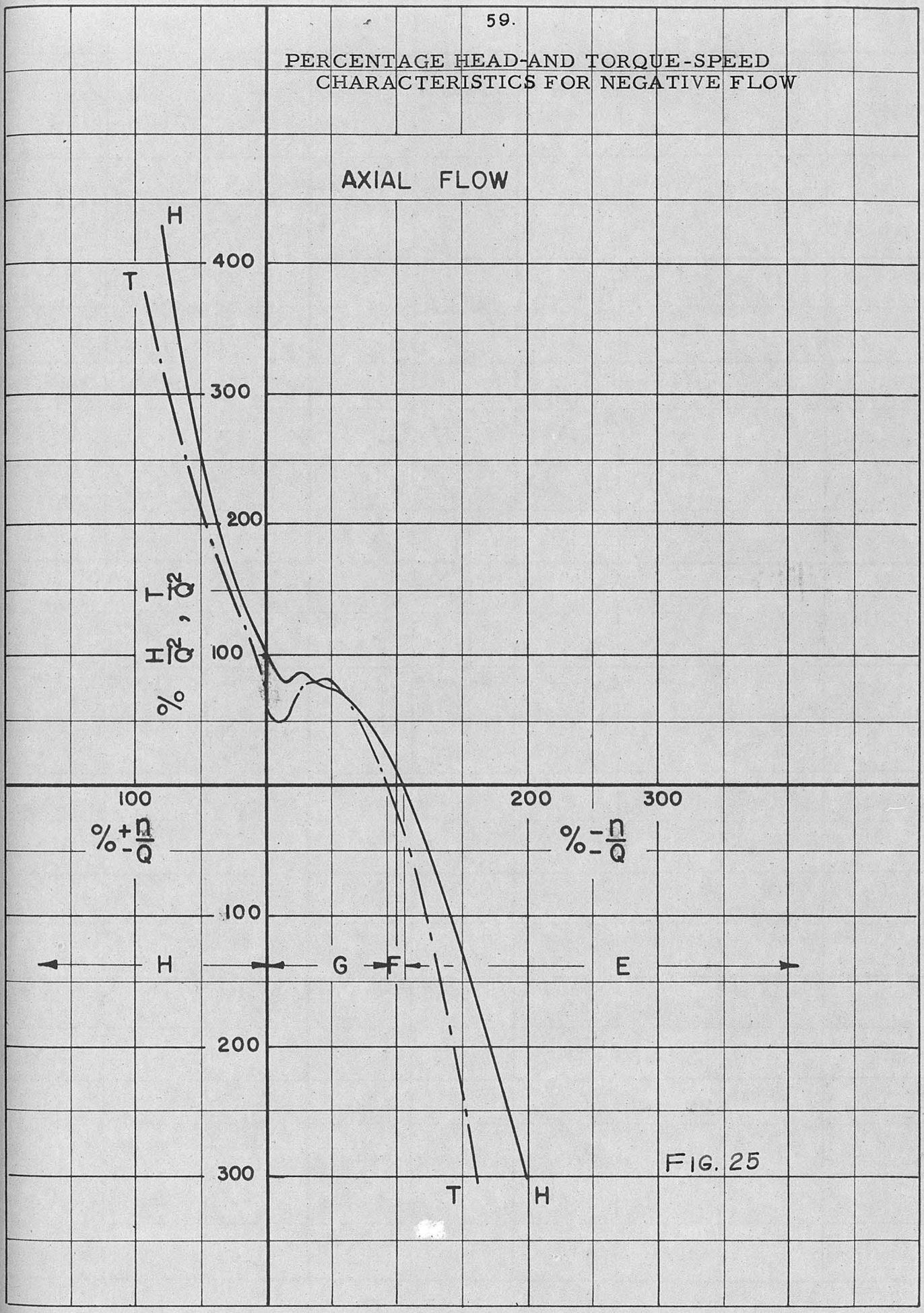

FIG. 25

HEAD-AND TORQUE - SPEED CHARACTERISTICS
FOR POSITIVE FLOW

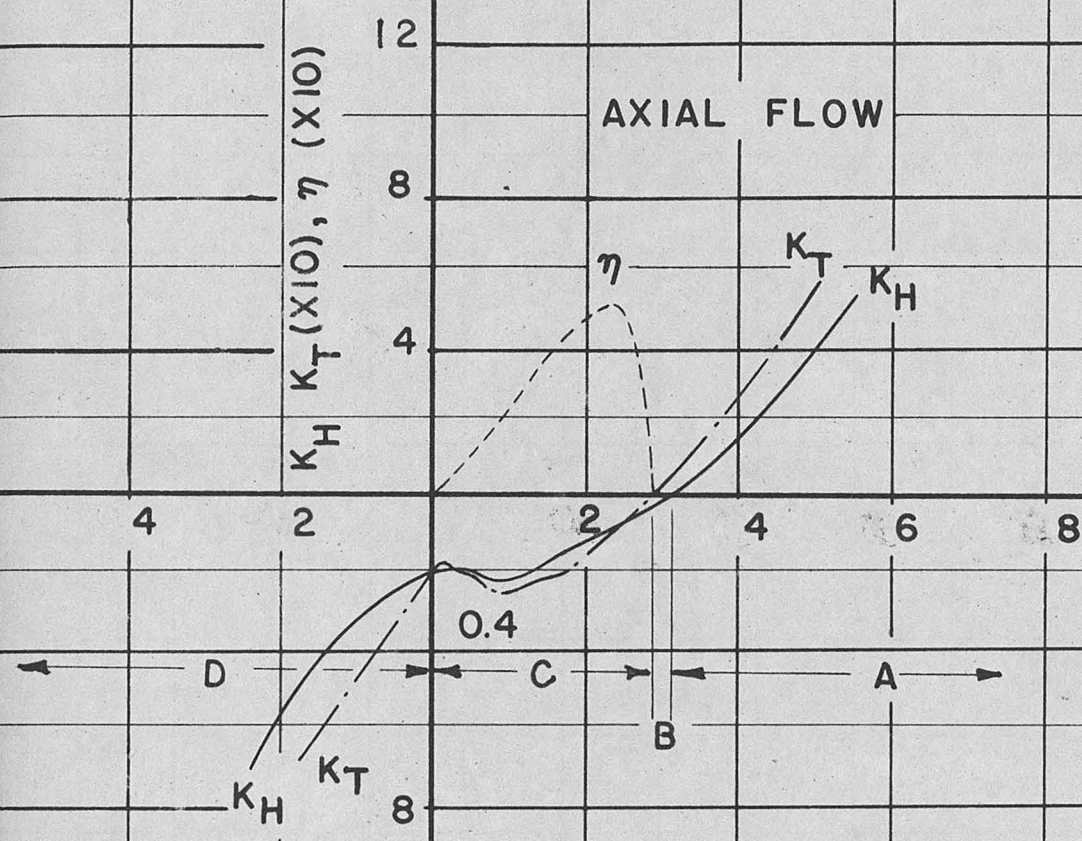

FIG. 26

PERCENTAGE HEAD-AND TORQUE - SPEED CHARACTERISTICS FOR POSITIVE FLOW

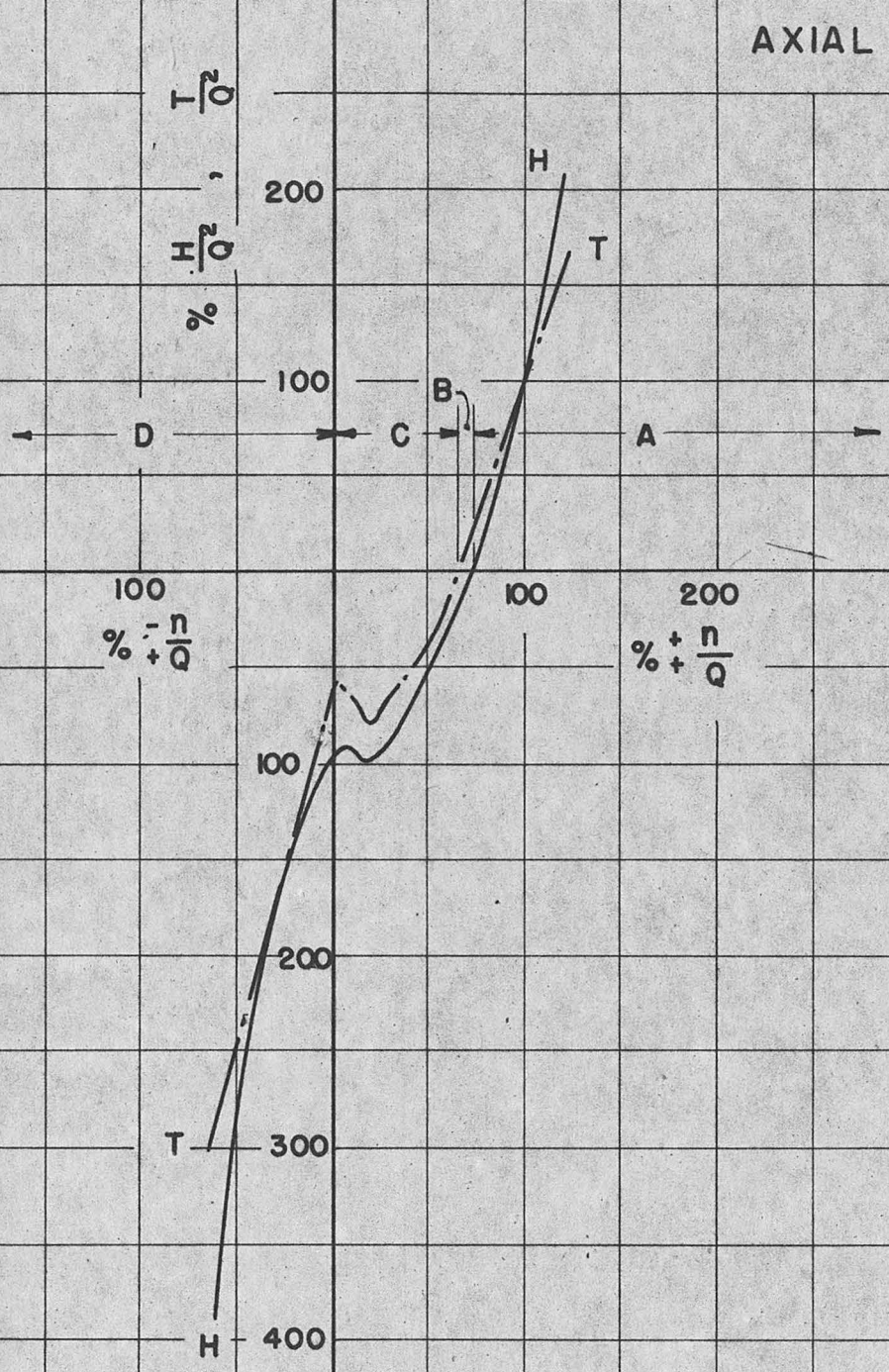

FIG. 27

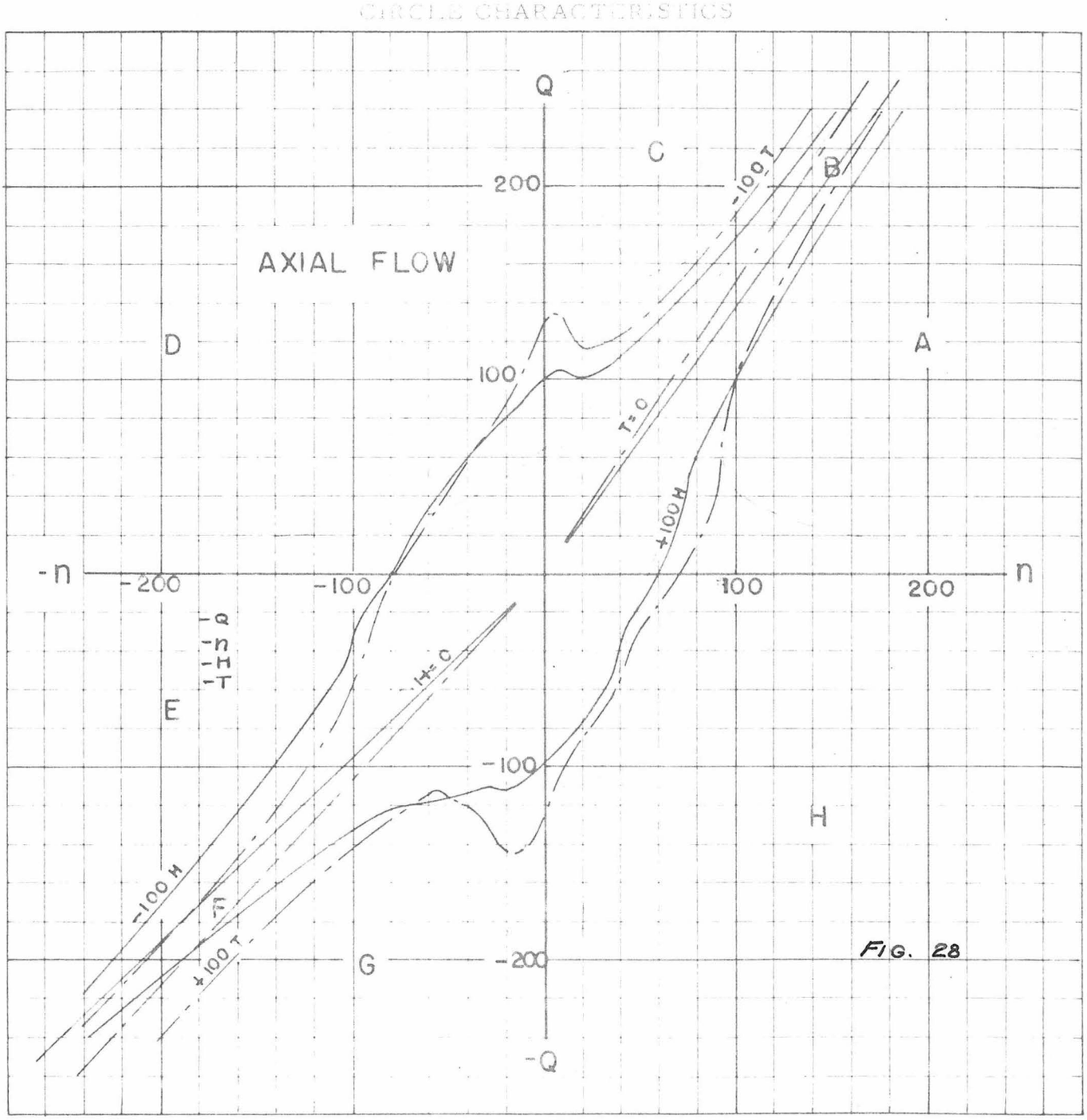
CIRCLE CHARACTERISTICS
Q
C
B
A
D
E
F
G
H
200
100
-100
-200
-Q
-n
n
-200
-100
100
200
AXIAL FLOW
-100 T
T=0
+100 H
H=0
-100 H
+100 T
-Q
-n
-H
-T

FIG. 28

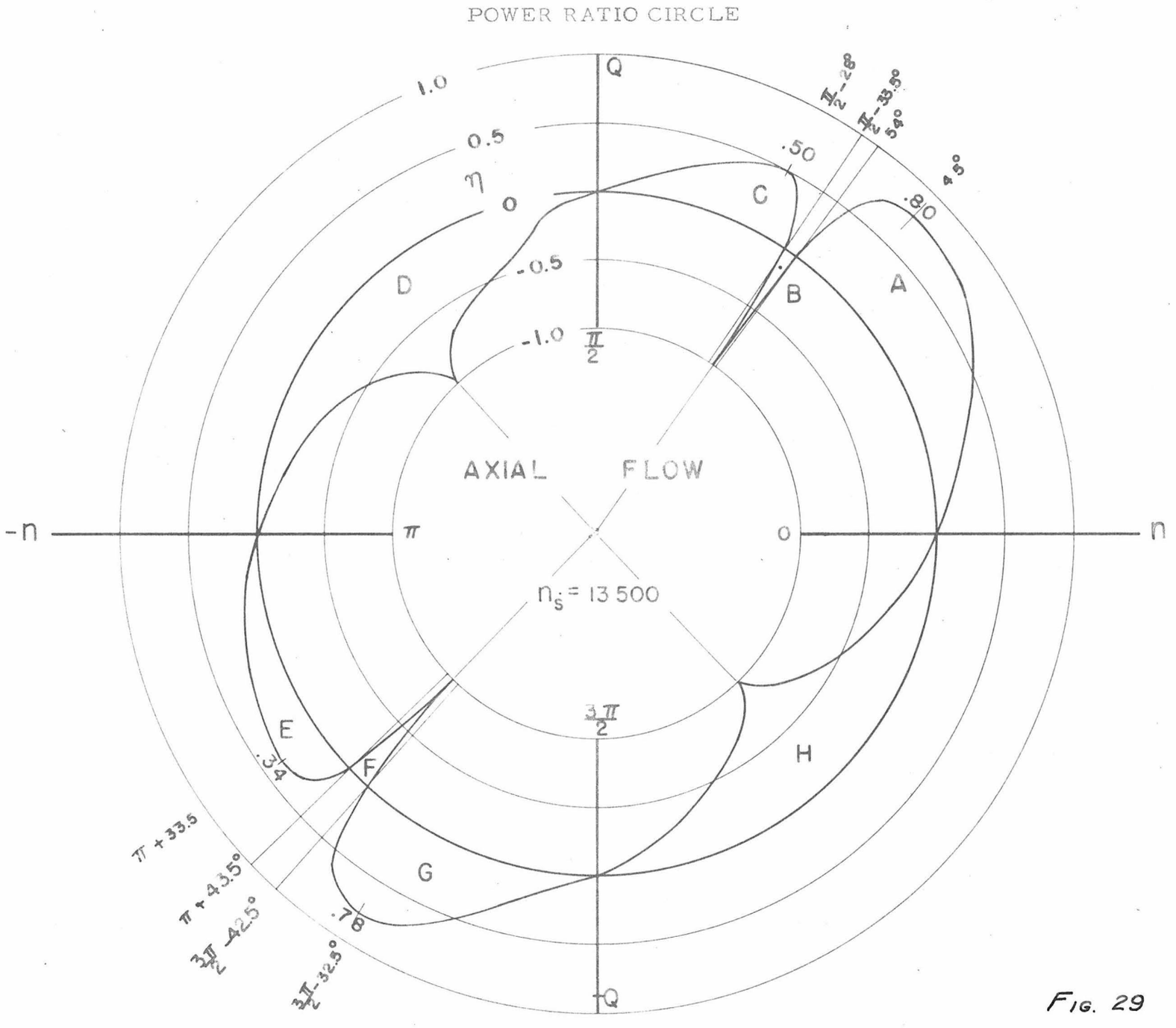
POWER RATIO CIRCLE
1.0
0.5
η
0
-0.5
-1.0
Q
-Q
-n
n
π
0
π/2
3π/2
AXIAL FLOW
n_s = 13 500
A
B
C
D
E
F
G
H
.50
.80
.34
.78
π/2 - 28°
π/2 - 33.5°
54°
4.5°
π + 33.5°
π + 43.5°
3π/2 - 42.5°
3π/2 - 32.5°

FIG. 29

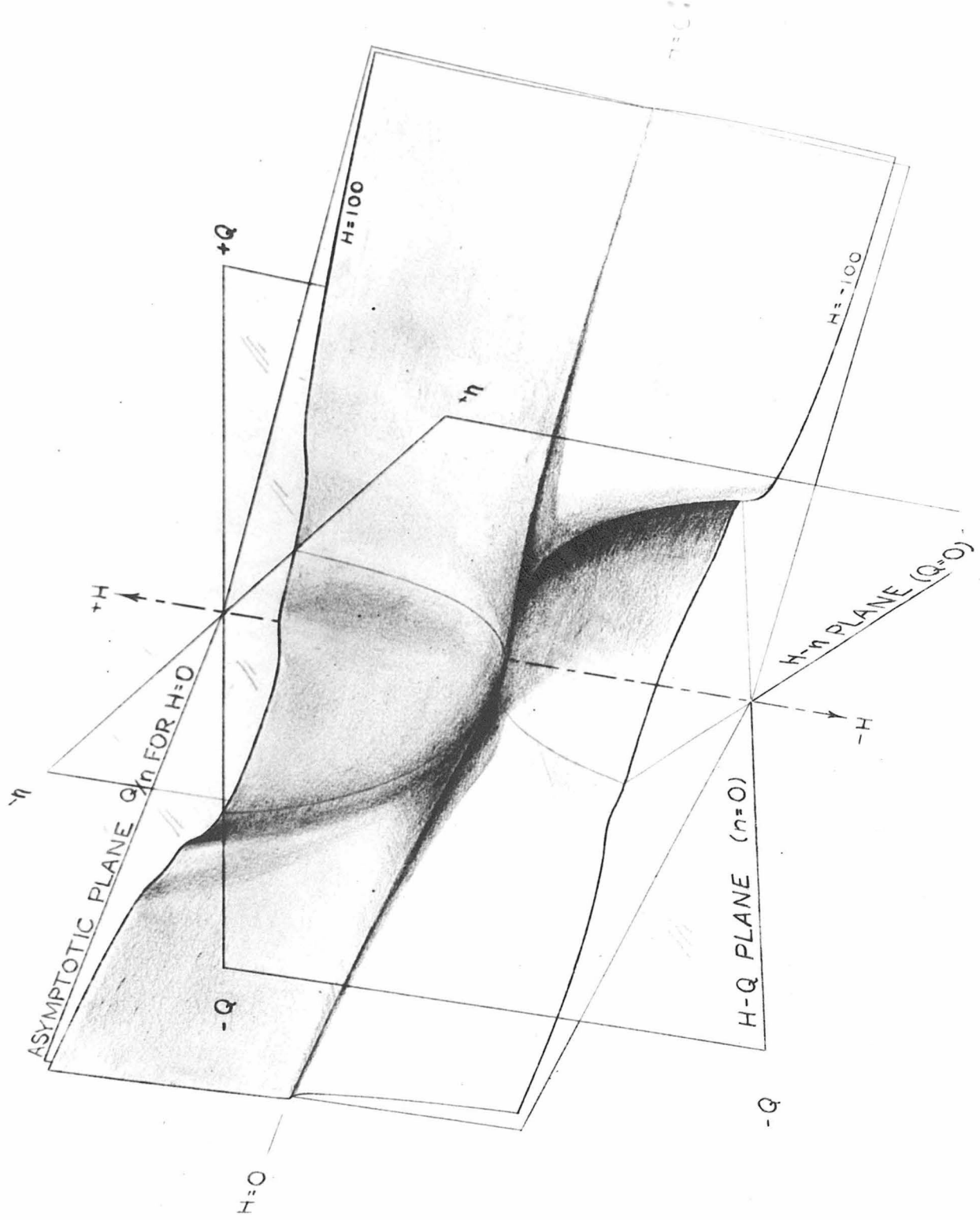
+Q
H=100
H=-100
+η
+H
-η
ASYMPTOTIC PLANE Q/η FOR H=0
-Q
H=0
H-η PLANE (Q=0)
-H
H-Q PLANE (η=0)
-Q

FIG. 30

IDEAL CIRCLE CHARACTERISTIC FOR RADIAL - FLOW IMPELLER

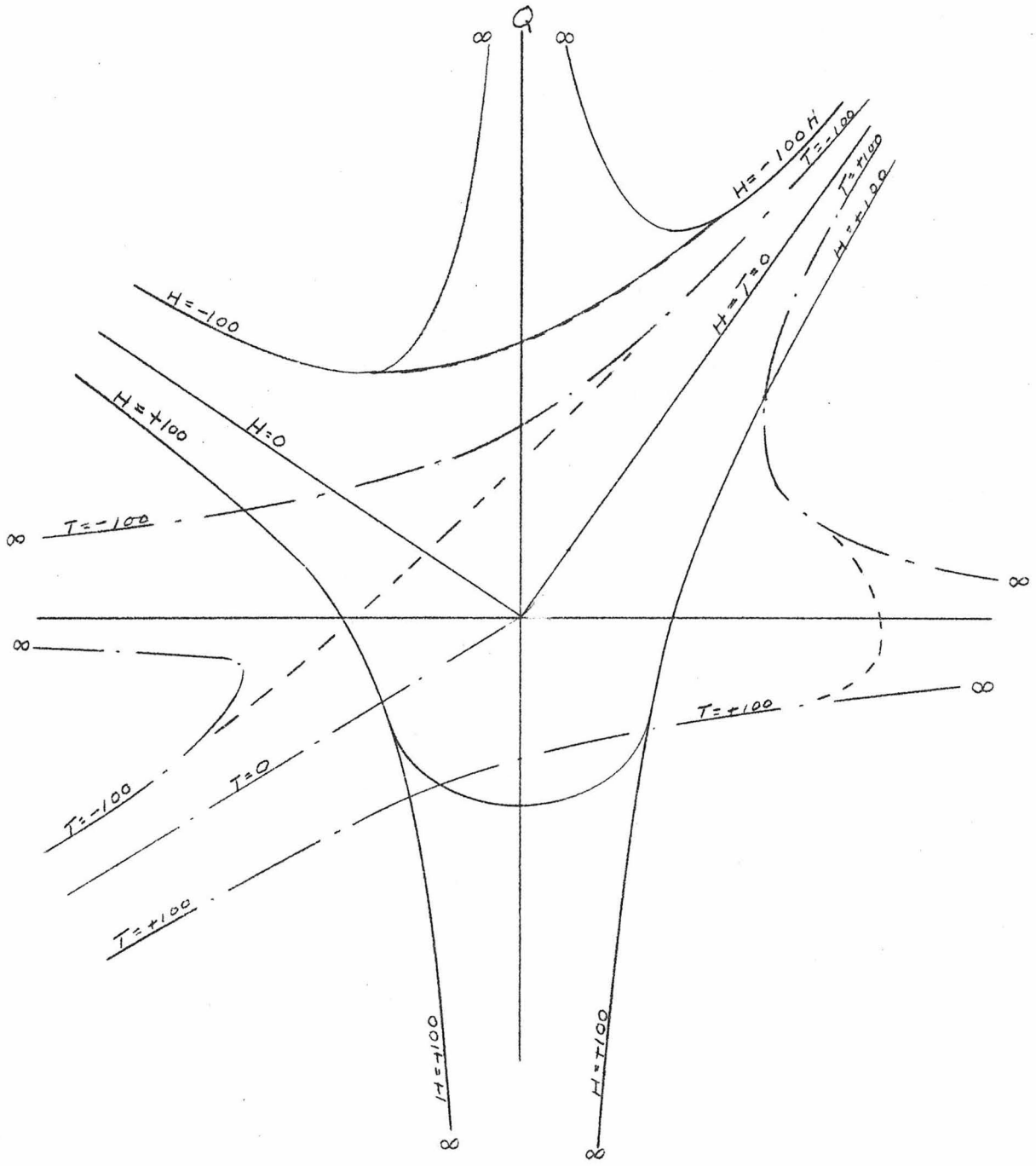

FIG. 31

HEAD-AND TORQUE - CAPACITY CHARACTERISTICS
FOR POSITIVE ROTATION

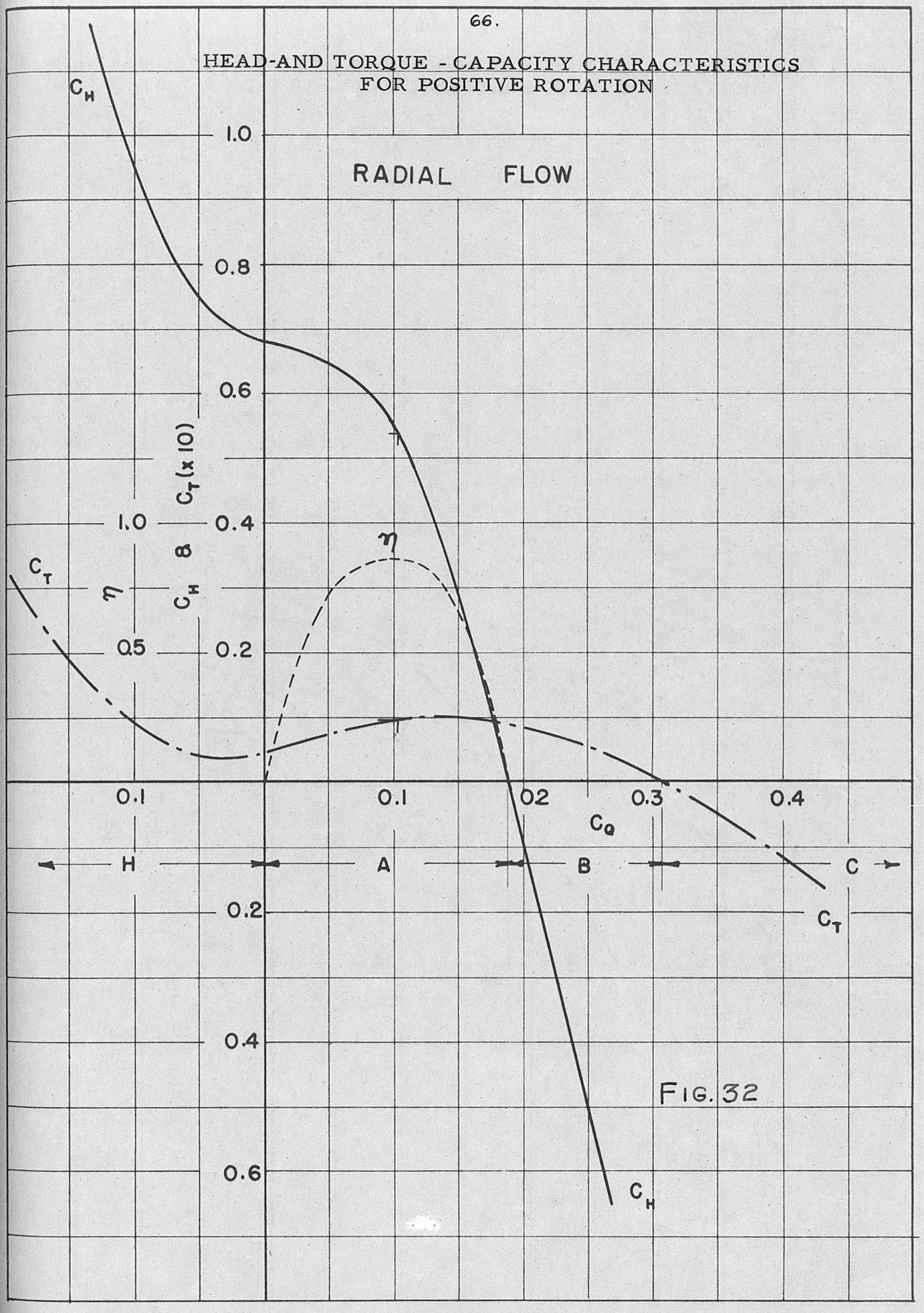

FIG. 32

PERCENTAGE HEAD-AND TORQUE - CAPACITY CHARACTERISTICS FOR POSITIVE ROTATION

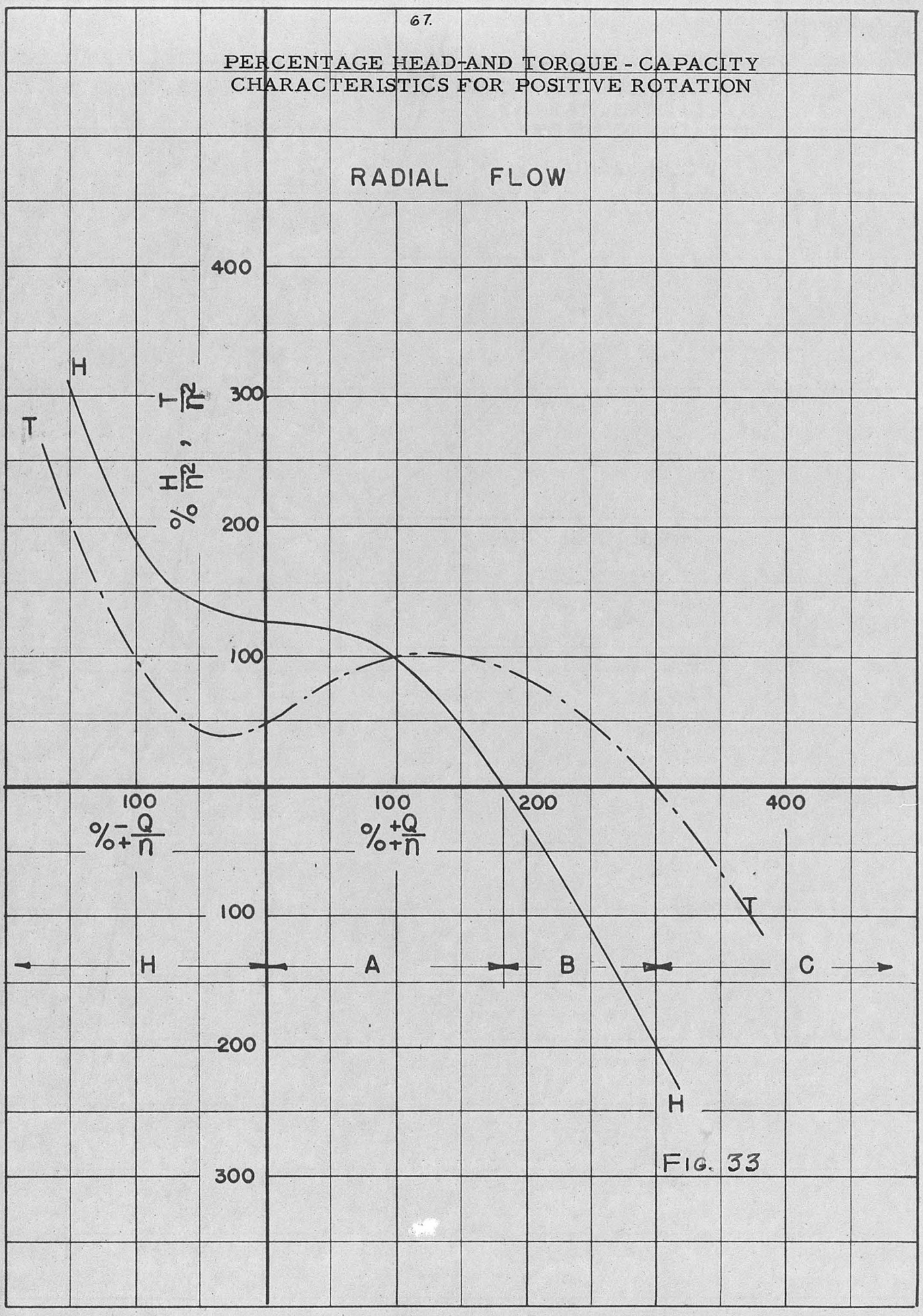

FIG. 33

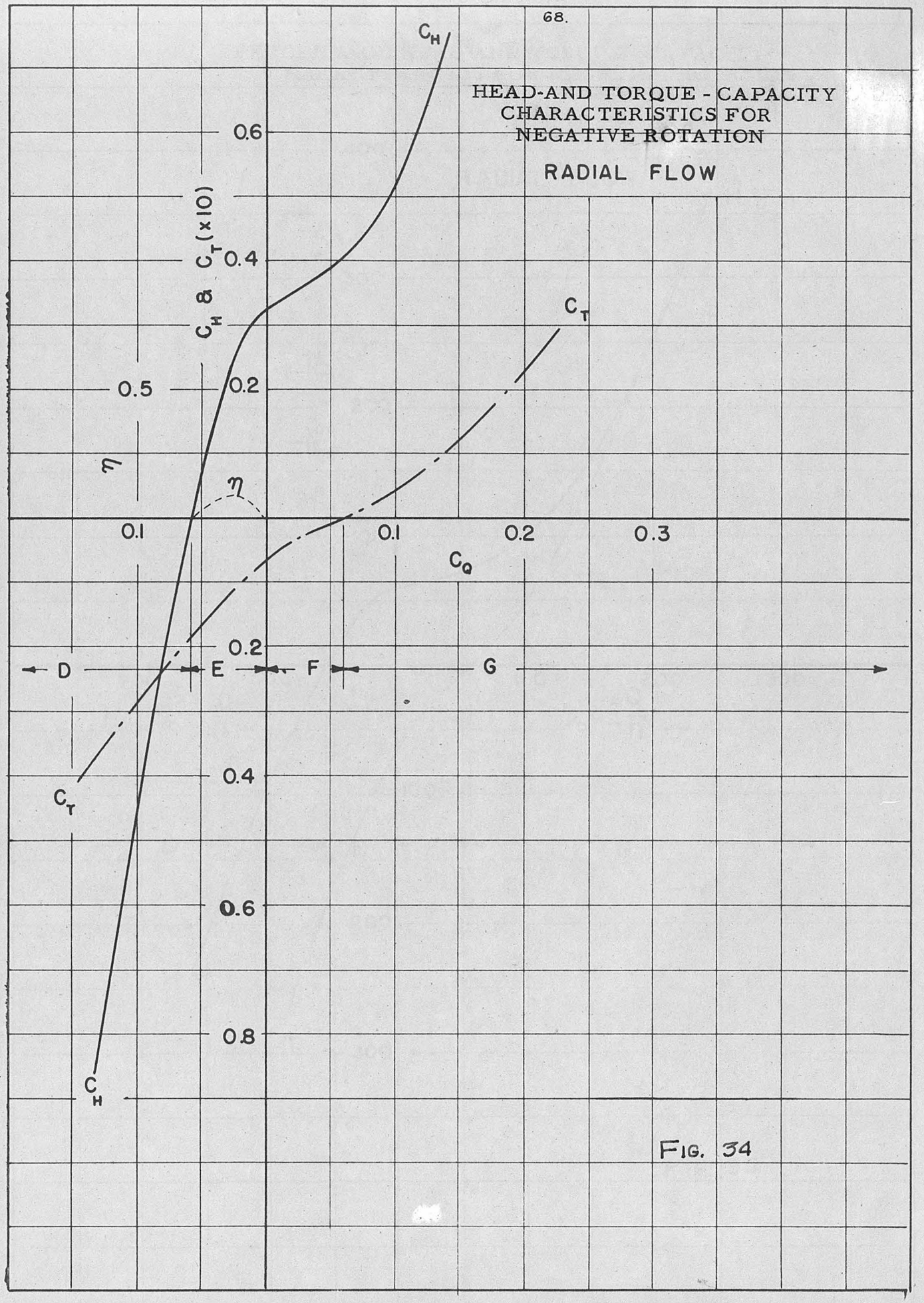
HEAD-AND TORQUE - CAPACITY CHARACTERISTICS FOR NEGATIVE ROTATION
RADIAL FLOW
C_H
C_T
C_H & C_T (x10)
η
C_Q
0.6
0.4
0.2
0.5
0.1
0.2
0.3
D
E
F
G
0.8

FIG. 34

PERCENTAGE HEAD-AND TORQUE - CAPACITY CHARACTERISTICS FOR NEGATIVE ROTATION

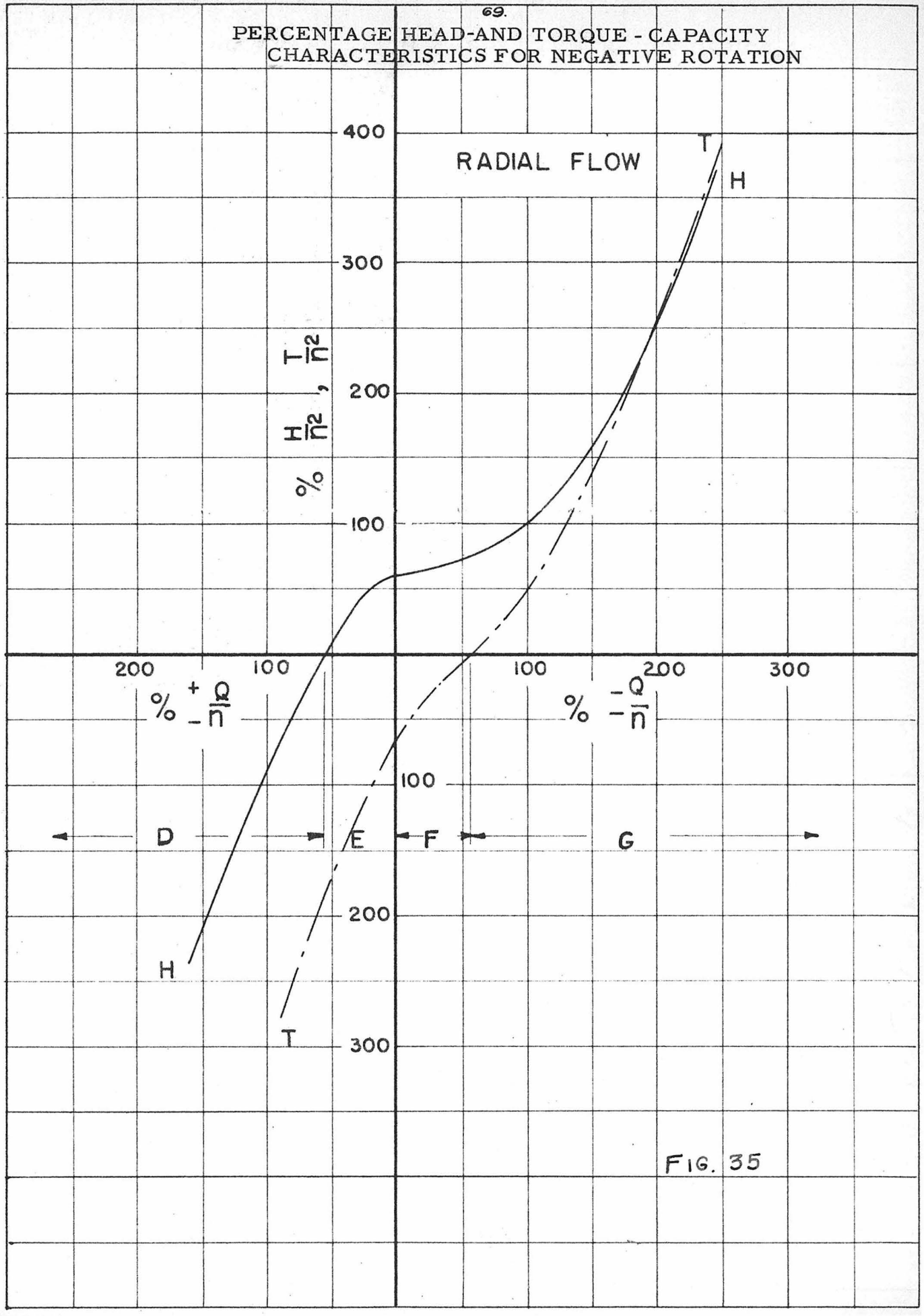

FIG. 35

HEAD-AND TORQUE - SPEED CHARACTERISTICS FOR NEGATIVE FLOW

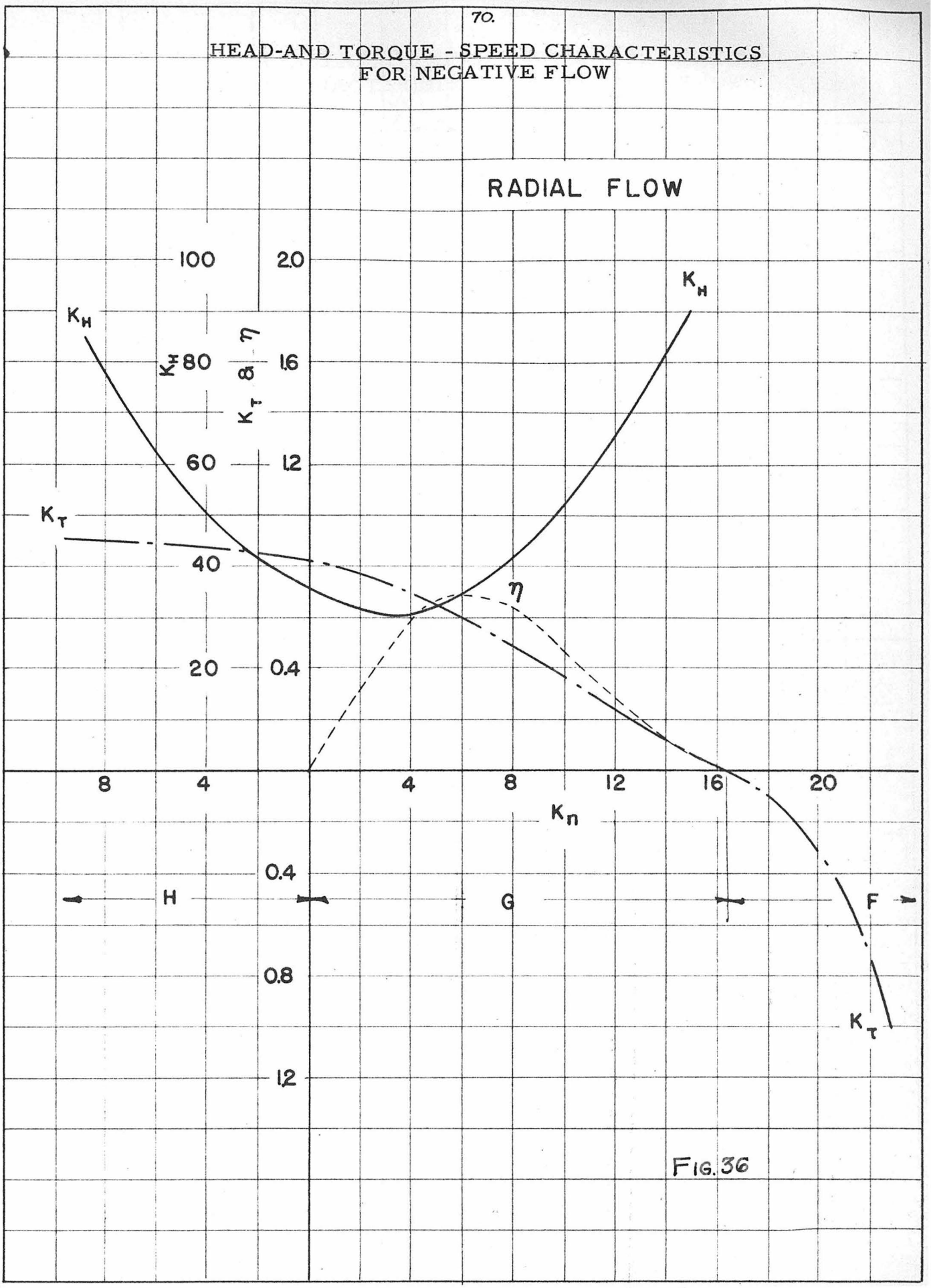

FIG. 36

PERCENTAGE HEAD-AND TORQUE - SPEED CHARACTERISTICS FOR NEGATIVE FLOW

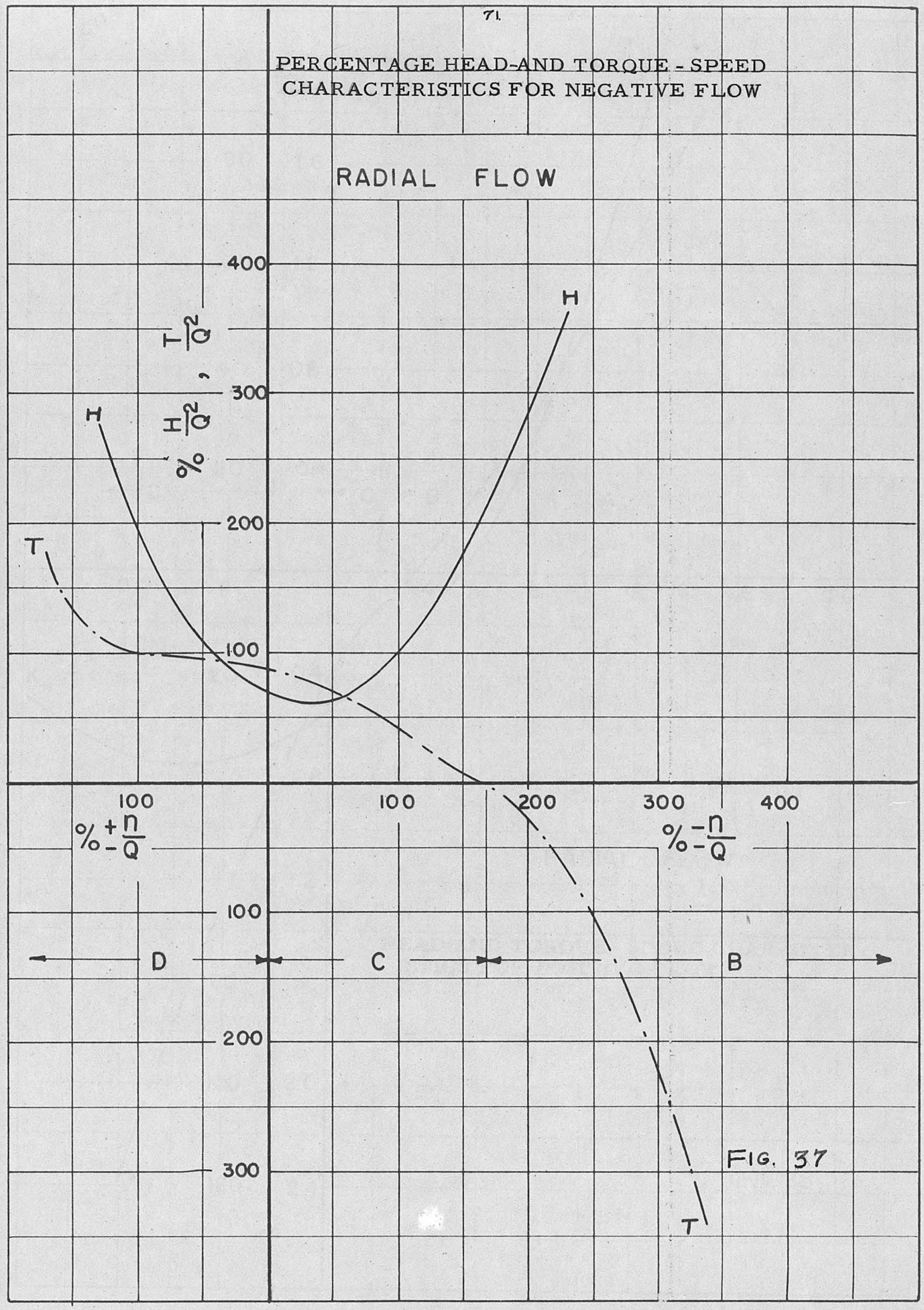

FIG. 37

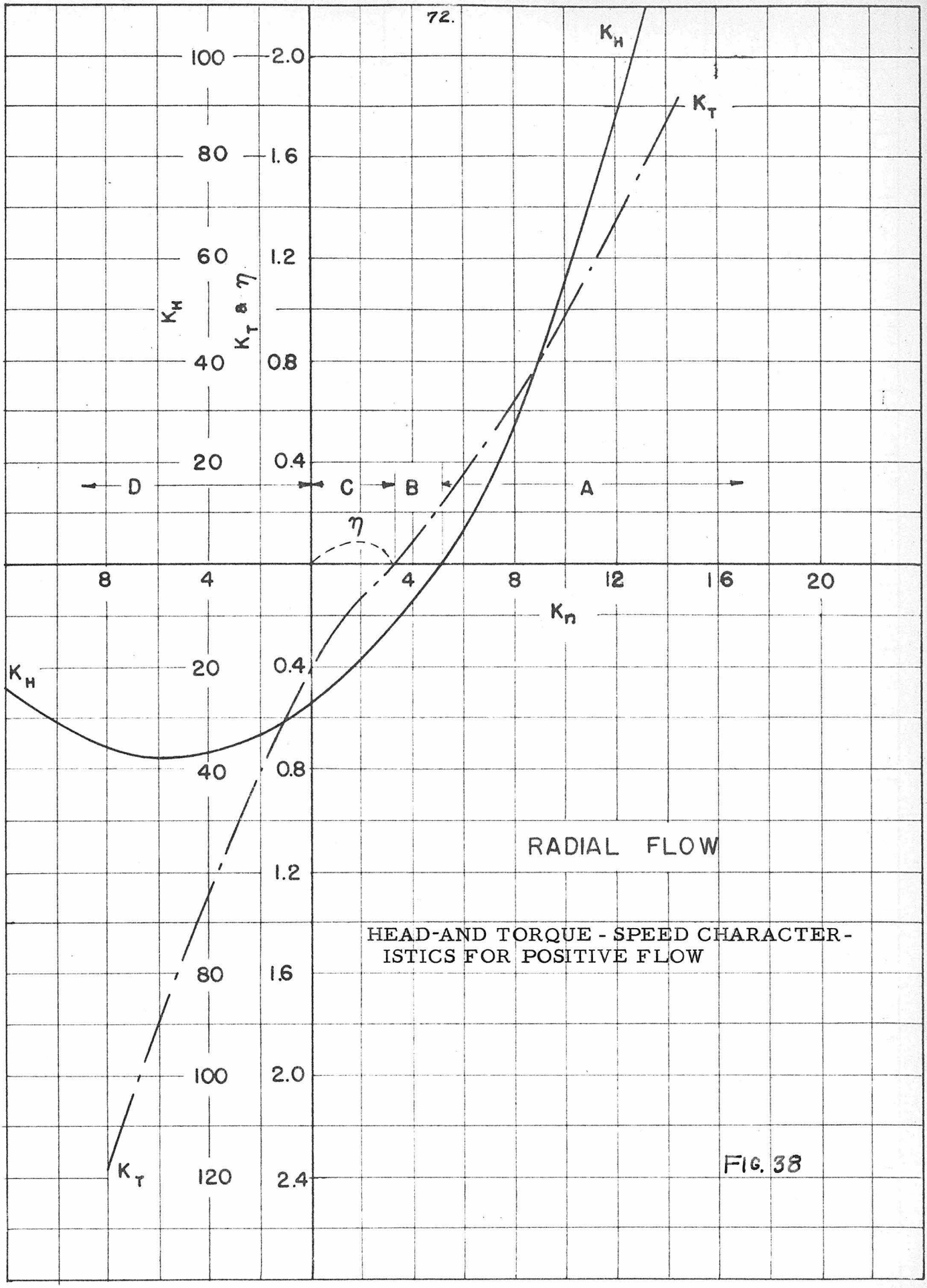

HEAD-AND TORQUE - SPEED CHARACTERISTICS FOR POSITIVE FLOW

FIG. 38

PERCENTAGE HEAD-AND TORQUE - SPEED CHARACTERISTICS FOR POSITIVE FLOW

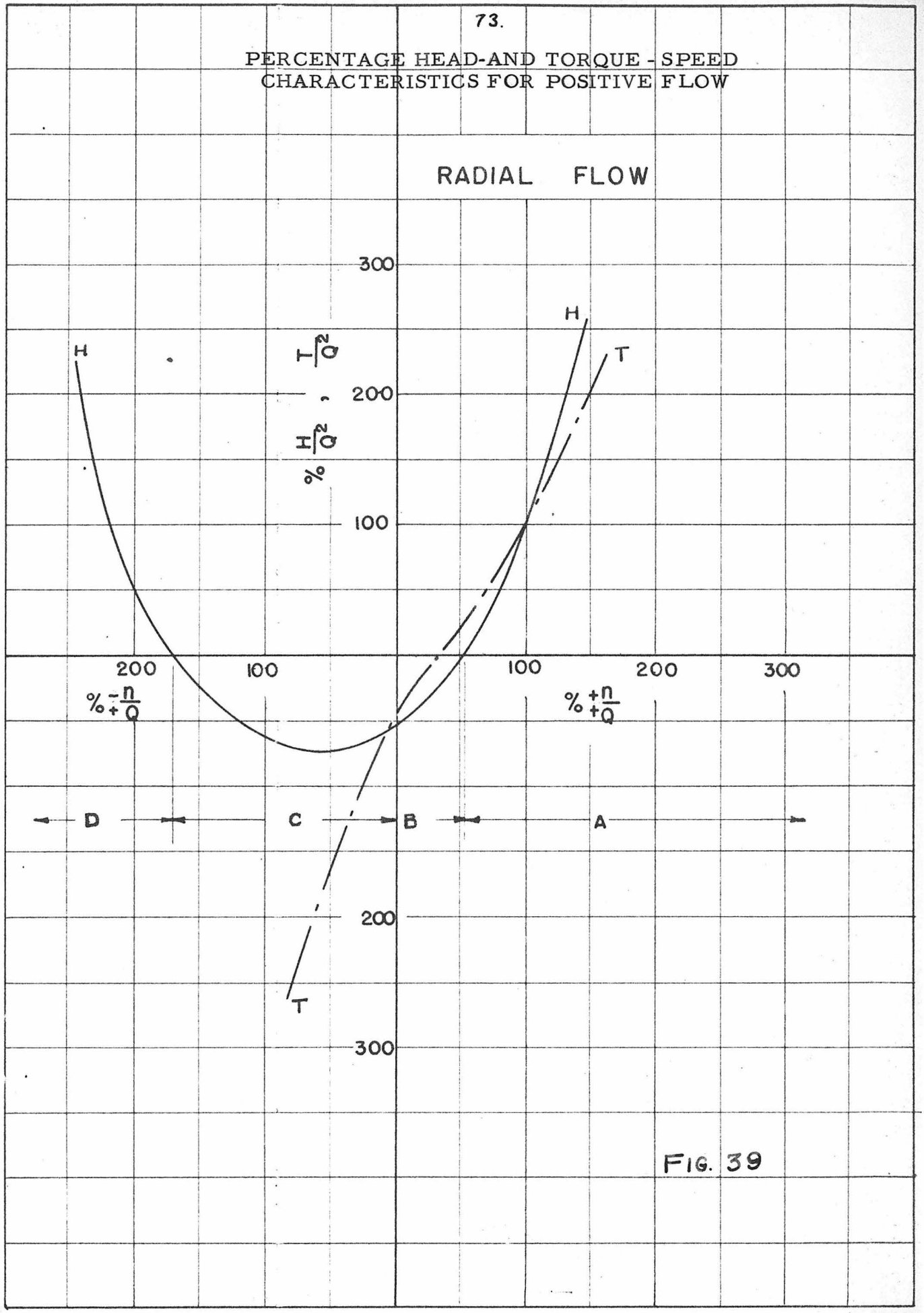

FIG. 39

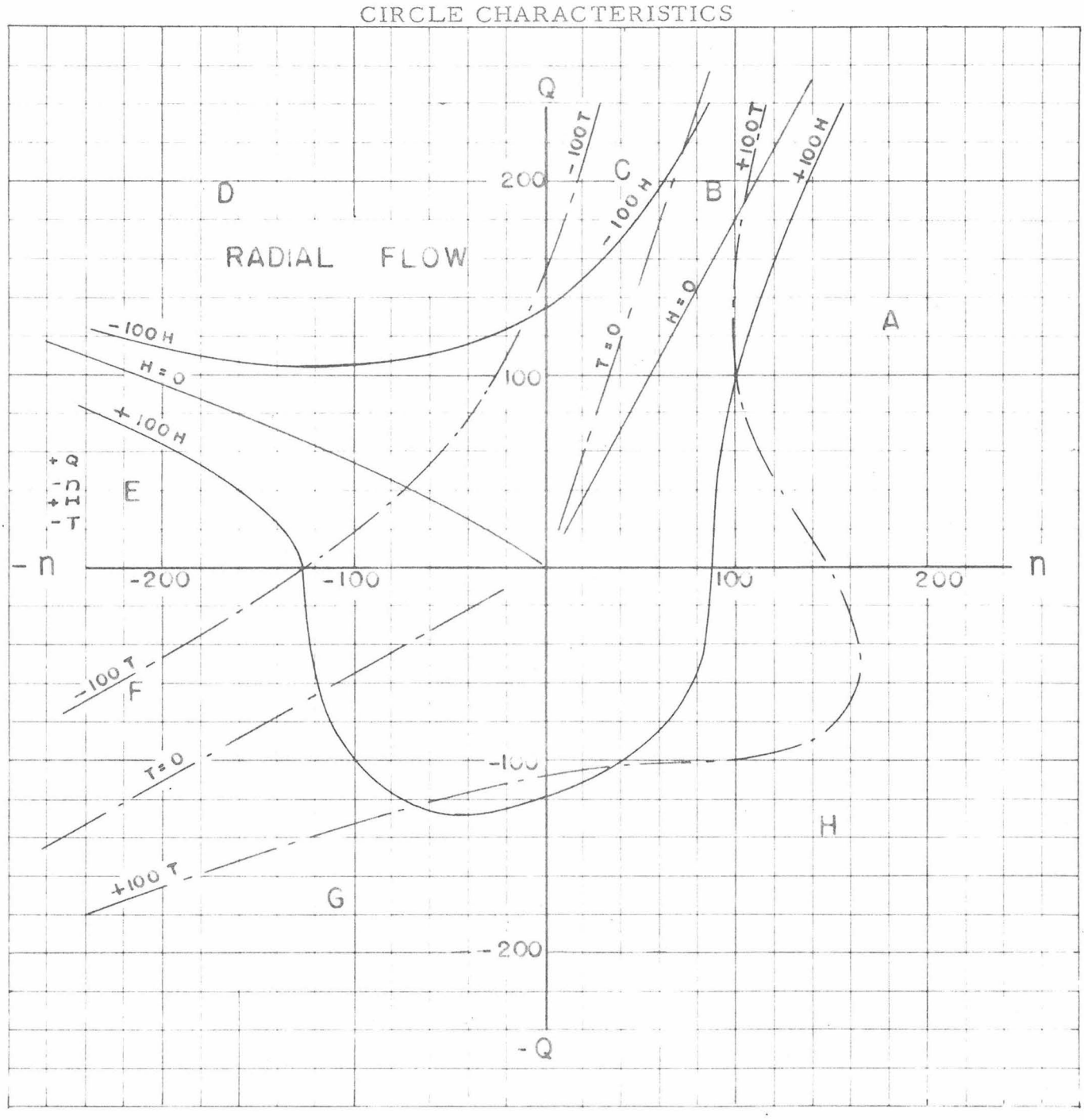
CIRCLE CHARACTERISTICS
Q
200
100
-100
-200
-Q
n
-n
-100 T
+100 T
-100 H
+100 H
H=0
T=0
A
B
C
D
E
F
G
H
RADIAL FLOW
+Q
-Q
+H
-T

FIG. 40

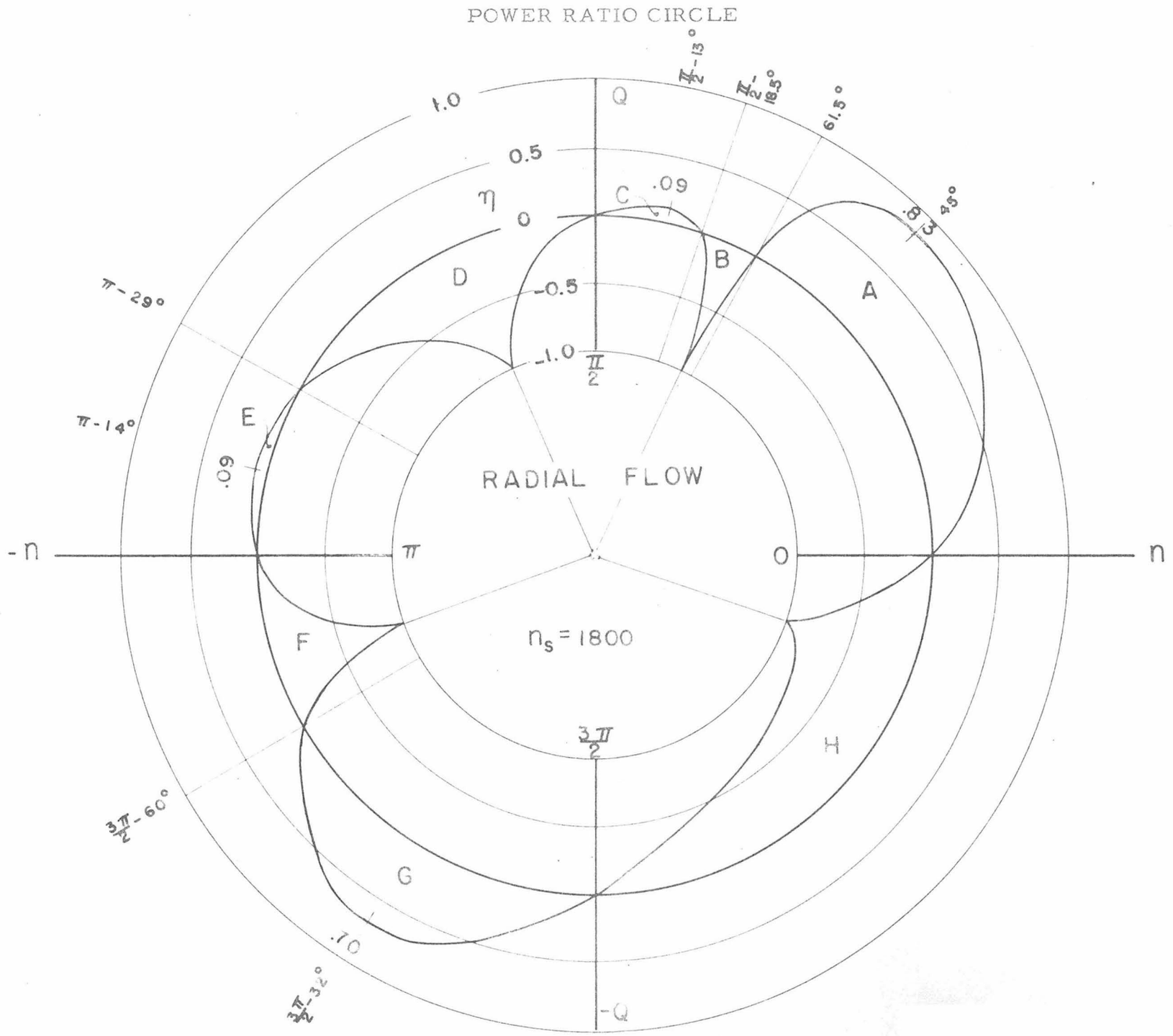
POWER RATIO CIRCLE
Q
-Q
-n
n
π
0
1.0
0.5
-0.5
-1.0
η
.09
.10
C
B
A
D
E
F
G
H
RADIAL FLOW
n_s = 1800
π/2 - 13°
π/2 - 18.5°
61.5°
π/3 - 45°
π - 29°
π - 14°
3π/2 - 60°
3π/2 - 32°
π/2
3π/2

FIG. 41

APPROXIMATE FLOW REPRESENTATIONS FOR VARIOUS ZONES OF OPERATION

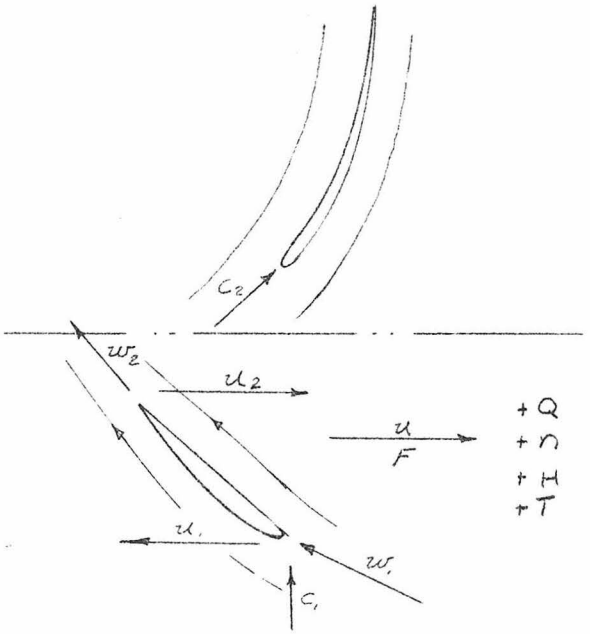

NORML PUMP ZONE A

(a)

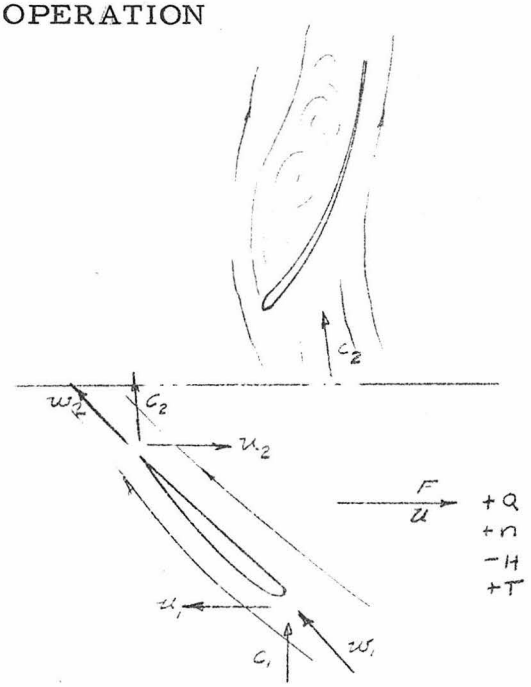

LOSS ZONE B

(b)

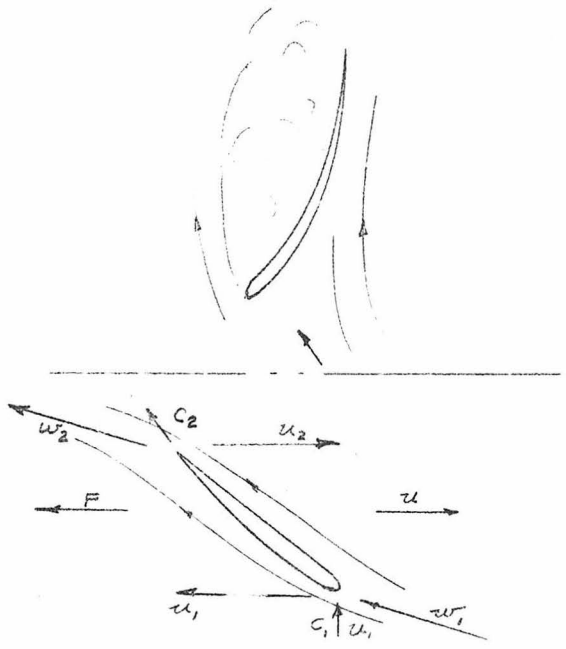

REVERSE TURBINE ZONE C

(c)

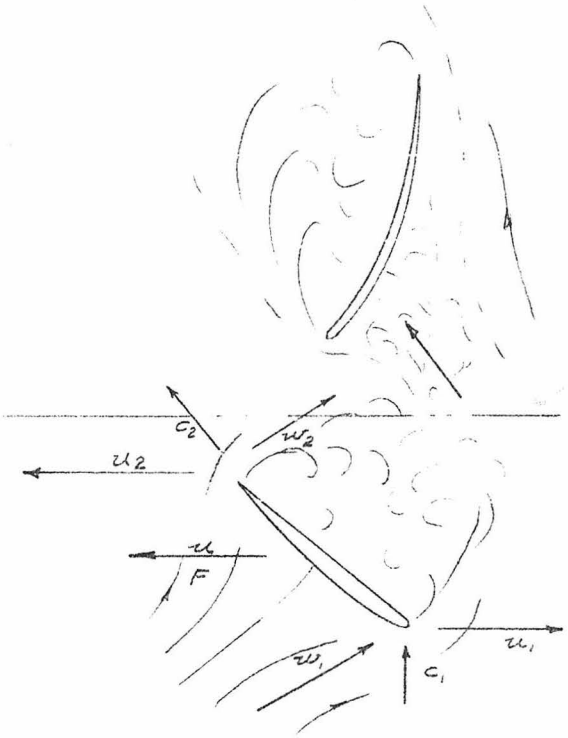

POWER DISSIPATION ZONE D

(d)

FIG. 42

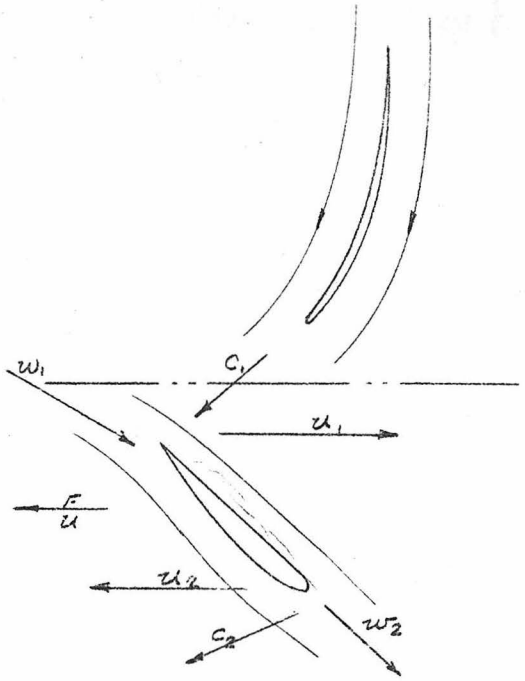

REVERSE PUMP ZONE E
(e)

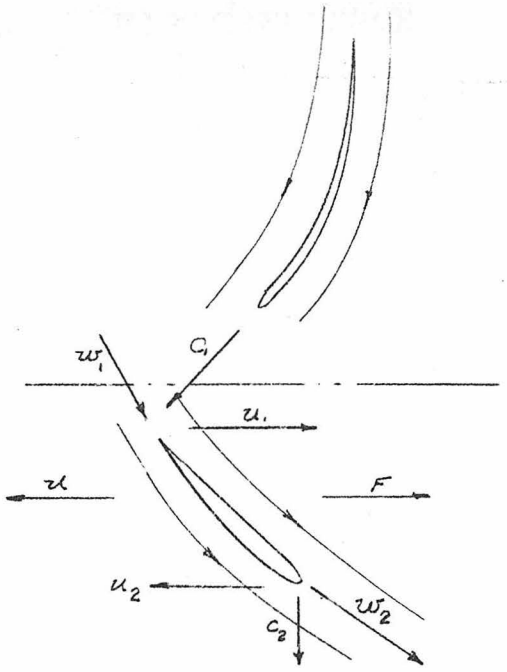

NORMAL TURBINE ZONE G
(f)

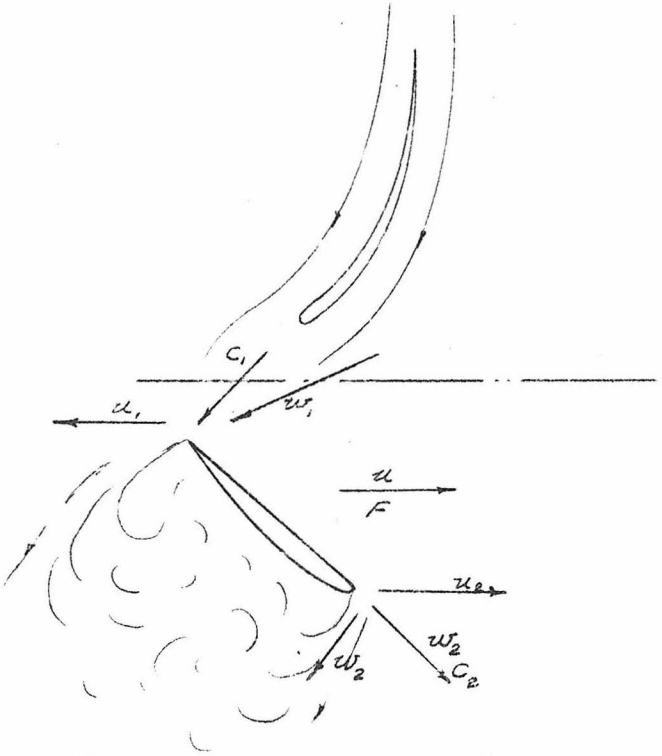

POWER DISSIPATION ZONE H
(g)

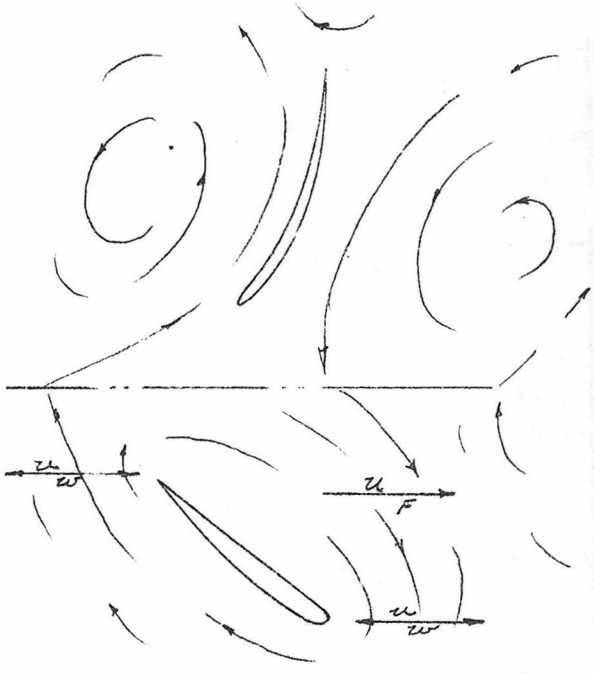

SHUT OFF (H-A)
(h)

FIG. 42

HEAD-AND TORQUE - CAPACITY CHARACTERISTICS
FOR POSITIVE ROTATION

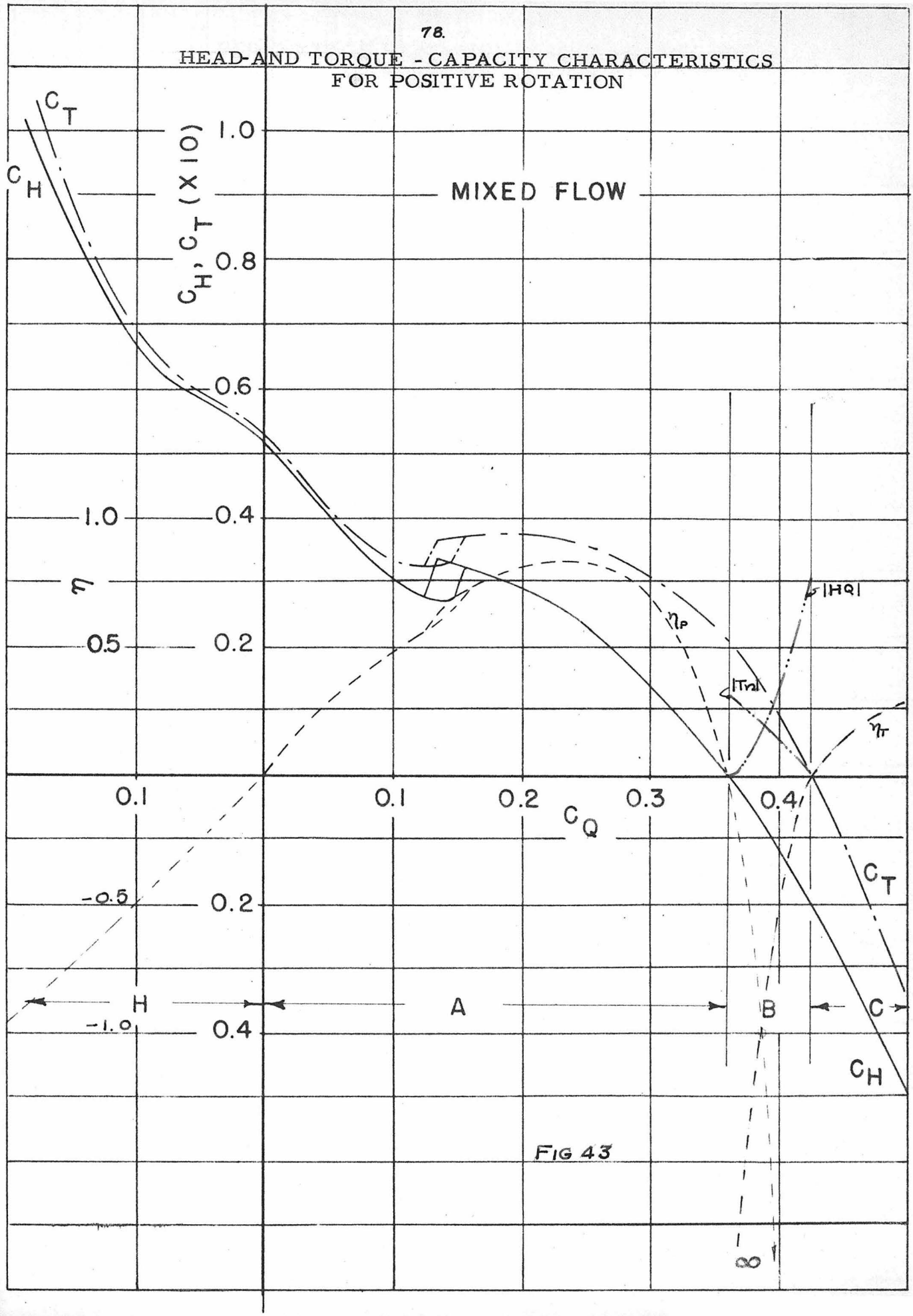

FIG 43

PERCENTAGE HEAD-AND TORQUE - CAPACITY CHARACTERISTICS FOR POSITIVE ROTATION

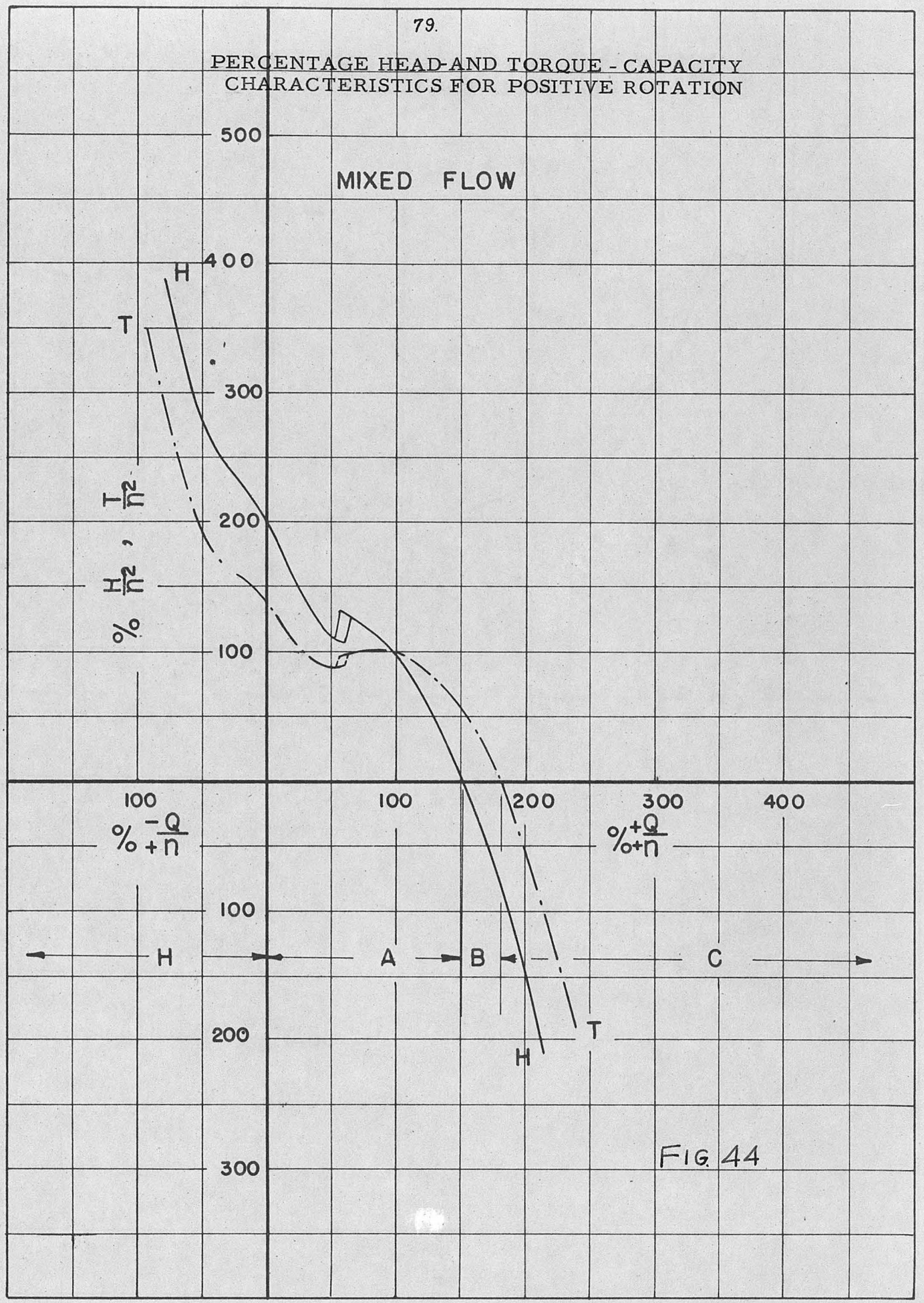

FIG. 44

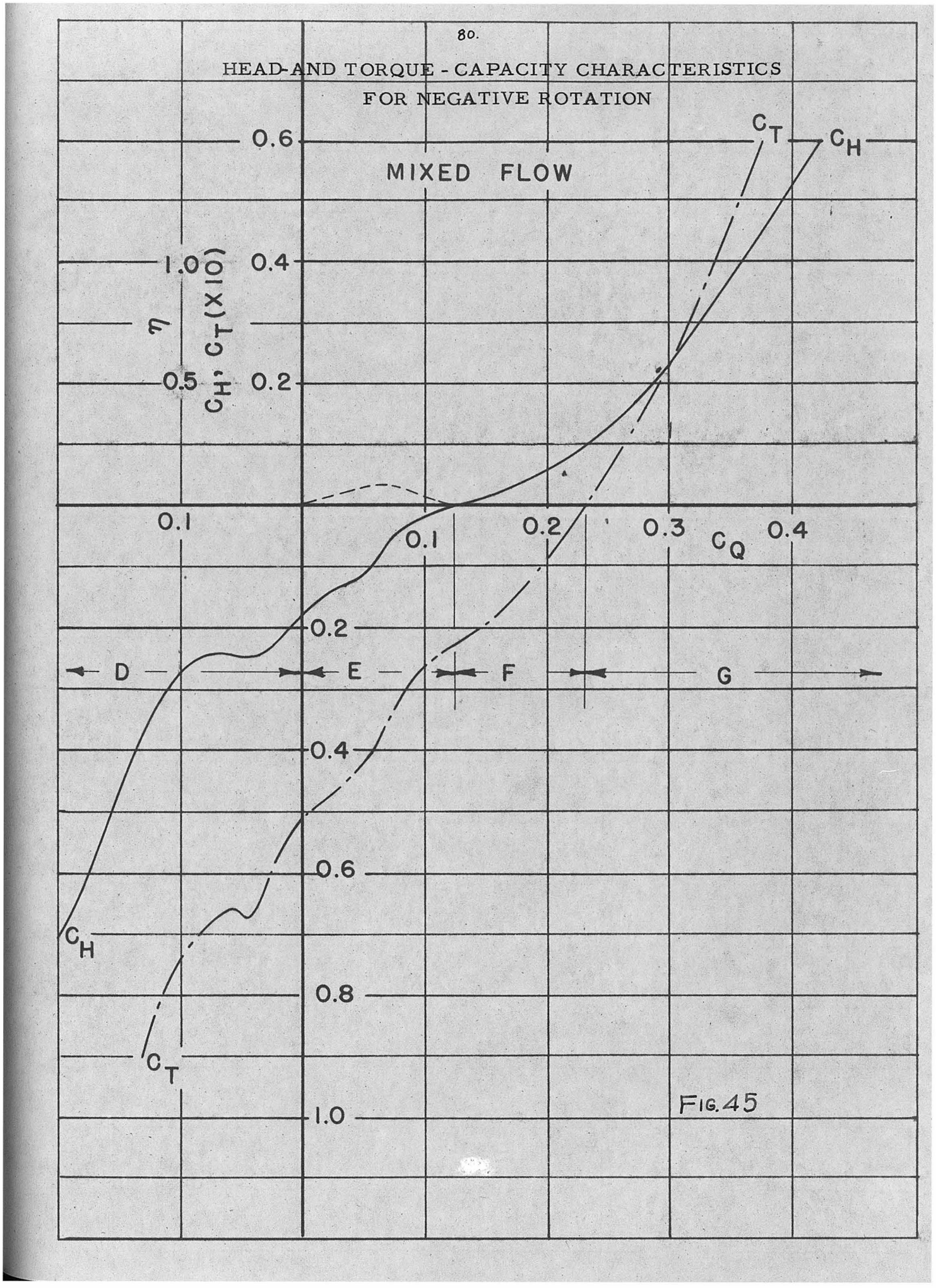
HEAD-AND TORQUE - CAPACITY CHARACTERISTICS
FOR NEGATIVE ROTATION
MIXED FLOW
C_T
C_H
η
C_H, C_T (X10)
C_Q
D
E
F
G
0.6
0.4
0.2
1.0
0.5
0.1
0.2
0.3
0.4
0.8

FIG. 45

PERCENTAGE TORQUE AND SPEED CHARACTERISTICS
FOR NEGATIVE ROTATION

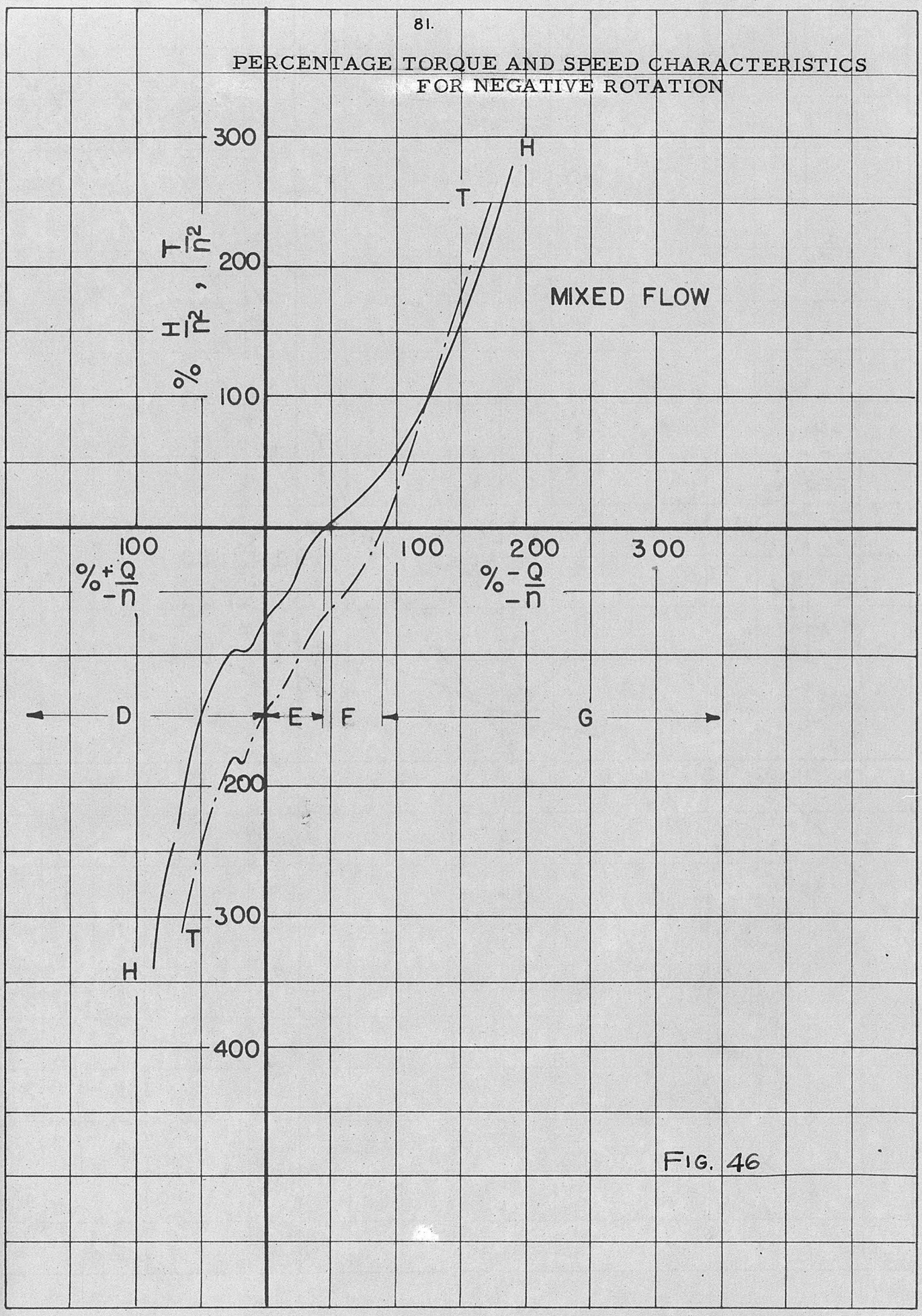

FIG. 46

HEAD-AND TORQUE - SPEED CHARACTERISTICS FOR NEGATIVE FLOW

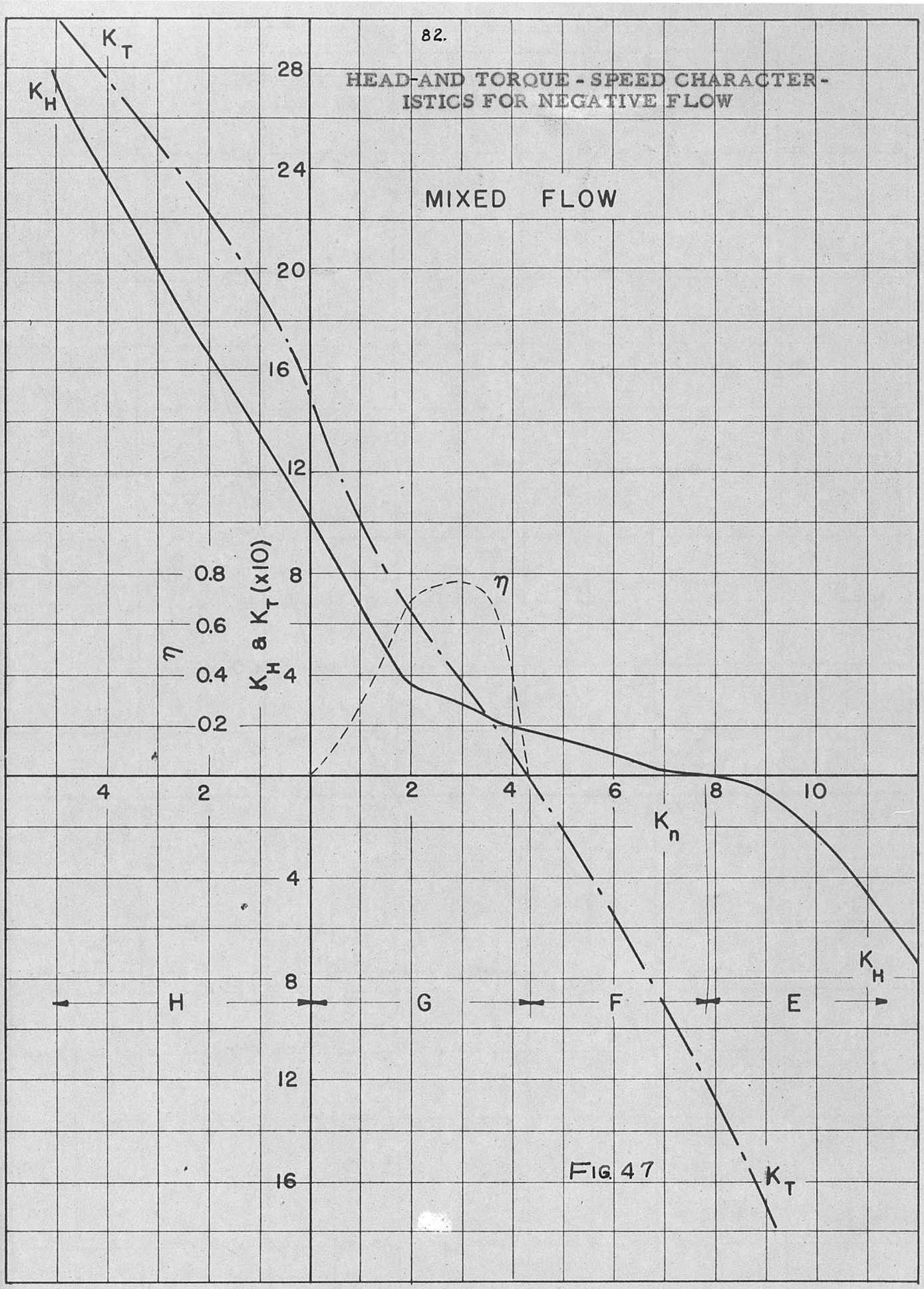

FIG. 47

PERCENTAGE HEAD AND TORQUE - SPEED CHARACTERISTICS FOR NEGATIVE FLOW

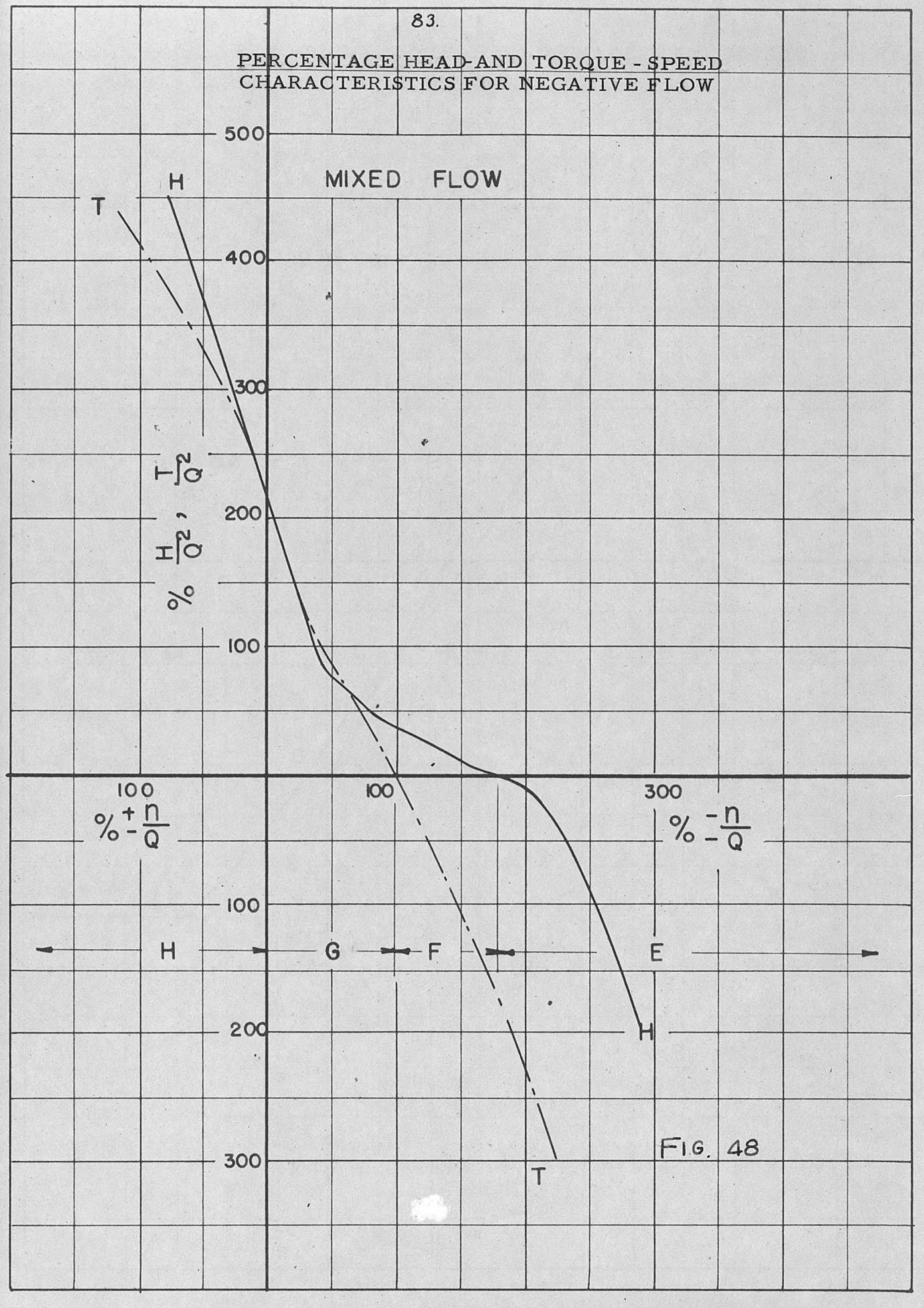

FIG. 48

HEAD-AND TORQUE - SPEED CHARACTERISTICS
FOR POSITIVE FLOW

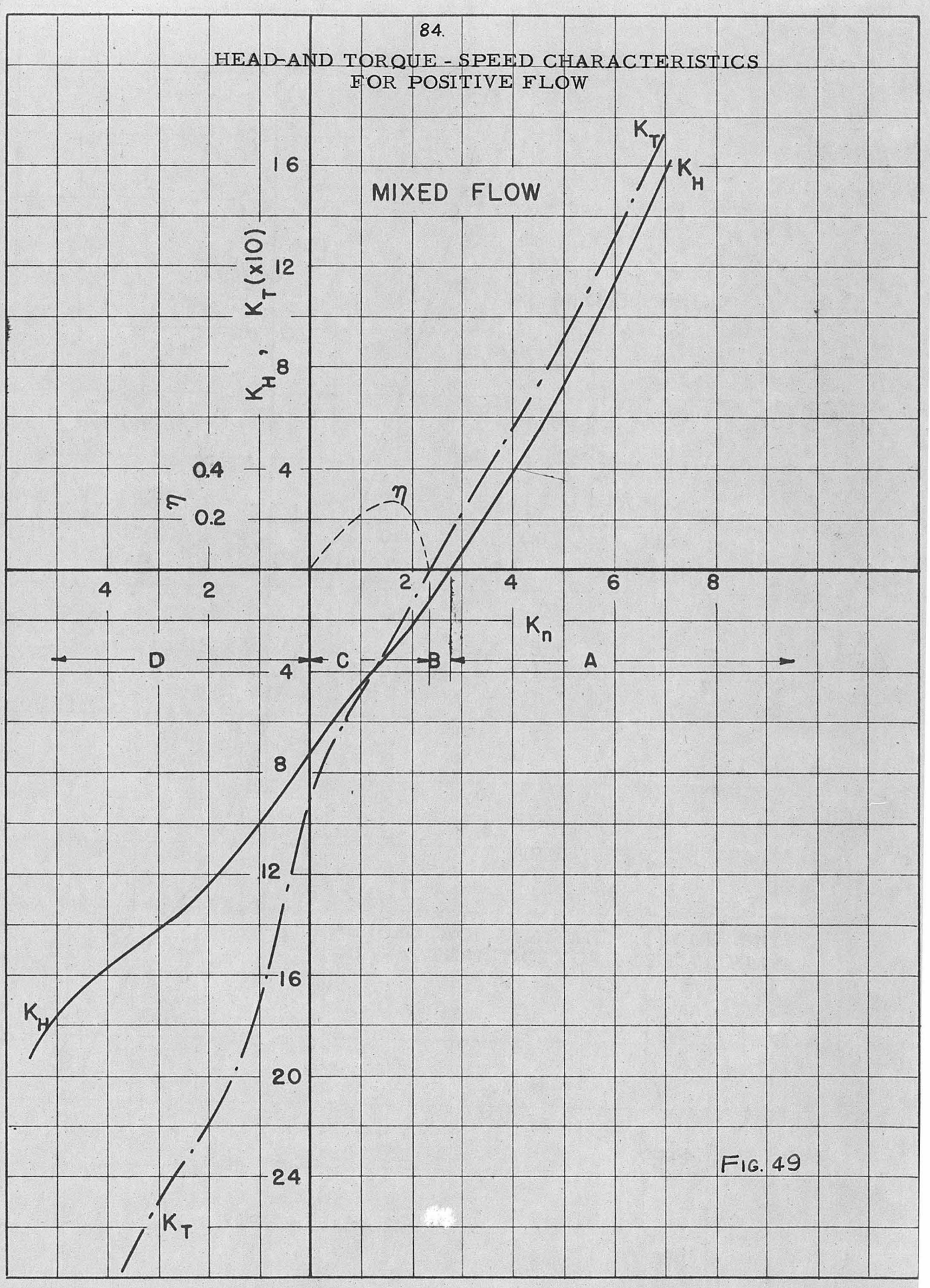

FIG. 49

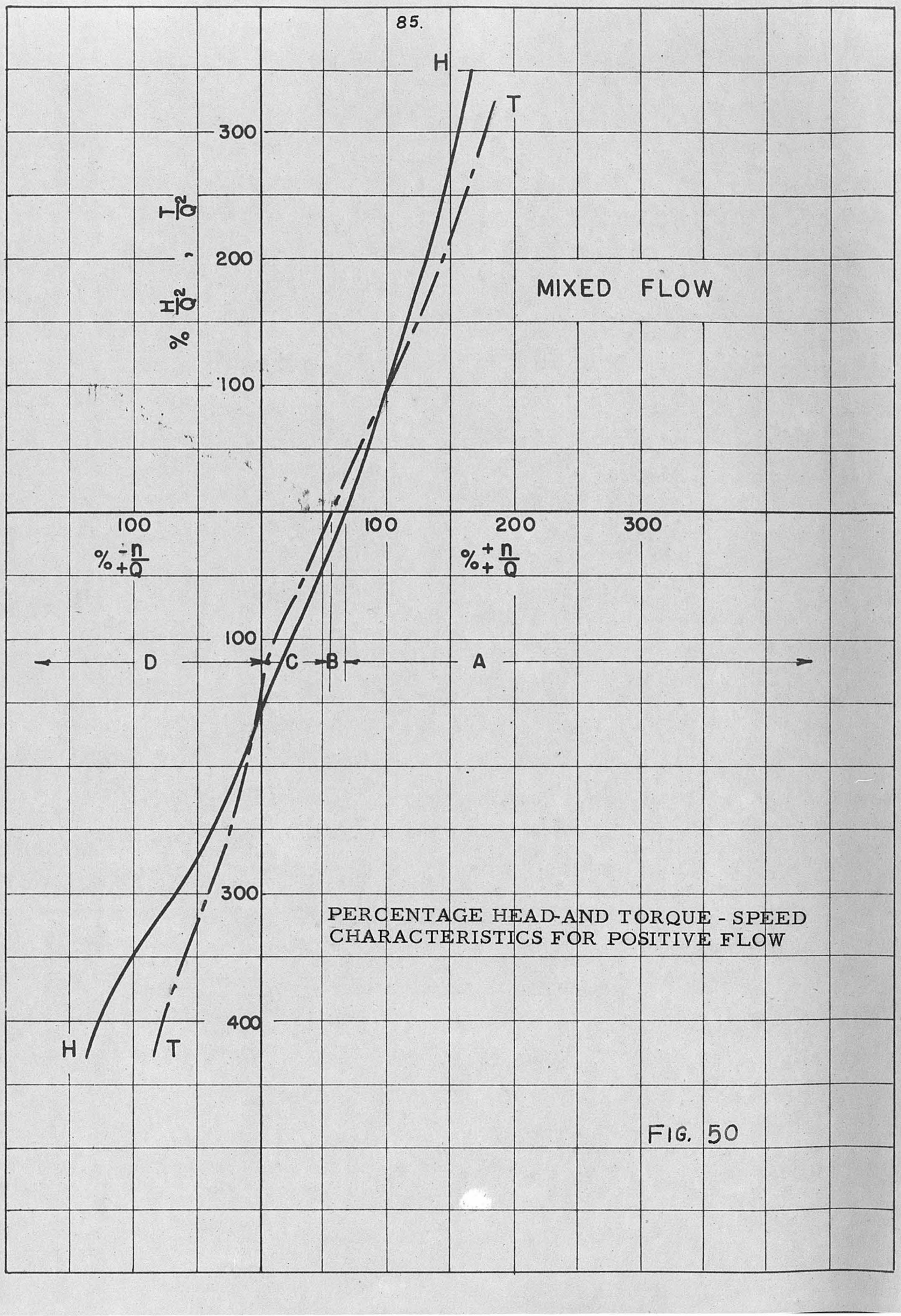

PERCENTAGE HEAD-AND TORQUE - SPEED CHARACTERISTICS FOR POSITIVE FLOW

FIG. 50

CIRCLE CHARACTERISTICS

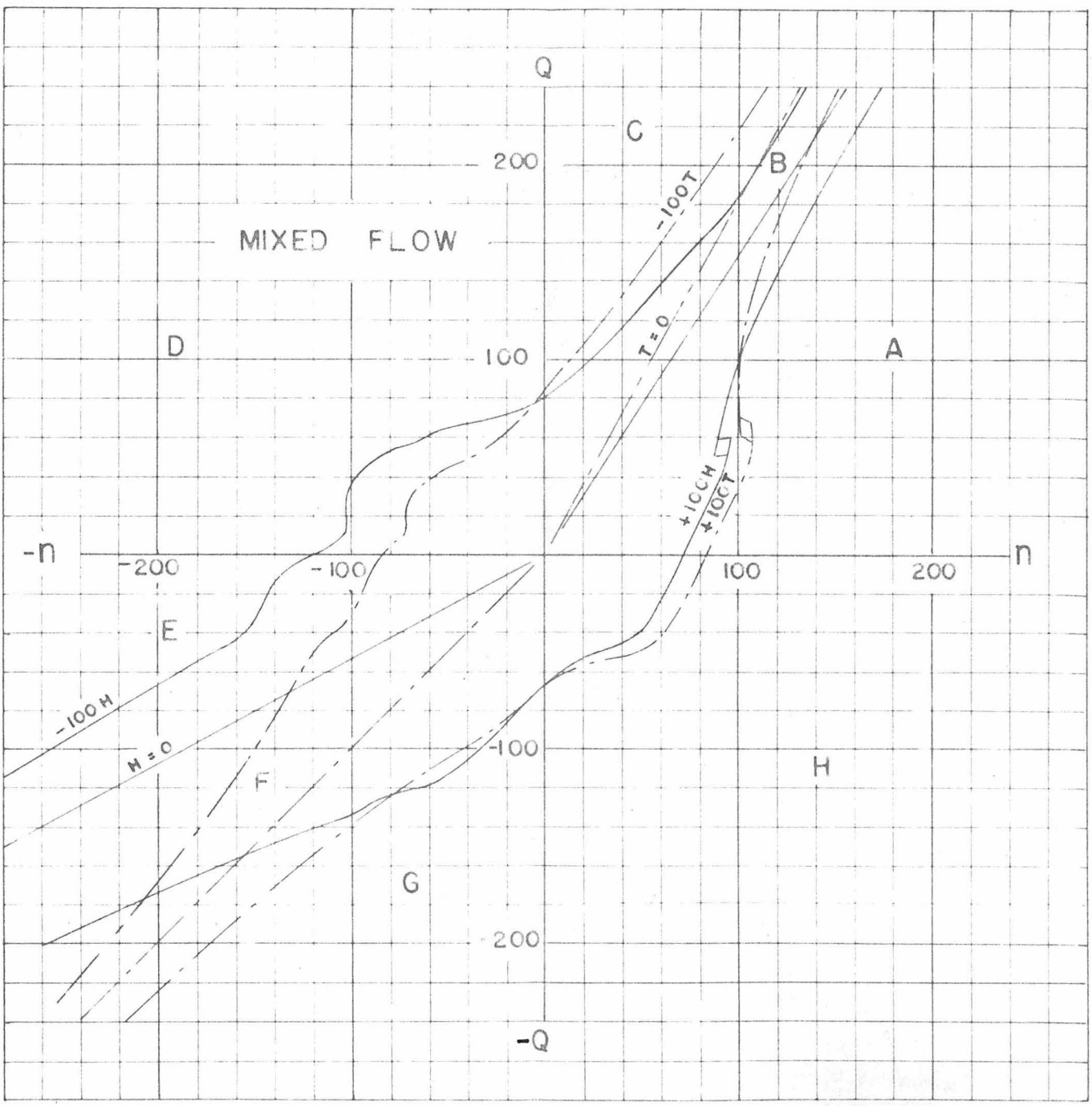

FIG. 51

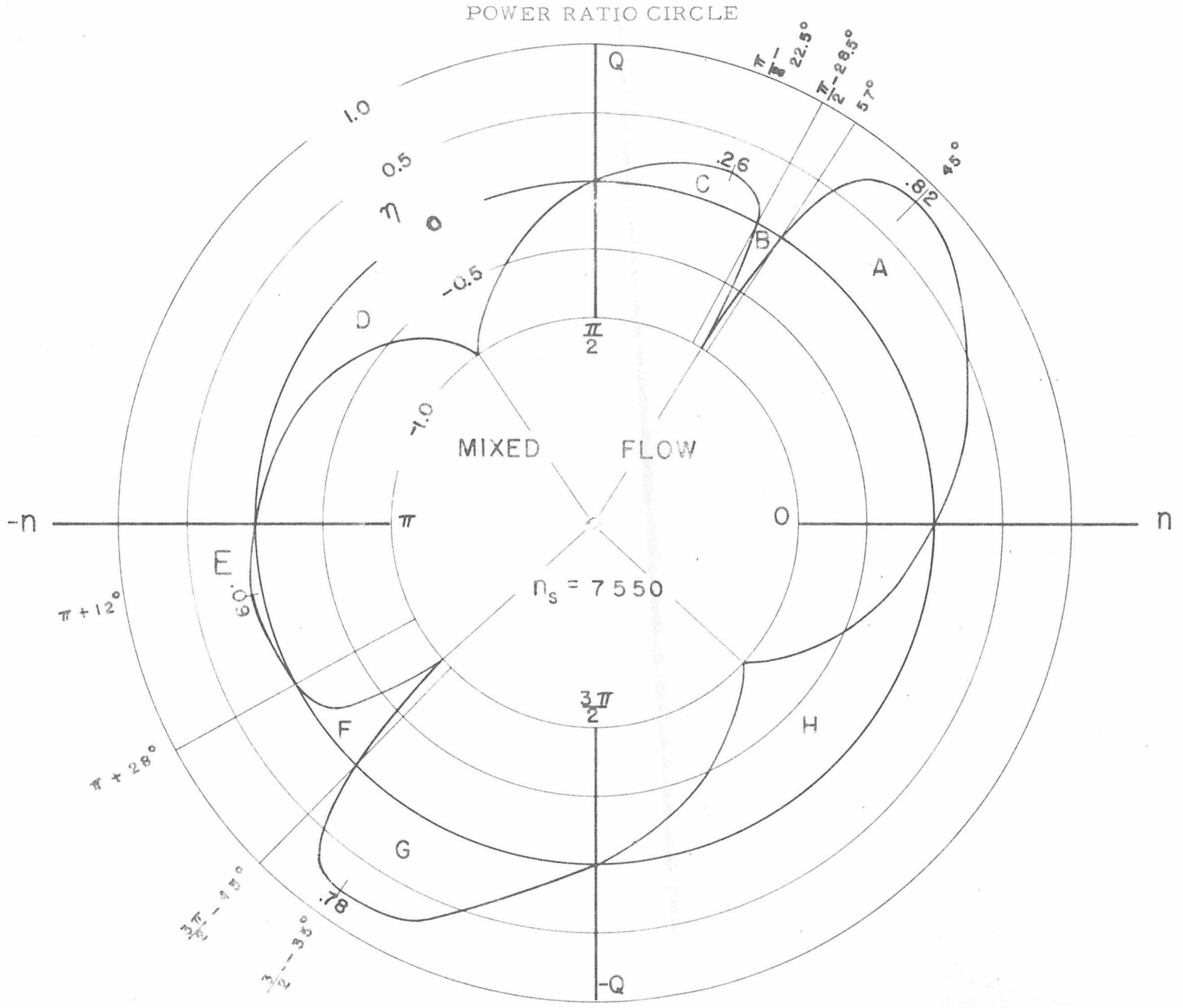
POWER RATIO CIRCLE
Q
1.0
0.5
η
0
-0.5
-1.0
.26
.82
45°
57°
π - 28.5°
π - 22.5°
π/2
A
B
C
D
MIXED
FLOW
-η
π
0
η
E
60°
π + 12°
π + 28°
F
G
H
.78
3π/2
-Q

FIG. 52

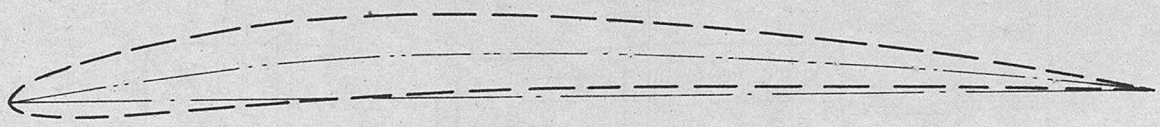

NACA 4407

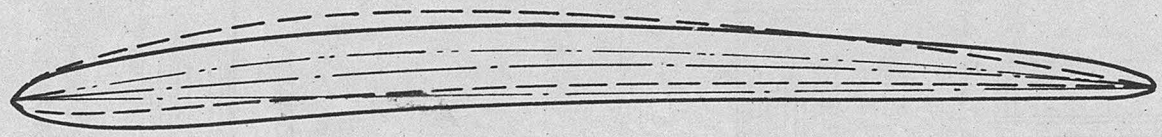

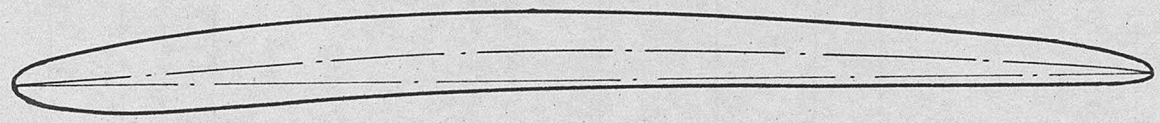

PUMP. BLADE PROFILE

FIG. 53

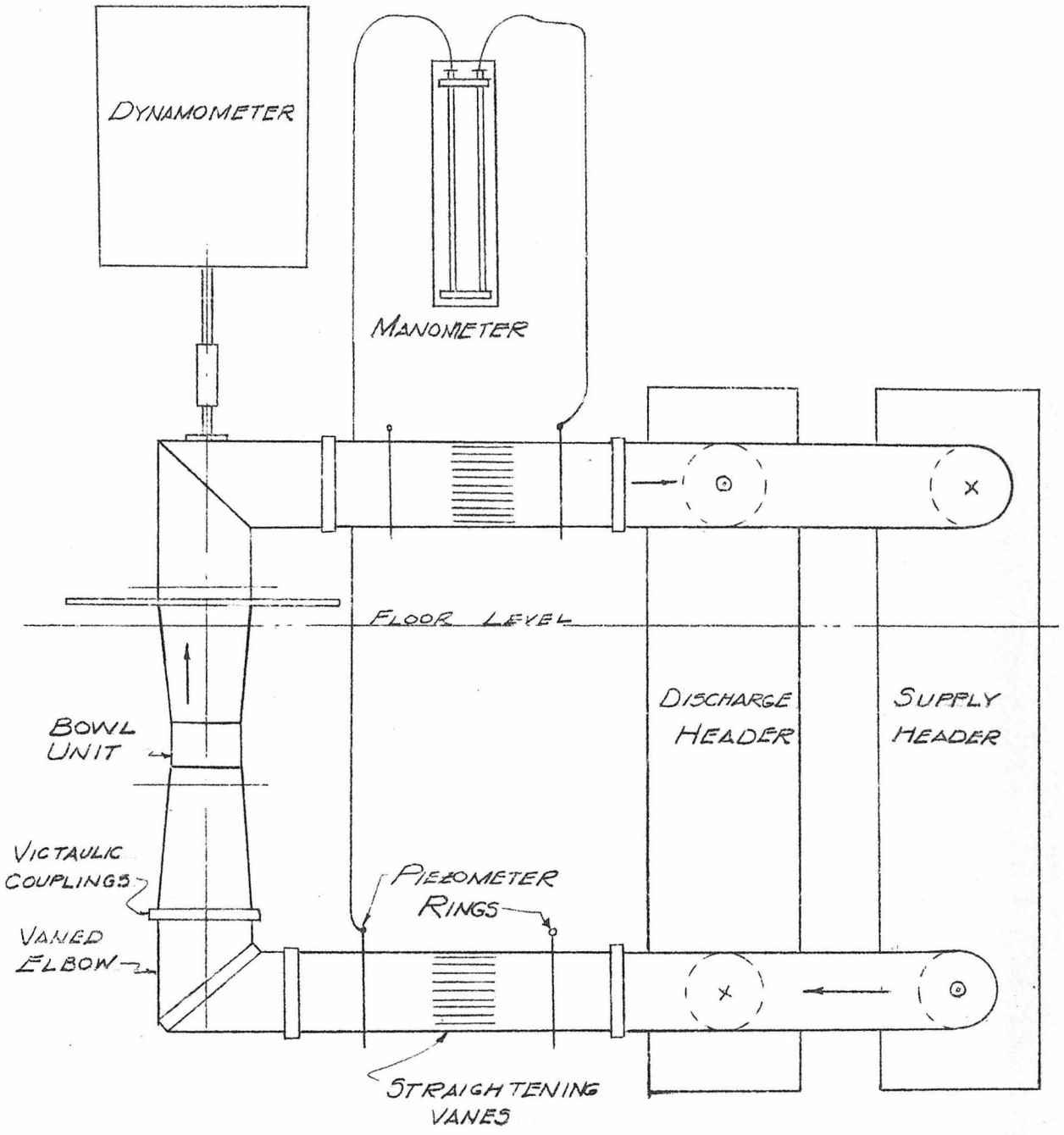

SKETCH OF PUMP INSTALLATION

FIG. 54

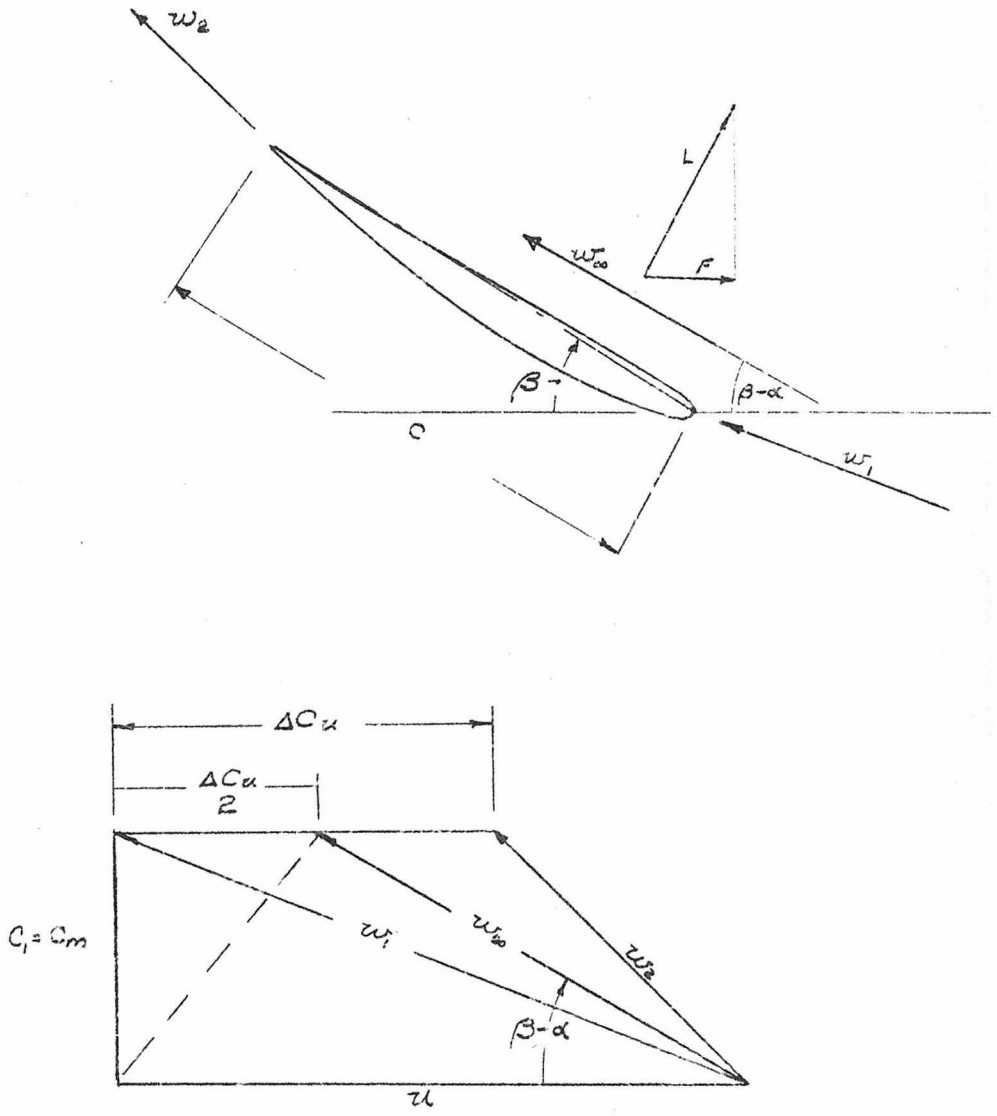

TWO - DIMENSIONAL AIRFOIL NOTATION

FIG. 55

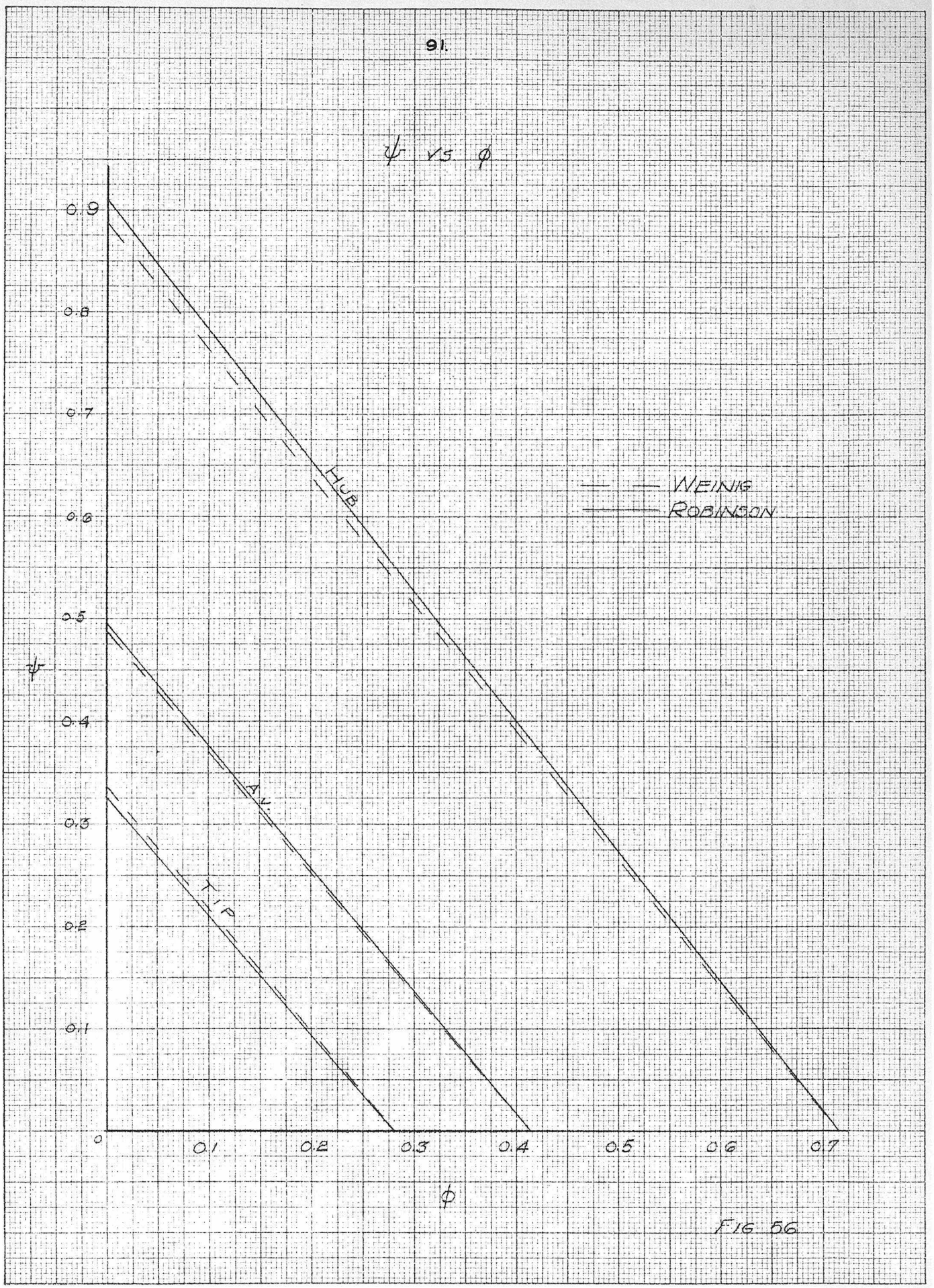
ψ vs φ
0.9
0.8
0.7
0.6
0.5
0.4
0.3
0.2
0.1
ψ
HUB
MID.
TIP
WEINIG
ROBINSON
0
0.1
0.2
0.3
0.4
0.5
0.6
0.7
φ

FIG 56

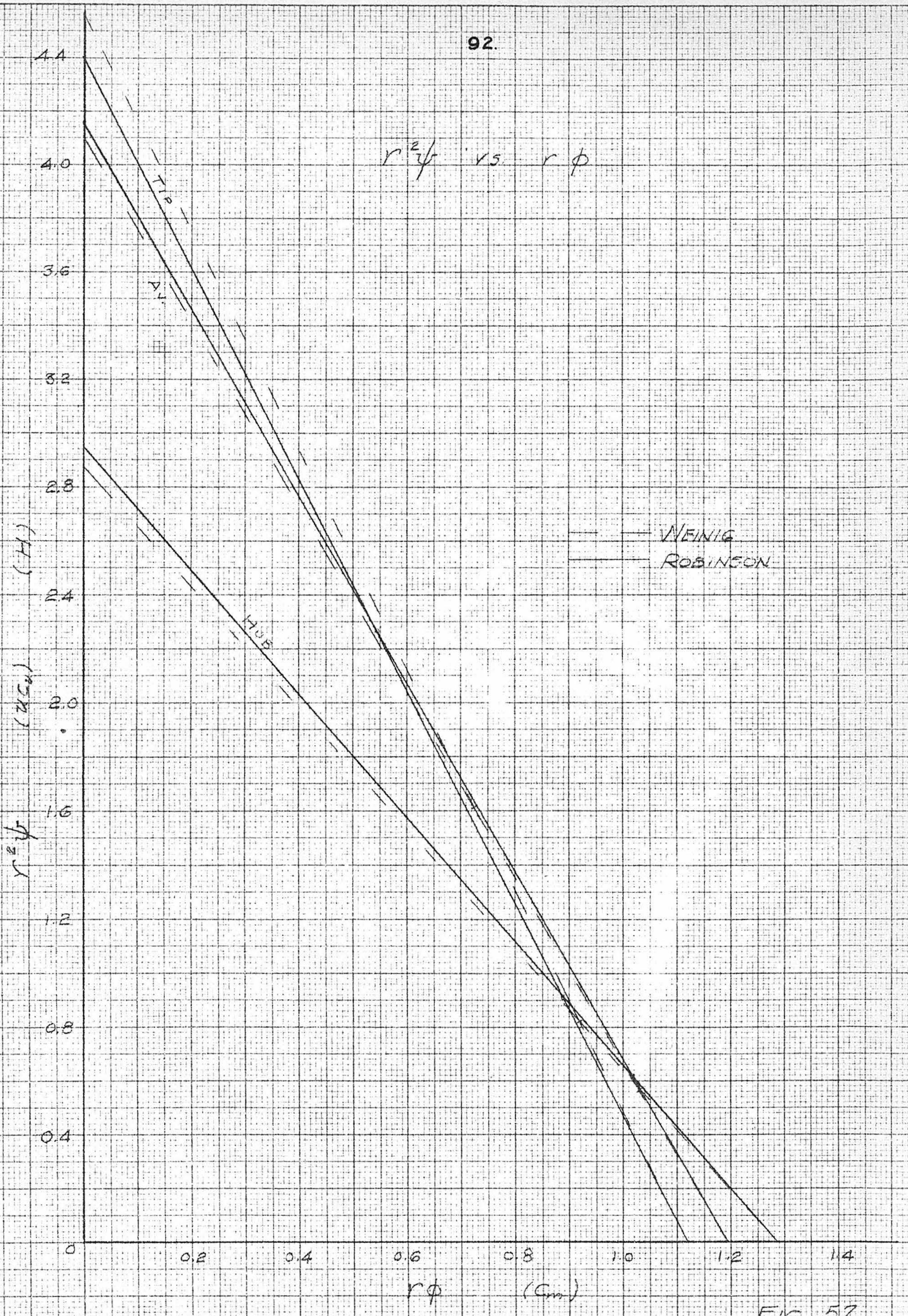

r²ψ vs rφ
TIP
AV.
HUB
WEINIG
ROBINSON
4.4
4.0
3.6
3.2
2.8
2.4
2.0
1.6
1.2
0.8
0.4
0
0.2
0.4
0.6
0.8
1.0
1.2
1.4
r²ψ (ψC_u) (H)
rφ (C_m)

FIG 57

MEAN VALUES OF ψ VS. ϕ

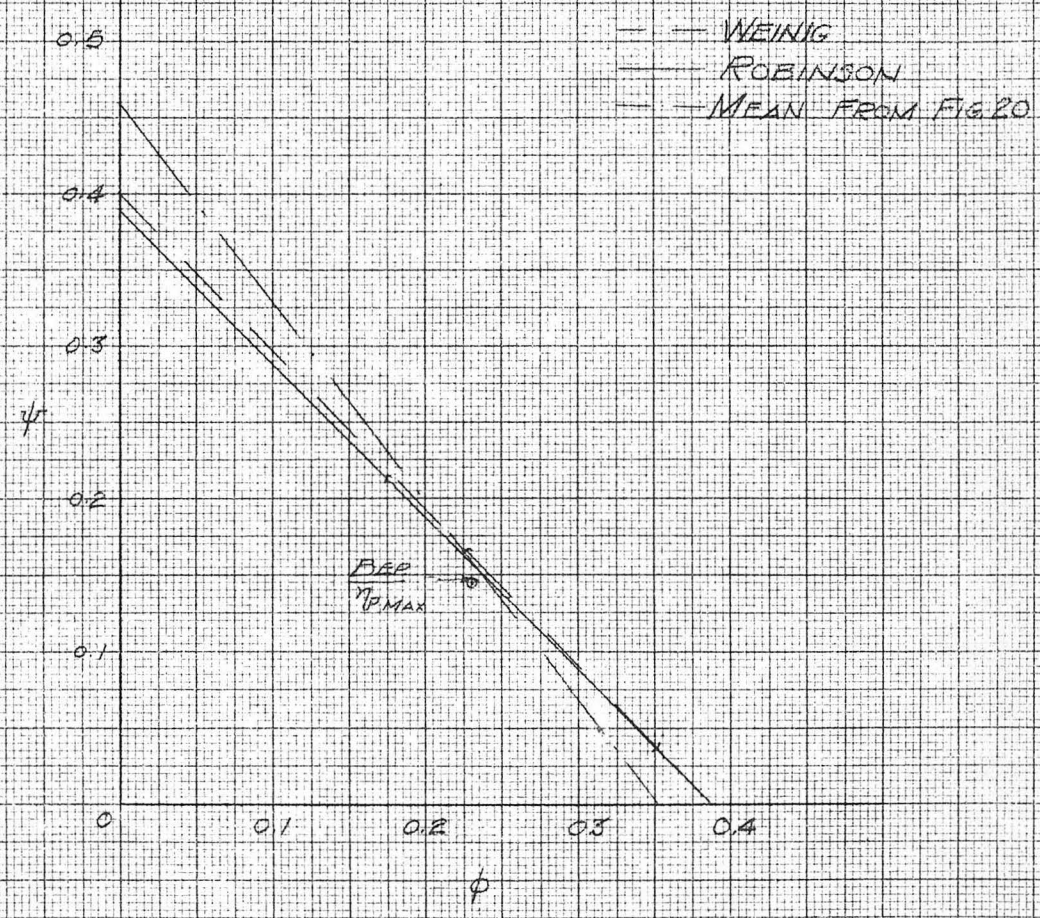

FIG 58

APPENDIX A

COMPARISON OF EXPERIMENTAL DATA WITH AIRFOIL CASCADE CALCULATIONS

In his Engineer's Degree thesis (12), R. L. Robinson calculated the relationships of lift coefficient vs. angle of attack for three section radii for the axial flow pump. He used a cascade theory utilizing a method whereby the slopes of the airfoil rather than the airfoil ordinates were used, thus getting around the operation of a differentiation in order to obtain the velocity and pressure distribution. The primary object of this was to be able to predict the zones of low pressure and consequently the cavitation behavior of the impeller. However, since no experimental determinations were made under cavitating conditions, it is only possible to check the ideal characteristics predicted by this method.

The two-dimensional cascade theory as applied to turbomachinery deals with the vector mean relative velocity, w_∞ which would be the free stream velocity far from the cascade, or would be the flight-path direction of the cascade moving through a fluid at rest (Fig. 55). This can be shown to be the vector mean of w_1 and w_2 by considering the combination of uniform and vortex flow in a plane where the airfoil is transformed into a circle, or by other methods such as considering that this vortex is equal in strength to the starting vortex that is washed downstream on initiation of the movement of the cascade or airfoil through the fluid. The simplest method, suggested by Wislicenus, is to assume that the force acting on the flow must be normal to the direction of w_∞ so that the rotational component of w_∞ is $\frac{1}{2}(w_{u1}+w_{u2})$.

(This is more a demonstration than proof, however.)

For axial inlet (Fig. 55),

$$F = L \sin(\beta - \alpha)$$

where

$$L = C_L c \frac{\rho w_\infty^2}{2},$$

and for three blades,

$$L = C_L (3c) \frac{\rho w_\infty^2}{2}$$

as before the power is given by

$$F \omega r = (\rho Q)(c_{u_2}) r = \rho Q g H,$$

or

$$H = \frac{Fu}{\rho g Q} .$$

The capacity per unit radius is

$$Q = 2\pi r \, c_m$$

and

$$c_m = w_\infty \sin(\beta - \alpha) ;$$

therefore,

$$H = \frac{3 C_L \, c \, u \, w_\infty}{4 \pi g r} .$$

The dimensionless head coefficient is defined as

$$\psi = H / \frac{u^2}{g} ,$$

the capacity coefficient as $\phi = c_m / u = \frac{Q/A}{u}$ so that

$$\psi = \frac{3 C_L \, c \, w_\infty}{4 \pi r u} \times \frac{c_m}{c_m} = \frac{3 C_L (c/r)}{4\pi} \cdot \frac{w_\infty}{c_m} \cdot \frac{c_m}{u}$$

$$\psi = \frac{3 C_L (c/r) \, \phi}{4 \pi \sin(\beta - \alpha)} .$$

Also since w_∞ is the mean of w_1 and w_2, $c_{u_\infty} = \frac{1}{2} c_{u_2}$; therefore, from the velocity triangle with w_∞ (Fig. 55)

$$\psi = 2 \left[1 - \phi \cot (\beta - \alpha) \right] \quad , \text{ or eliminating } \phi \, ,$$

$$\psi = \frac{2}{\dfrac{\cos(\beta - \alpha)}{1 + \left(\dfrac{3C_L}{8\pi} \dfrac{c}{r}\right)}} \, .$$

Solving for ϕ ,

$$\phi = \frac{\sin (\beta - \alpha)}{\cos(\beta - \alpha) - \dfrac{3C_L c}{8\pi r}} \, .$$

These two equations will give the characteristic for varying angles of attack.

The data determined from the theory as presented by Robinson gives the following:

r inches	c inches	β degrees	C_L
1.80 (hub)	3.25	33.60	$6.59 \sin (\alpha + 2)$
2.90 (av.)	2.91	18.65	$7.18 \sin (\alpha + 3.84)$
4.00 (tip)	2.88	11.88	$6.89 \sin (\alpha + 3.84)$

The results are plotted in Fig. 56 for the three radii along with the curves as predicted by Weinig. This pump was designed after still another method as worked out by Folsom and O'Brien (13) using NACA single blade airfoil data and assuming a lattice coefficient of 1. The lattice coefficients obtained by Robinson compare quite closely with those determined by Weinig as is seen;

	Lattice Coefficient		
	Hub	Av.	Tip
Robinson	1.05	1.14	1.10
Weinig	1.04	1.14	1.13

It is seen from Fig. 56 that the two methods give nearly the same results, the deviation being only a small percentage. This is interesting since Weinig's results are for a flat plate airfoil cascade and Robinson's are for cambered airfoils of finite thickness. Both methods were developed by the same basic mapping procedures.

Having obtained the curves of ψ vs. ϕ , these may be integrated in some fashion to give a mean characteristic. Since $\psi = \frac{u\, c_u}{u}$, or $H/\frac{u^2}{g}$ and $u = \omega r$, if ψ is multiplied by r^2, the product $(H/\frac{\omega^2}{g})$ is directly proportional to H, or $u\, c_u$ which is constant for all radii at the design point (assuming the free vortex or constant energy criterion of design). Also, assuming no prerotation and a uniformly distributed inlet velocity, c_m must be constant for all radii, or since $\phi = \frac{c_m}{u}$, $r\phi = \frac{c_m}{\omega}$. Thus if $r^2\psi$ is plotted vs. $r\phi$, the curves for all radii should intersect at the design point. For the three section radii calculated in Robinson's paper, these curves are plotted in Fig. 57, both after the method of Robinson and that of Weinig. These also fall in close proximity to each other for each radius. However, no single point of intersection is noted for either set. This is not surprising considering that a totally different design method was

employed, a constant lattice coefficient of unity was assumed and single airfoil data used.

The manner in which to integrate, or sum these characteristics is the next problem. It can be done either by summing the head over a line of constant capacity, or c_m, or summing the through flow over a line of constant H, or u c_u. Neither of these is accurate in so far as the assumptions of irrotational and two-dimensional flow can be maintained at any condition other than that occurring at the point of intersection. Also the two methods will not produce the same results. This can be seen by considering the shut-off condition and the results obtained if both methods are compared. The means were calculated in both ways and found to be essentially coincident (due to a not too large spread between the three curves in each case). These mean values based on the mean section radius of 3.10 inches are plotted in Fig. 58. The ranges of possible design points are noted on the curves as the ranges of intersections of the section curves in Fig. 57. Since these mean curves indicate the hydraulic input head, the value of experimental head coefficient (C_H) must be divided by the maximum efficiency to obtain a representative comparison. This point is also indicated on Fig. 58 and is seen to be in good agreement. However, it must be remembered that this efficiency is for the complete unit so that there are fluid and bearing friction losses entering into the experimental determination even if these are, for the most part, compensating effects.

From either of these types of analyses it would seem like a good method to begin with a single curve in a plot such as Fig. 58 and derive all section characteristics from this one plot. This would mean that both the head and through-flow velocity would be constant for all radii at any one operating point.

APPENDIX B

DERIVATION OF COEFFICIENTS FOR AN AXIAL FLOW MACHINE

The experimental dimensionless head, capacity and torque coefficients were determined as shown below. The coefficients referred to a constant speed basis are referred to as head-speed coefficients, etc., while those based on a constant capacity reference are called head-capacity coefficients, etc.

This appendix gives the coefficients generally for any purely axial flow machine of constant passage area. These are given in terms of the geometric parameters of the machine and the flow parameters. These general parameters are then specialized to give the conversion from the quantities of Q, n, H and T as they were read in the laboratory directly into the dimensionless values as plotted.

This particular axial flow unit was a 10 inch PL unit manufactured by the Peerless Pump Division of the Food Machinery Corporation.

The following definitions and values of terms apply to the derivations:

$$D_o = 8 \text{ in. (Bowl diameter)}$$

$$D_h = 3.6 \text{ in. (Hub diameter)}$$

$$\rho = 3.6/8 = 0.45 \text{ (Radius ratio)}$$

$$(1 - \rho^2) = 0.7975$$

$$\frac{1 + \rho^2}{2} = 0.60125$$

$$A = \frac{\pi}{4}\left[\left(\frac{D_o}{12}\right)^2 - \left(\frac{D_h}{12}\right)^2\right] = \frac{\pi}{4} \cdot \left(\frac{D_o}{12}\right)^2 \cdot (1 - \rho^2) \text{ square feet.}$$

$$\frac{D_m}{12} = \frac{1}{12}\sqrt{\frac{D_o^2 + D_h^2}{2}} = \frac{D_o}{12}\cdot\left(\frac{1+\rho^2}{2}\right)^{\frac{1}{2}} \quad \text{feet.}$$

$$u_m = \frac{\pi n}{60}\,\frac{D_m}{12} = \frac{\pi n}{60}\,\frac{D_o}{12}\cdot\left(\frac{1+\rho^2}{2}\right)^{\frac{1}{2}} \quad \text{fps.}$$

CAPACITY-SPEED COEFFICIENT

$$C_Q = \frac{c_m}{u_m} = \frac{Q}{A\,\frac{\pi n}{60}\cdot\frac{D_m}{12}} = \frac{Q}{\frac{\pi n}{60}\,\frac{D_o}{12}^3\,\frac{\pi}{4}} \times \frac{1}{(1-\rho^2)(\frac{1+\rho^2}{2})^{\frac{1}{2}}}$$

$$C_Q = \frac{Q}{n\,D_o^3}\;\frac{1728}{\pi^2(1-\rho^2)(\frac{1+\rho^2}{2})}\;\frac{1}{2}$$

$$C_Q = 42000\,\frac{Q}{nD_o^3(1-\rho^2)(\frac{1+\rho^2}{2})}\;\frac{1}{2}$$

$$C_Q = 132.5\,\frac{Q}{n}$$

$D_o = 8"$ $\rho = .45$

HEAD-SPEED COEFFICIENT

$$C_H = \frac{H}{\frac{u_m^2}{g}} = \frac{gH}{\left[\frac{\pi m}{60}\,\frac{D_m}{12}\right]^2} = \frac{gH}{\left[\frac{\pi m}{60}\,\frac{D_o}{12}\right]^2\left[\frac{1+\rho^2}{2}\right]}$$

$$C_H = \frac{H}{n^2\,D_o^2}\;\left[\frac{32.2(3600)(144)}{\pi^2\;\frac{1+\rho^2}{2}}\right]$$

$$C_H = 1{,}691{,}000\,\frac{H}{n^2\,D_o^2\left[\frac{1+\rho^2}{2}\right]}$$

$$C_H = 0.04395\,\frac{H(\text{ft } H_2O}{\left[\frac{n}{1000}\right]^2}$$

$D_o = 8"$ $\rho = .45$

$$C_H = 0.555\,\frac{H\ (\text{ft.Hg})}{\left[\frac{n}{1000}\right]^2}$$

TORQUE-SPEED COEFFICIENT

$$C_T = \frac{T}{\left(\frac{\gamma}{g}\right)\left(\frac{D_m}{12}\right)^3 u_m^2} = \frac{T}{\frac{\gamma}{g}\left(\frac{D_o}{12}\right)^5\left(\frac{\pi m}{60}\right)^2\left(\frac{1+\rho^2}{2}\right)^{\frac{5}{2}}}$$

$$C_T = \frac{T}{n^2 D_o^5} \cdot \frac{(12)^5 g \cdot 3600}{\pi^2\left(\frac{1+\rho^2}{2}\right)^{\frac{5}{2}}} = \frac{T}{n^2 D_o^5} \cdot \frac{(12)^5\, 32.2(3600)}{62.4\,\pi^2\left(\frac{1+\rho^2}{2}\right)^{\frac{5}{2}}}$$

$$C_T = 46{,}800{,}000 \frac{T}{n^2 D_o^5 \left(\frac{1+\rho^2}{2}\right)^{\frac{5}{2}}}$$

$$C_T = 51.1 \times 10^{-3} \frac{T}{\left(\frac{n}{1000}\right)^2} \; ; \; C_T = 0.4255 \times 10^{-3} \frac{T}{\left(\frac{n}{1000}\right)^2}$$

T Ft. lbs. T In. lbs.

$D_o = 8"$ $\rho = 0.45$

PUMP EFFICIENCY

$$\eta_P = \frac{WHP}{BHP} = \frac{QH}{T \cdot \frac{2\pi m}{60}}$$

$$\eta_P = \frac{\gamma}{\frac{2\pi m}{60}} \cdot \frac{\frac{n D_o^3 C_Q (1-\rho^2)\left(\frac{1+\rho^2}{2}\right)^{\frac{1}{2}}}{42000} \cdot \frac{n^2 D_o^2 \left(\frac{1+\rho^2}{2}\right) C_H}{1691000}}{\frac{n^2 D_o^5 (1+\rho)^{\frac{5}{2}} C_T}{46{,}800{,}000}}$$

$$\eta_P = \frac{62.4(30)(46.8)(1-\rho^2)\, C_Q\, C_H}{\pi\,(42000)(1.691)\left(\frac{1+\rho^2}{2}\right) C_T}$$

$$\eta_P = 0.392 \cdot \frac{1-\rho^2}{\frac{1+\rho^2}{2}} \cdot \frac{C_Q\, C_H}{C_T}$$

SPEED-FLOW COEFFICIENT $\propto n/Q^2$

$$K_n = \frac{u_m}{c_m} = \frac{1}{C_Q}$$

HEAD-FLOW COEFFICIENT $\propto H/Q^2$

$$K_H = \frac{H}{\frac{c_m^2}{g}} = \frac{C_H}{C_Q^2}$$

TORQUE-FLOW COEFFICIENT

$$K_T = \frac{T}{\frac{\gamma}{g}\left(\frac{D_m}{12}\right)^3 c_m^2} = \frac{C_T}{C_Q^2}$$

TURBINE EFFICIENCY

$$\eta_T = \frac{1}{\eta_P}$$

SPECIFIC SPEED

$$n_S = \frac{Q^{\frac{1}{2}}}{H^{\frac{3}{4}}} \cdot n$$

$$Q = \frac{n C_Q}{132.5}$$

$$H = \frac{n^2 C_H}{43950}$$

$$n_S = \frac{\left[\frac{n C_Q}{132.5}\right]^{\frac{1}{2}} n}{\left[\frac{n^2 C_H}{43950}\right]^{\frac{3}{4}}} = \left[\frac{C_Q}{132.5}\right]^{\frac{1}{2}} \left[\frac{43950}{C_H}\right]^{\frac{3}{4}}$$

$$n_S = 262 \frac{C_Q^{\frac{1}{2}}}{C_H^{3/4}}$$

$$\left.\begin{aligned} C_Q &= 0.230 \\ C_H &= 0.115 \end{aligned}\right\} \text{ at b.e.p.}$$

$$n_S = 13500 \text{ (Based on gpm.)}$$

$$\eta_P = 0.520 \frac{C_Q C_H}{C_T}$$

$$\rho = .45$$

EXAMPLE: Run No.5, Data Sheet 5-11-50(2)

Q = 1.605 c.f.s.

n = 1000 r.p.m.

H = 0.239 ft. Hg.

T = 44.6 in. lbs.

$$C_Q = 132.5 \frac{1.605}{1000} = 0.213 = C_Q$$

$$C_H = 0.04395(.239)(12.65) = 0.556(.239) = \underline{0.133 = C_H}$$

$$C_T = 0.4255 \cdot 10^{-3}(44.6) = \underline{0.019 = C_T}$$

$$\eta_P = 0.520 \frac{(.213)(.133)}{.019} = \underline{77.5\% = \eta_P}$$

APPENDIX C

DERIVATION OF COEFFICIENTS FOR A MIXED FLOW MACHINE

These are derived in the same general way as those for the axial flow unit. However, since there is so much possibility for variation in the various geometric parameters of a mixed flow unit, no attempt is made to present a general form for the coefficients as was done with the axial flow unit.

The particular unit tested was a 10 inch MF unit manufactured by the Peerless Pump Division of the Food Machinery Corporation.

The following definitions, sketch and values apply to the derivations of coefficients for this unit:

$$A_2 = \pi \left[\frac{D_o + D_h}{2} \right] s$$

$$= \pi \left[\frac{8\frac{1}{4} + 4\frac{19}{64}}{2} \right] 2\frac{9}{32} \cos 5^o$$

$$A_2 = 4.48 \text{ sq. in.}$$
$$0.311 \text{ sq. ft.}$$

$$D_{m_2} = \sqrt{\frac{D_o^2 + D_h^2}{2}}$$

$$D_{m_2} = 6.67 \text{ in.}$$

$$\frac{D_{m_2}}{12} = 0.548 \text{ ft.}$$

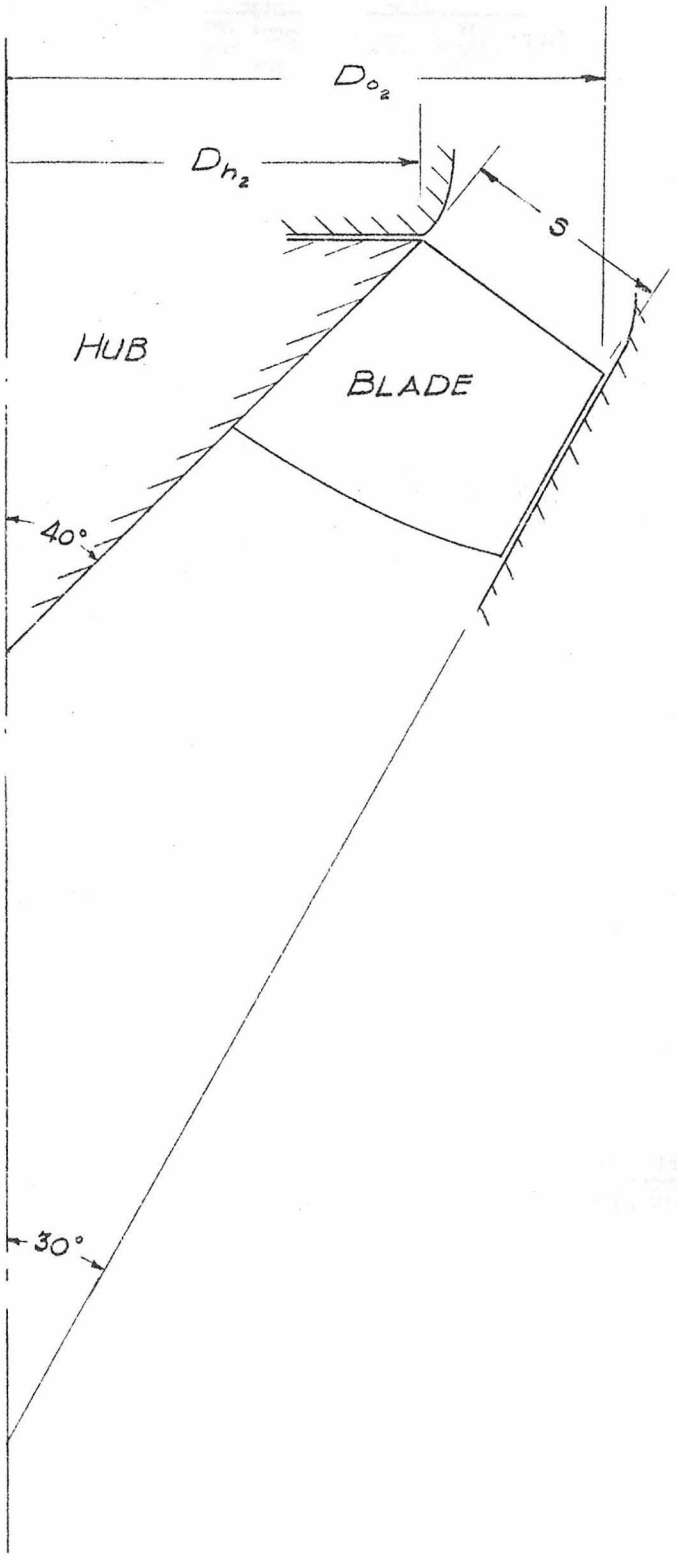
D_{o_2}
D_{h_2}
S
HUB
BLADE
40°
30°

CAPACITY-SPEED COEFFICIENT

$$C_Q = \frac{c_{m_2}}{u_{m_2}} = \frac{Q/A}{\frac{\pi n}{60}\frac{D_{m_2}}{12}} = \frac{Q/n}{(.311)\frac{\pi}{60}(.548)}$$

$$\boxed{C_Q = 111.8\,\frac{Q}{n}}$$

HEAD-SPEED COEFFICIENT

$$C_H = \frac{H}{\frac{u_{m_2}^2}{g}} = \frac{gH}{\left(\frac{\pi n}{60}\right)^2\left(\frac{D_{m_2}}{12}\right)^2} = \frac{32.14 \cdot H/n^2}{\frac{\pi}{60}(.548)^2}$$

$$C_H = \frac{0.0391 \cdot H(ft.H_2O)}{(n/1000)^2}$$

$$\boxed{C_H = \frac{0.495\ H(ft.\ Hg)}{(n/1000)^2}}$$

TORQUE-SPEED COEFFICIENT

$$C_T = \frac{T}{\left(\frac{\gamma}{g}\frac{D_m}{12}\right)^3 \cdot u_{m_2}^2} = \frac{gT}{\gamma\left(\frac{D_{m_2}}{12}\right)^3 \cdot \left(\frac{\pi D_{m_2} n}{60\ 12}\right)^2} = \frac{32.14\ (60^2)}{62.4(.548)^5 \cdot \pi^2}\,\frac{T}{n^2}$$

$$C_T = \frac{3810\ T\ (\text{ft. lbs.})}{n^2} = \frac{0.3174 \times 10^{-3}\ T(\text{in. lbs.})}{(n/100)^2}$$

PUMP EFFICIENCY

$$\eta_P = \frac{QH}{T \cdot \frac{2\pi n}{60}} = \frac{62.4\ (60)3810\ n\ n^2\ C_Q\ C_H}{2\pi(111.8)39100\ n\ n^2\ C_T}$$

$$\eta_P = 0.520 \cdot \frac{C_Q\ C_H}{C_T}$$

SPEED-FLOW COEFFICIENT

$$K_n = \frac{c_{m_2}}{u_{m_2}} = \frac{1}{C_Q} = \frac{1}{111.8}\ \frac{n}{Q} = \frac{0.895\ n/100}{Q}$$

$$K_n = \frac{0.895\ n/100}{Q}$$

HEAD-FLOW COEFFICIENT

$$K_H = \frac{H}{\frac{c_{m_2}^2}{g}} = \frac{C_H}{C_Q^2} = \frac{39100\ H/n^2}{(111.8)^2\ Q^2/n^2} = \frac{3.13\ H(\text{ft. } H_2O)}{Q^2}$$

$$K_H = \frac{3.96\ H(\text{ft. Hg.})}{Q^2}$$

TORQUE-FLOW COEFFICIENT

$$K_T = \frac{T}{\frac{\gamma}{g}\left(\frac{D_{m_2}}{12}\right)^3 (c_{m_2})^2} = \frac{C_T}{C_Q^2} = \frac{3810\ T/n^2\ (\text{ft. lbs.})}{(111.8)^2\ Q/n^2}$$

$$K_T = \frac{0.305\ T(\text{ft. lbs.})}{Q^2} = \frac{0.0254\ T\ (\text{in. lbs.})}{Q_2}$$

TURBINE EFFICIENCY

$$\eta_T = \frac{1}{\eta_P} = \frac{1}{.520}\ \frac{C_T}{C_Q\ C_H} = \frac{K_T \cdot C_Q^{\,2}\ K_n}{.52\ K_H \cdot C_Q^{\,2}}$$

$$\eta_T = \frac{1.922\ K_n\ K_T}{K_H}$$

SPECIFIC SPEED

$$n_s = \frac{Q^{\frac{1}{2}}}{\frac{3}{4}}\ n = \frac{(39100)^{\frac{3}{4}}\ C_Q^{\frac{1}{2}}\ n^{\frac{1}{2}}\ n}{(111.8)^{\frac{1}{2}}\ C_H^{\frac{3}{4}}\ n^{\frac{3}{2}}}$$

$$n_s = \frac{263\ C_Q^{\frac{1}{2}}}{C_H^{\frac{3}{4}}} = \frac{263\ (.23333)^{\frac{1}{2}}}{(.253)^{\frac{3}{4}}}$$

$$n_s = 356 \text{ on c.f.s.}$$
$$7550 \text{ on g.p.m.}$$